

# 博士学位论文

## 高浓度旋风分离器气固流动与分离特性的 数值模拟

### NUMERICAL SIMULATION OF DENSE GAS-SOLID SEPARATION IN CYCLONE SEPARATORS

**M'BOUANA No éLandry-Privace**

**2014 年 6 月**

国内图书分类号: TQ051.8  
国际图书分类号: 621.6

学校代码: 10213  
密级: 公开

## 工学博士学位论文

# 高浓度旋风分离器气固流动与分离特性的 数值模拟

博 士 研 究 生: M'BOUANA No éLandry-Privace

导 师: 陆慧林 教授

申 请 学 位: 工学博士

学 科: 热能工程

所 在 单 位: 能源科学与工程学院

答 辩 日 期: 2014 年 6 月

授予学位单位: 哈尔滨工业大学

Classified Index: TQ051.8

U.D.C: 621.6

Dissertation for the Doctoral Degree in Engineering

**NUMERICAL SIMULATION OF DENSE  
GAS-SOLID SEPARATION IN CYCLONE  
SEPARATORS**

<b>Candidate:</b>	M'BOUANA No éLandry-Privace
<b>Supervisor:</b>	Prof. LU Huilin
<b>Academic Degree Applied for:</b>	Doctor of Engineering
<b>Speciality:</b>	Thermal Energy Engineering
<b>Affiliation:</b>	School of Energy Science and Engineering
<b>Date of Defence:</b>	June, 2014
<b>Degree-Conferring-Institution:</b>	Harbin Institute of Technology

## Abstract

Multiphase flow is a fundamental physical phenomenon prevalent in nature and industrial processes, and has very wide range of application, such as dust air, debris flows, sandstorms flow, powder pneumatic conveying, separation and collection of coal combustion and conversion, other applications where multiphase flow problem occur include the fluidized bed reactor in the coal combustion, petroleum processing industry spray combustion, solid propellant rocket nozzle flow and materials industry.

In industrial applications, we often encounter the phenomenon of separation of multiphase flow. Many industrial processes, such as coal and waste materials combustion, mineral processing, food processing, soil remediation, waste treatment, oil refining, apply the phenomenon of particle separation.

Several technologies, including fabric filters, dust collectors and cyclone separators can be used for gas-solid separation. Some separators are not suitable for many industrial applications, but Cyclones play a critical role in separation of solid particles in a flowing fluid. Cyclones Separators are widely used in many industrial sectors such as in the petrochemical and process industries to separate dust from gas steams or for product recovery.

In the last decade, Cyclones separators have been the subject of several experimental and numerical researches to improve and this involves trying to treat several parameters involved in modifying the behavior of their efficacy. However, due to factors, that affect the performance of cyclones and the gas-solid two-phase flow is extremely complex and then involves many of the basic disciplines of fluid mechanics, thermodynamics, heat and mass transfer, combustion and rheology.

With the development of computer technology and computational method, numerical simulation has become one of the most promising methods for studying gas-solid flows. Continuous improving of the numerical simulation methods has important significance to further study of the complex mechanism and effect factors of gas-solid flows. The present contribution aims to add more to the existing knowledge on the functioning of cyclones which represents one of the most recent applications of the technique of separation by centrifugal force. The main objective

of the present research is to study the behavior of dense gas solid separator within different type of cyclones. The research aims to provide a better understanding of the effect of cyclone geometry. Two turbulence model and Eulerian-Eulerian approach will be combined to study and describe the dense fluid flow and the performance of cyclone. The effect of cyclone geometry, the effect of turbulence model and the effect of solid concentration on the cyclone separators are investigate.

The scope covered in the present research is outlined in the following paragraphs:

(1) Firstly, the numerical simulation of gas and solid flow were performed using conventional cyclone separator with four types of inlet configuration. In this section, we used Renormalization group k-epsilon (RNG k- $\epsilon$ ) and Reynolds stress model (RSM) model in Fluent to study numerical simulation of gas and particle flow in cyclone separator. The turbulent model is verified by comparing the RNG k- $\epsilon$  and RSM results in term of gas pressure field, gas and solid volume fraction. The effects of turbulent model, solid inlet volume fraction and inlet geometry are investigated based on the velocity components, pressure drop and cyclone efficiency.

(2) In the second part simulations are relative to the square cyclone separator, the flow behavior of gas and particles within a square cyclone separator is simulated by means of computational fluid dynamics. The RNG k- $\epsilon$  model and the RSM were used to model gas turbulence, and Eulerian approach to model gas-solid two phase flow. The flow behavior is examined in terms of tangential velocity components, static pressure and pressure drop contour plots for flow field and solid volume fraction. The effects of the turbulence model and solid volume fraction on the square cyclone are discussed. The results indicate that the pressure drop increases with increasing solid volume fraction, and increase with increasing inlet velocities for two turbulence models, moreover, simulations were compared with pressure field. For all runs, the RSM model gives a higher pressure drop compared to the RNG k- $\epsilon$  model. The RSM model provides well the forced vortex and free vortex, and captures better the phenomena occurring during intense vortex flow in the presence of walls within cyclone separators. The results showed that square cyclone

with different inlet geometries would increase the pressure drop and decrease the separation efficiency as function of inlet angle  $\alpha$ . Note that the effects of the cyclone inlet configuration angle on pressure drop and collection efficiency are opposite. Increasing the inlet width will save more driving power but leads to reduced collection efficiency.

(3) Finally, The RNG k- $\varepsilon$  and RSM and Eulerian approach will be combined to study and describe the dense fluid flow and the performance of cyclone in horizontal cyclone separator. The effect of two turbulence model and solid inlet volume fraction based on the distributions of the flows fields, and cyclone performance were studied and the results illustrated that by increasing of solid volume fraction the pressure drop in horizontal cyclone increases but the collection efficiency decreases.

**Keywords:** Computational Fluid Dynamic; Cyclone separator; Dense gas-solid two phase flow; Turbulence model; Solid volume fraction.

## 摘 要

多相流是一种在自然界和工业过程中很常见的物理现象，实际生活中也有很多方面涉及到多相流动，比如扬尘、泥石流、沙尘暴、气力输送、煤粉燃烧产物的分离与捕集等等。此外，多相流动现象还大量出现在石油化工、流化床反应器、固体火箭喷管和材料工业等领域。

在工业应用中，我们经常需要考虑如何分离多相流体。在许多工业工程中，比如矿物加工、食品加工、土壤改良、废物处理、石油提纯等，都包含有颗粒分离现象。

目前，在气固分离方面已经有一些比较成熟的技术和设备，布袋除尘器、电除尘器和旋风分离器都是使用较广的气固分离手段。一些分离器可能不适用工业生产，但是旋风分离器在分离多相流体中的固体颗粒方面有着很好的效果。并且旋风分离器在很多工业领域都有着广泛的应用，比如在石油化工中从气流中分离出灰尘以及在工业过程中进行产品修复。

在过去的十年里，科研工作者通过一系列的实验研究和数值模拟来提高旋风分离器的性能，通过修改一些参数来修正分离器的参数是研究手段之一。然而，影响旋风分离器和气固两相流动的因素是非常复杂的，并且其中涉及到大量的流体力学、传热传质、热力学、燃烧学等方面的内容。

旋风分离器是离心力分离技术应用的典范，现在的研究旨在拓展旋风分离器已成的知识体系。目前研究的主要目标是运用不同形式的旋风分离器进行稠密气固分离。本文研究的主要范围如下所示：

(1) 对由传统的旋风分离器产生的气固流动进行了数值模拟，该分离器有四个不同形式的进口结构。在这个章节中，我们采用 FLUENT 中的 RNG  $k-\varepsilon$  和 RSM 模型对旋风分离器中的气流和颗粒流进行数值模拟。依据速度分布，压降和分离效率对湍流模型，固相的入口体积分数和入口结构的作用进行了考察。

(2) 对方形旋风分离器中的气体和颗粒的流动进行了 CFD 模拟。RNG  $k-\varepsilon$  模型和 RSM 模型用来模拟气体的湍流，欧拉法模拟气固两相流动。通过切向

速度、静压力和压降在流场中的等高线和固体体积分数对流动进行了检验。讨论了湍流模型和固体体积分数对方形旋风分离器的影响。模拟结果表明，随着固体体积分数的增加压降增加，并且压降随着两个湍流模型的入口速度的增加而增加。同时，本文比较了两种数值模拟结果中的压力场。综上所述，相比于 RNG k- $\epsilon$  模型，用 RSM 模型模拟可以获得更高的压降。运用 RSM 模型可以获得更好的强制涡流和自由涡流，并且能够更好的反应旋风分离器壁面发生强烈的涡流这一现象。结果表明不同进口结构的方形旋风分离器可以增加压降和降低分离效率，该结果可以表示成进口角度的一个函数。需要注意的是，旋风分离器的入口角度对压降和捕集效率的影响效果是相反的。增加进口的宽度会进一步的节省驱动能耗但是会导致收集效率的降低。

(3) 湍流模型 (RSM 和 RNG k- $\epsilon$  模型) 和欧拉法被联合使用去研究和描述稠密流体流动和水平旋风分离器分离现象。依据流场的分布和分离性能对湍流模型和入口固相体积分数的影响进行了分析，结果表明水平旋风分离器中的压降随着固相体积分数的增加而增加，但是捕集效率随着固相体积分数的增加而降。

**关键词：**CFD；旋风分离器；稠密气固两相流；湍流模型；两相流动；固相体积分数



## Contents

<b>Abstract .....</b>	<b>I</b>
<b>摘 要 .....</b>	<b>IV</b>
<b>Nomenclature .....</b>	<b>IX</b>
<b>扩展中文摘要 .....</b>	<b>1</b>
<b>Chapter 1 Introduction .....</b>	<b>15</b>
1.1 Background of the research .....	15
1.2 State of the art of gas-solid cyclone separators .....	16
1.2.1 Cyclone separators: A state of the art review .....	16
1.2.2 Description and geometry of cyclone .....	19
1.2.3 Performance characteristics of cyclone separators .....	22
1.2.4 Parameters affecting the performance of cyclone .....	24
1.3 Gas-solid two-phase flow modeling: A state of the art review .....	26
1.3.1 Turbulence model .....	27
1.3.2 Gas-solid two phase flow model.....	27
1.3.3 Kinetic theory of granular flow .....	29
1.4 The objectives of this research .....	30
<b>Chapter 2 Description of numerical model .....</b>	<b>32</b>
2.1 Introduction .....	32
2.2 Turbulence modeling for the fluid phase .....	32
2.2.1 RNG k- $\epsilon$ model .....	33
2.2.2 Reynolds Stress Model .....	34
2.3 Gas-solid two phase flow model description .....	37
2.4 Brief summary .....	41
<b>Chapter 3 Numerical study of a cylindrical cyclone separators .....</b>	<b>42</b>
3.1 Introduction .....	42
3.2 Description of numerical model .....	42
3.2.1 Configuration of cyclone separators .....	42
3.2.2 Turbulence model .....	45
3.2.3 Gas-solid two phase flows .....	45
3.2.4 Boundary conditions .....	46

3.2.5 Grid independence .....	46
3.3 Results and discussion .....	47
3.3.1 Effect of turbulence model on cyclone separator .....	47
3.3.2 Effect of inlet geometry on the flow pattern and performance .....	56
3.4 Brief summary .....	63
<b>Chapter 4 Numerical study of square cyclone separators .....</b>	<b>65</b>
4.1 Introduction .....	65
4.2 Numerical simulation methods .....	66
4.2.1 Geometry configuration of four squares cyclones.....	66
4.2.2 Turbulence model .....	68
4.2.3 Gas-solid two phase flow model.....	68
4.2.4 Boundary condition .....	69
4.2.5 Grid independence studies .....	69
4.3. Validation of the numerical model.....	70
4.4 Results and discussions .....	71
4.4.1 Comparison of turbulence model.....	71
4.4.2 Effect of solid concentration on square cyclones .....	77
4.4.3 Effect of inlet configuration on square cyclone separators .....	83
4.5 Brief summary .....	90
<b>Chapter 5 Separation and pressure drop in horizontal cyclone separator .....</b>	<b>92</b>
5.1. Introduction .....	92
5.2. Mathematical model and numerical solution method.....	93
5.2.1 Gas–solid two-fluid model .....	93
5.2.2 Turbulence model .....	93
5.2.3 Geometry of horizontal cyclone separator .....	94
5.2.4 Boundary conditions .....	96
5.3 Results and discussion .....	96
5.3.1 Flow fields .....	96
5.3.2 Tangential velocity.....	98
5.3.3 Volume fraction.....	101
5.3.4 Pressure drop .....	101
5.3.5 Collection efficiency.....	103
5.4. Brief summary .....	105
<b>Summary and Conclusion .....</b>	<b>106</b>

---

<b>Reference .....</b>	<b>109</b>
<b>Papers published in the period of Ph.D education .....</b>	<b>121</b>
<b>哈尔滨工业大学学位论文原创性声明及使用授权说明 .....</b>	<b>122</b>
<b>Statement of copyright and Letter or authorization .....</b>	<b>123</b>
<b>Acknowledgements .....</b>	<b>124</b>
<b>Resume .....</b>	<b>125</b>

## Nomenclature

$a$	Cyclone inlet height, m
$b$	Cyclone inlet width, m
$B$	Exit solid diameter, m
$C_D$	Drag coefficient
$C_{ij}$	Convection term
$D$	Cyclone diameter, m
$De$	Exit gas (or vortex finder) diameter, m
$D_{T,ij}$	Turbulent diffusion term
$D_{L,ij}$	Molecular diffusion
$d_s$	Solid particle diameter, m
$F_{ij}$	Production by system rotation
$G_b$	Generation of turbulence kinetic energy due to buoyancy
$G_k$	Generation of turbulence kinetic energy due to mean velocity
$G_{ij}$	Buoyancy production
$g_0$	Radial distribution function (.)
$g$	Gravitational acceleration, $m/s^2$
$H$	Cyclone height, m
$h$	Cyclone(or cylindrical ) body height, m
$k$	Turbulent kinetic energy, $m^2/s^2$
$m$	Mass flow rate, kg/s
$m_p$	Particle mass, kg
$P$	Pressure, Pa
$P_{ij}$	Stress production term
$P_s$	Solid pressure, Pa
$P_{si}, P_{so}$	Solid pressure at inlet and outlet of cyclone, Pa
$\Delta P$	Pressure drop between separator inlet and gas outlet, Pa
$r, \theta, z$	Cylindrical coordinates
$Re$	Reynolds number, dimensionless
$r_f$	Radius of free vortex
$S$	Exit tube length, m

$S_{\text{user}}$	User-defined source term
$t$	Time, s
$U, V, W$	Velocity components
$\mathbf{u}$	Velocity vector, m/s
$V_{\text{in}}$	Inlet velocity, m/s
$V_g, V_s$	Gas velocity, solid velocity, m/s

**Greek letters**

$\alpha$	Volume fraction (.)
$\alpha$	Cyclone inlet angle( $^{\circ}$ )
$\alpha_k$	Inverse Prandtl number
$\alpha$	Swirl constant
$\beta_{gs}$	Interface momentum transfer coefficient
$\Gamma$	Represents the circulation.
$\Delta$	Change in variable, final-initial
$\varepsilon$	Turbulent dissipation rate ( $\text{m}^2/\text{s}^3$ )
$\varepsilon_{ij}$	Dissipation
$\mu_s$	Solid shear viscosity
$\mu_g$	Gas viscosity, kg/m-s
$\lambda_s$	Solid bulk viscosity
$\theta$	Granular temperature, $\text{m}^2/\text{s}^2$
$\Phi_{ij}$	Pressure strain
$\phi_s$	Exchange of fluctuating energy
$\eta$	Collection efficiency
$\rho_g$	Gas density, $\text{kg}/\text{m}^3$
$\rho_s$	Solid density, $\text{kg}/\text{m}^3$
$\tau$	Stress tensor
$\omega$	Angular velocity, rad/s

**Subscript**

$g$	Gas
$s$	Solid
$q$	Gas or solid phase

**Abbreviation**

CFD	Computational fluid dynamic
CFBC	Circulating fluidized bed combustion
DEM	Discrete Element Method
DPM	Discrete Phase Models
DRSM	Differential Reynolds Stress Model
KTGF	Kinetic Theories of Granular Flows
LDA	Laser Doppler anemometry
LES	Large Eddy Simulation
PDA	Particle Dynamic Analyzer
RNG	Renormalization group
RSM	Reynolds Stress Model
VOF	Volume of fluid

## 扩展中文摘要

气固分离单元是燃煤流化床和催化裂化反应器等工业过程中的重要过程之一，高效、低阻的气固分离器保证了流化床反应器的高固体通量和高循环倍率运行，故成为流态化技术的关键单元技术之一。旋风分离器作为一种广泛应用于燃煤、石油化工、煤化工、电力等工业部门的气固分离设备，由于其结构简单、造价低并可耐受高温高压操作条件、分离效率较高等优点，成为气固分离装置的首选。

燃煤流化床锅炉中气固分离单元一般由旋风分离器组成，因此，旋风分离器性能是影响分离整体效率的最重要因素之一。同时，高固体通量操作使得旋风分离器处于高入口浓度操作工况，而高循环倍率运行要求分离器必须在许可的压降下尽可能的提高效率，高温恶劣环境需要分离器在结构上加以优化以减弱结焦、磨损的可能性。

鉴于分离器结构和布置的不同，旋风分离器主要有：立式“筒锥式”、立式方形和卧式圆柱型等。分离器结构和布置的差异导致分离器性能的不同，适用于不同的燃煤流化床过程。不同结构和布置的旋风分离器的工作过程具有共同的特征：进入旋风分离器的含尘气体在壁面的约束下，由直线运动变为圆周运动，旋转气流绝大部分沿壁面螺旋运动，被称为外旋涡。气体中的颗粒在离心力作用下被甩向旋风分离器壁面，与壁面碰撞、摩擦后，动量逐渐损失，并随着外旋涡气流最终落入排尘口被分离出来。外旋涡气流导致净化后的气体沿轴线螺旋运动，从排气管排出，被称为内旋涡。由此可见，旋风分离器内部的流动为三维气固强旋流动，其复杂性表现为：（1）三维旋转流动：表现出强烈的各向异性特征，对实验研究和数值模拟造成了很大困难；（2）“二次流”：强旋流运动引起的压力梯度将在旋风分离器内壁产生“二次流”，包括排气管末端的“短路流”以及自排出口向上的“二次返混流”。（3）气固两相流：气体和颗粒间的相互作用对流动和分离过程造成很大影响；（4）流场边界复杂：筒锥式结构、入口等结构使得旋风分离器的流场边界比重力沉降分离器、惯性撞击式

分离器以及过滤式分离器等都要复杂的多。

旋风分离器内气固两相流体动力特性的研究主要分为三类方法：一类方法是采用各种实验手段；二类方法是采用理论分析的方法建立性能模型；三类方法是采用计算流体力学(CFD)的方法。旋风分离器的数值模拟可分为纯气流流场的数值模拟和气固两相流场的数值模拟。

总之，高入口浓度是燃煤流化床旋风分离器的最重要特征。前人的工作以性能实验、模型研究和数值模拟为主要研究手段，研究对象则集中于低入口浓度下的“筒锥式”旋风分离器。因此，研究高入口浓度下不同型式旋风分离器的性能、流动结构、分离机理和计算模型具有重要意义。

基于燃煤流化床对高浓度气固分离的技术需求和前人的研究成果，本文的研究目标为：在高入口浓度条件下，对“筒锥式”旋风分离器、方形分离器和卧式分离器进行气固两相流动、分离的规律和性能计算方法，从而为燃煤流化床旋风分离器的设计和优化提供理论参考和实践依据。

本文的主要研究内容和结构安排如下：

第二章：对于分离器气固两相流场，数值计算方法主要有离散相模型(DPM)和双流体模型(TFM)两种方法。双流体模型(Two fluid model)是在欧拉坐标系中考察流体相与颗粒相的模型。给出双流体模型的计算模型。其中：采用颗粒动力学 (Kinetic theory of granular flow, KTGF) 封闭固相的本构方程。颗粒动力学类比稠密气体分子运动论，使用“颗粒温度”的概念反映了基于层流机制的颗粒相速度脉动，从理论上获得了颗粒相粘度和颗粒相压力的表征方法，并提出了以颗粒的非弹性碰撞为颗粒相能量的耗散形式。通过采用颗粒动力学方法，预测分离器内高浓度颗粒碰撞作用对颗粒流体动力特性的影响。气相湍流的数值模拟方法主要有：直接数值模拟方法(DNS)、基于大涡模拟的亚网格尺度方法(LES)、雷诺应力平均方法(RANS)、谱方法和基于概率密度函数的 PDF 方法等。本文研究采用 RANS 方法研究气体流体动力特性。分别应用重整化  $k-\varepsilon$  双方程模型和雷诺应力模型(RSM)模拟气相湍流流动过程，分析分离器内气体湍流流动特性。

第三章：分别采用 RNG  $k-\varepsilon$  模型和 RSM 模型，结合颗粒动力学模型，数



值模拟“筒锥式”旋风分离器内气固两相流动过程。获得了浓度和速度分布以及气体压力的分布。图 1 表示气体速度在进口位置高度的分布特性。分别采用 RMS 模型和 RNG k- $\epsilon$  模型预测气体湍流流动特性, 计算结果表明气体速度分布基本相同, 在进入分离器气体速度达到最大, 之后, 气体速度逐渐降低。在中心筒体区域, 气体速度达到最小, 表明在筒体内速度分布高度不均匀。

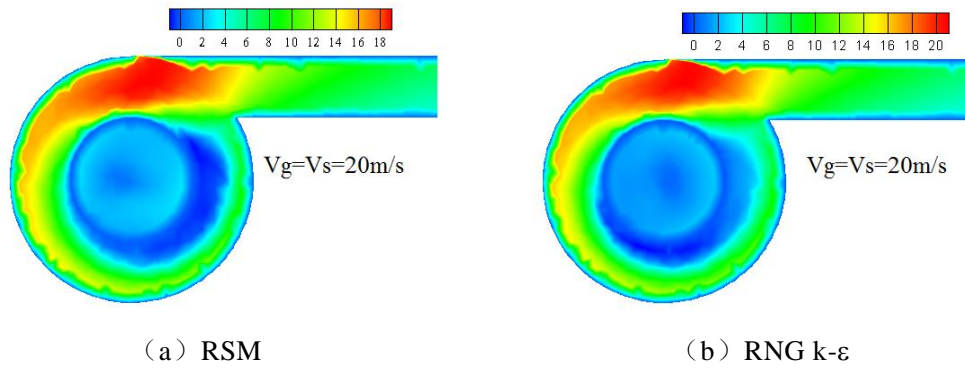


图 1 不同气体湍流模型对气体速度分布的影响

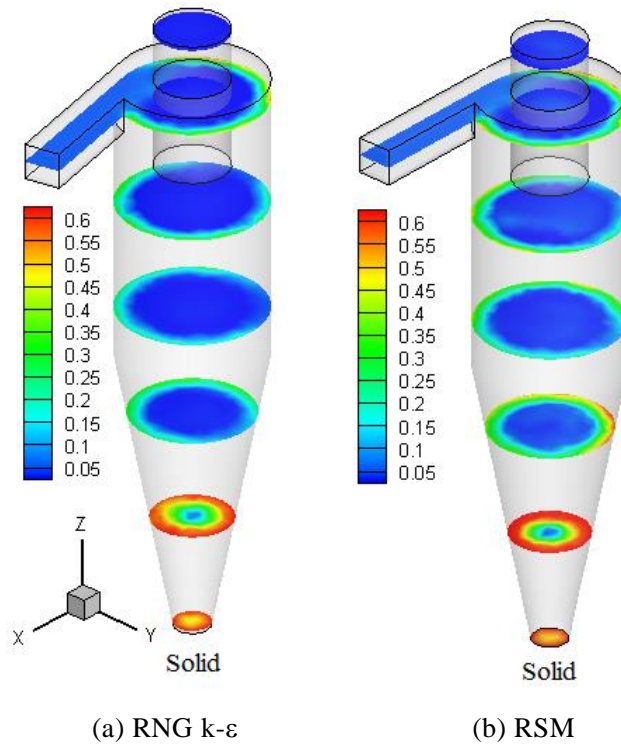


图2 不同气体湍流模型对颗粒浓度变化的影响

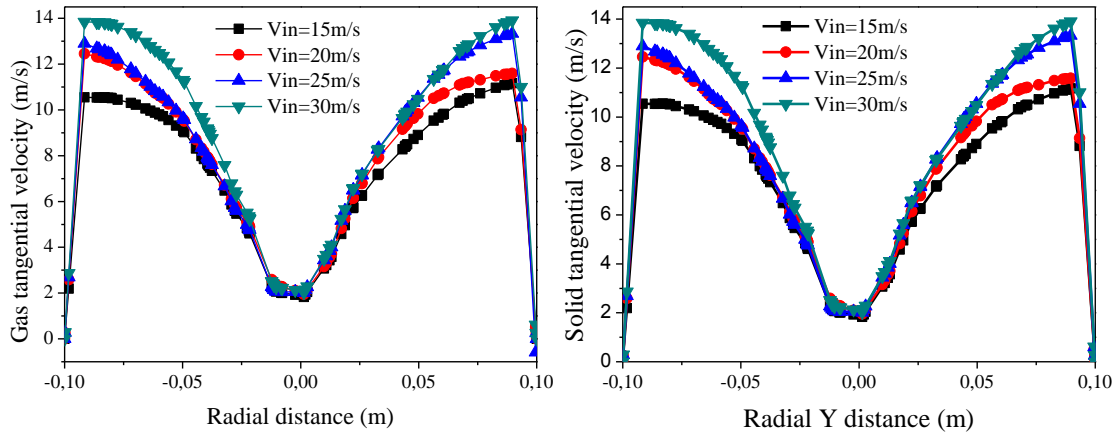


图3 不同进口气体速度下气体和颗粒切向速度的分布

图2表示颗粒浓度的变化。在分离器入口，颗粒浓度最低。当气体和颗粒进入筒体后，颗粒被集中在筒体壁面区域。沿锥体出口方向，颗粒浓度逐渐增大，在锥体出口处颗粒浓度达到最大，表明颗粒被分离。由图可见，采用气体 RNG  $k-\varepsilon$  湍流模型和 RSM 模型所得到的颗粒浓度分布的变化趋势是一致的。但是，采用 RSM 模型预测的筒体区域和锥体区的颗粒浓度相对较大，而 RNG  $k-\varepsilon$  模型预测的颗粒浓度相对较小，即 RSM 模型预测的颗粒分离比 RNG  $k-\varepsilon$  模型预测结果要高。

图3表示气体和颗粒切向速度的分布。随着进口气体速度的增加，气体和颗粒切向速度增大。在分离器筒体壁面处切向速度为零是由于在数值模拟计算中壁面采用无滑移边界条件，使得气体和颗粒速度为零，随着径向距离离开筒体壁面，气体和颗粒气相速度迅速增大，并且达到最大值，之后，气体和颗粒切向速度逐渐降低，在筒体中心处气相和颗粒切向速度达到最小。由此可见气体和颗粒切向速度最大是位于筒体壁面区域。

图 4 表示气体和颗粒轴向速度的分布。由图可见，在筒体中心气体和颗粒轴向速度最大，之后，气体和颗粒轴向速度逐渐降低，由正值变为负值。在筒体壁面附近，气体和颗粒轴向速度达到最小（负值为最大），在筒体壁面，气体和颗粒轴向速度为零，这是由于在数值模拟计算中采用无滑移边界条件所致。气体和颗粒轴向速度为正值表明气体和颗粒沿筒体轴向向上流出。相反，当气体和颗粒轴向速度为负值表明气体和颗粒向锥体处方向流动。对颗粒相实现了

颗粒的分离。计算结果表明沿筒体径向方向，气体和颗粒切向速度分布是不对称的。

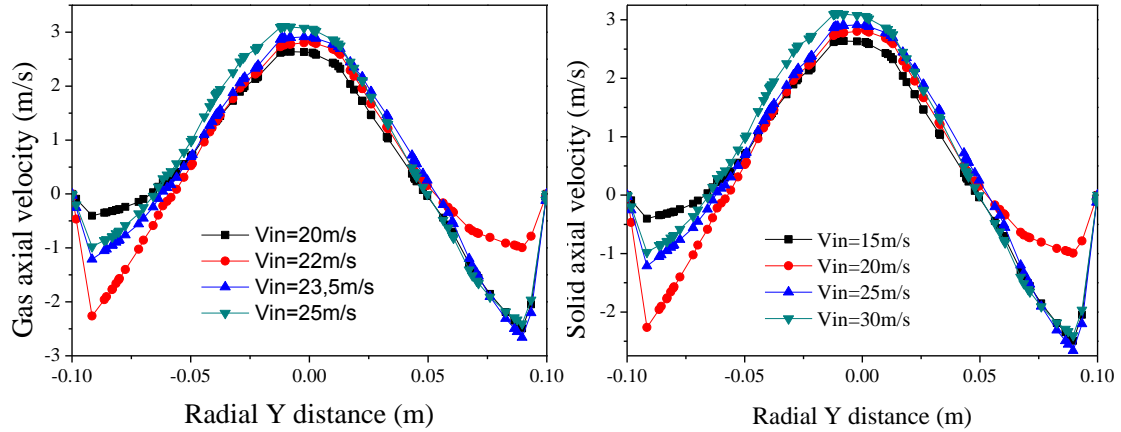


图 4 不同进口气体速度时气体和颗粒轴向速度的分布

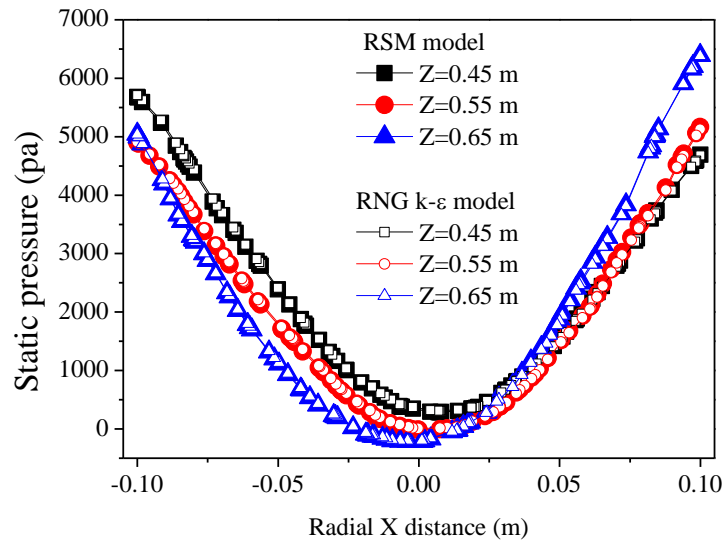


图 5 不同气体湍流模型预测气体压力径向分布

图 5 表示气体压力的径向分布。在壁面处气体压力最大，沿径向方向气体压力逐渐降低，在筒体中心区域气体压力达到最小。表明相对于筒体壁面区域的气体，在筒体中心区的气体处于低压区，气在壁面的气体向筒体中心区域流动，从而实现气体的分离。在不同高度气体压力是不同的。越往锥体出口处气体压力就越低，表明沿筒体轴向方向气体压力分布是不同的。并且沿筒体径向方向气体压力分布是不对称的。气体压力分布的非对称性导致速度分布是不

对称的。气体速度和压力的径向不对称分布将影响颗粒的流动很分离，最小气体压力并非位于筒体中心，而是偏离筒体中心。

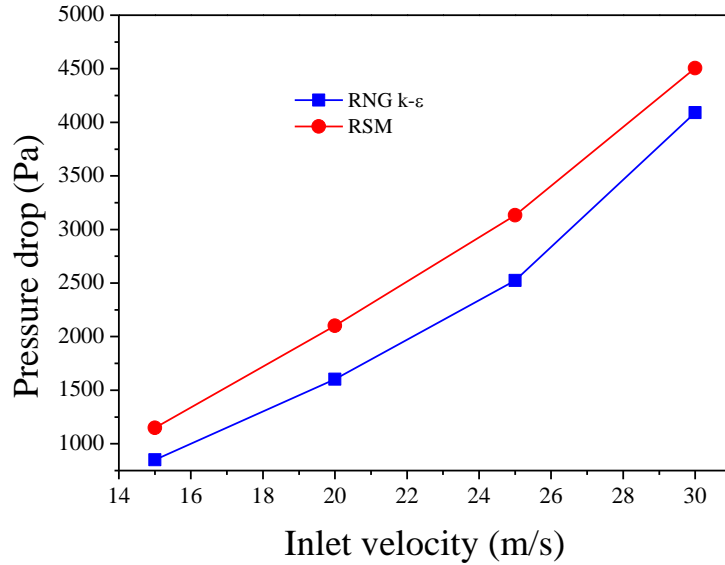


图 6 不同气体速度对分离器压降的影响

图 6 表示分离器压降随气体速度的变化。随着进口气体速度的增加，分离器压降增大。这是因为随着气体速度增加，气体和颗粒与筒体壁面的相对速度增大，形成的流动阻力或者压降就增大，因此，分离器的压降就增大。计算结果表明，采用 RNG k-ε 模型预测的压降与 RSM 预测的压降的变化趋势是一致的，但是采用 RSM 模型预测的分离器压降大于 RNG k-ε 模型预测结果，也反映出气体湍流模型影响分离器内气体和颗粒速度和浓度分布。模拟预测的分离器压降相对较大是由于进口气体速度较高的缘故。

对不同进口结构（改变进口通道收缩角）的分离器内气体和颗粒流动特性进行了数值模拟，分析进口通道收缩角对速度、浓度和气体压降的影响，表明进口通道收缩角对分离器性能有较大的影响。进口通道收缩角越大，产生的分离器就越大。

第四章：分别 RNG k-ε 模型和 RSM 模型，结合颗粒动力学模型，数值模拟方形分离器内气固两相流动过程。方形分离器的结构布置见图 7 所示。气体和颗粒混合物通过进口进入方形分离器，颗粒被离心力所分离。分离下来的颗粒通过排料口排出。气体通过底部中心管排出，故称为下排气分离器。

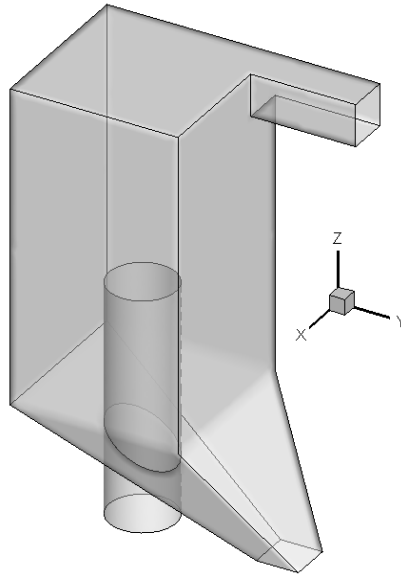


图7 方形分离器的结构布置

图8表示气体和颗粒速度矢量分布。气体进入分离器后做旋转流动，同时在底部形成气体和颗粒的漩涡流动。尽管结构是对称的，但是气体和颗粒速度场是不对称的，气体和颗粒流动的中心与方形体的几何中心是不重合的，与圆形分离器相比，方形分离器内气体和颗粒流动过程更为复杂。

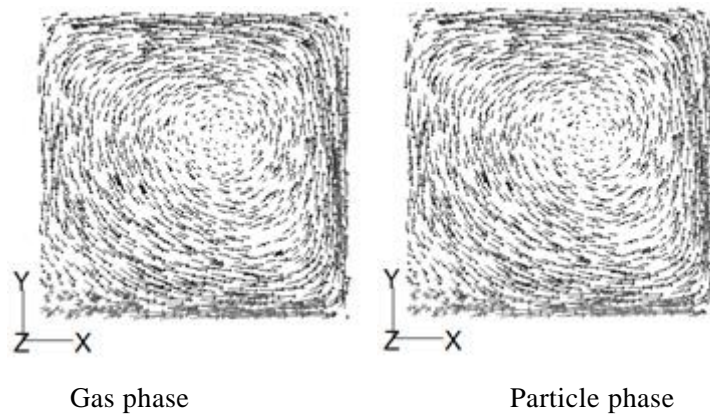


图8 气体和颗粒速度矢量分布

图9表示气体切向速度的变化。总体变化趋势是：随着进口气体速度的增加，分离器内切向速度提高。在分离器壁面处气体切向速度为零。之后，气体切向速度迅速提高，达到最大值后，切向速度开始降低，逐渐降低到最小值后，又开始增大。在分离器的中心区域，气体切向速度出现回升，可能的原因是在

分离器内部形成回流，如在方形分离器的四个角部形成涡流，导致气体速度场的变化，进而影响气体的切向速度分布。结果表明随着颗粒浓度的增加，气体切向速度分布的趋势基本不变。方形分离器中心区域的气体切向速度减小，有利于气体-颗粒的分离。

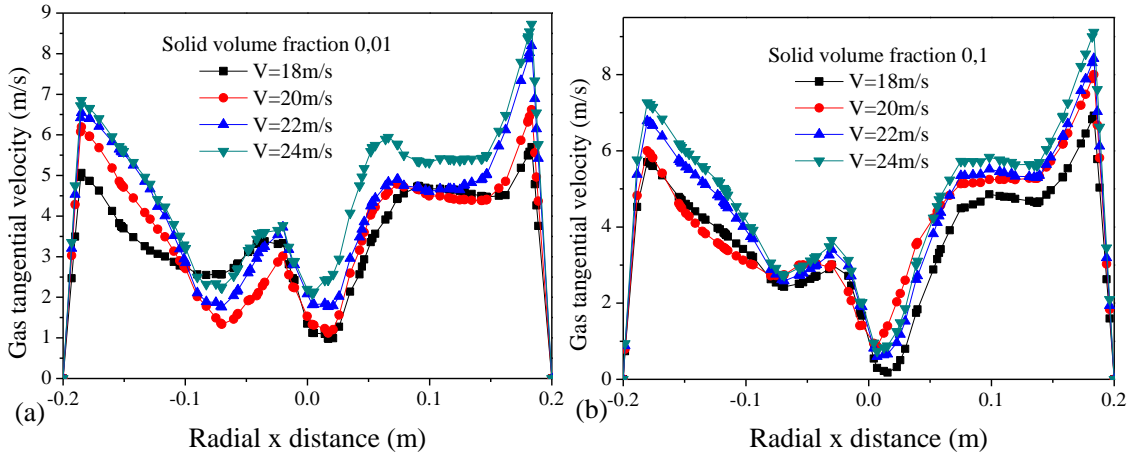


图 9 不同进口气体速度时气体切向速度的变化

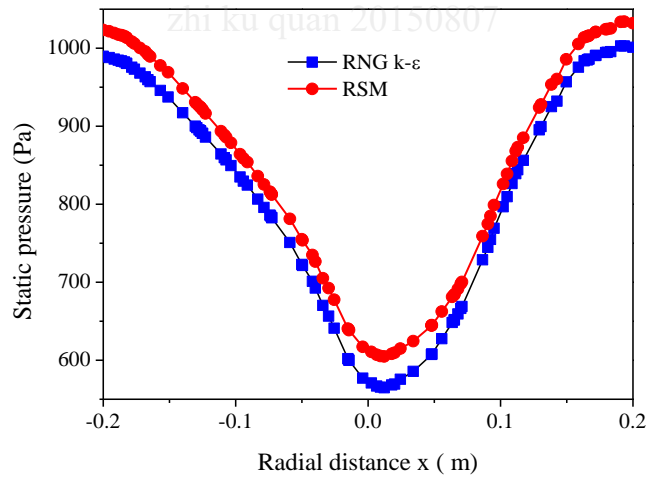


图 10 方形分离器内气体压力的变化

图 10 表示气体压力在方形分离器内变化。在方形分离器壁面区域气体压力最大。之后，气体压力逐渐降低，在方形分离器的中心区域，压力达到最小。由此可见，在方形分离器内部气体和颗粒的高速旋转，导致气体压力沿径向逐渐降低，使得气体朝中心区域流动，有利于颗粒的分离。由计算结果表明，采用 RNG  $k-\epsilon$  模型和 RSM 模型预测的气体压力变化趋势是相同的。与 RSM 模型

预测气体压力相比，RNG k- $\epsilon$  模型预测的气体压力降低。

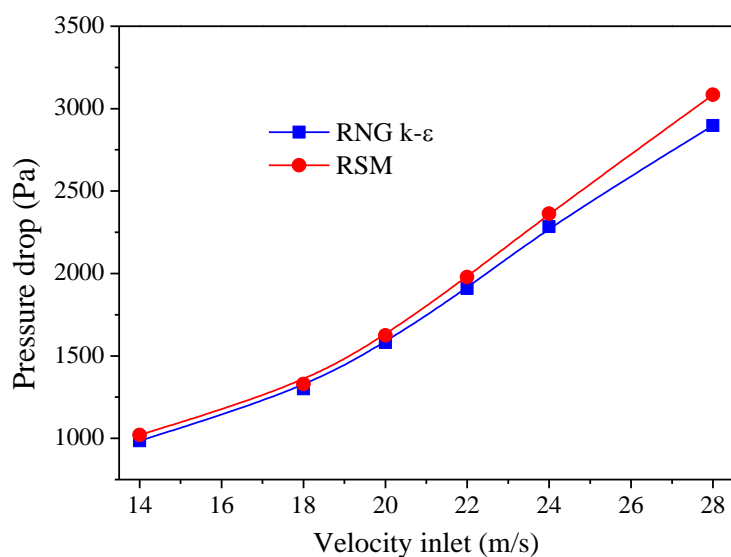


图 11 方形分离器气体压降的变化

图 11 表示方形分离器压降随进口速度的变化。随着进口气体速度的增加，气体和颗粒与壁面之间产生的流动阻力就越大，方形分离的气体压降就越大。采用 RNG k- $\epsilon$  模型和 RSM 模型预测的方形分离器压降变化趋势是相同的。与 RNG k- $\epsilon$  模型预测的方形分离器气体压降相比，RSM 模型预测的方形分离器压降相对较大，但是，两者之间预测的气体压降相差不大。

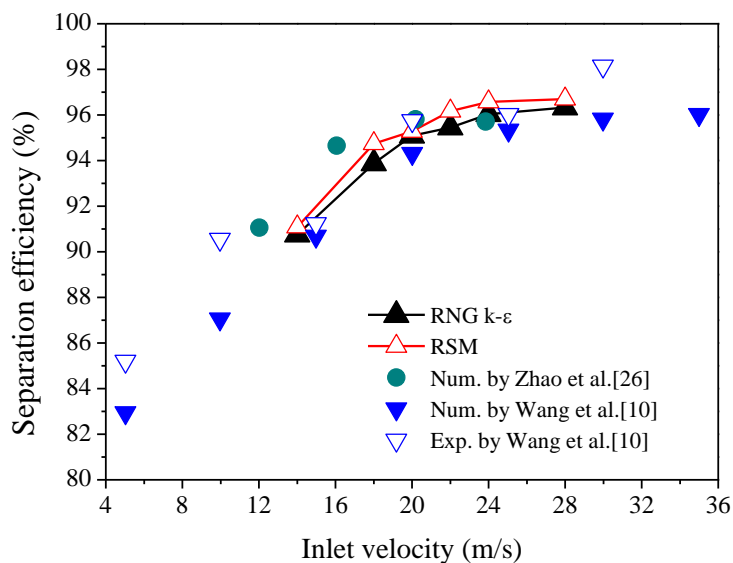


图 12 方形分离器分离效率的变化



图 12 表示方形分离器分离效率的变化趋势。随着进口速度的增加，分离效率增大。这是因为进口速度增大，提高气体和颗粒的切向速度，增大离心力，提高颗粒分离的能力，进而提高分离器分离效率。采用 RNG k- $\epsilon$  模型和 RSM 模型预测的方形分离器分离效率的变化趋势是相同的。但是，模型预测的方形分离器的分离效率是有差异的。与 RNG k- $\epsilon$  模型预测方形分离器分离效率相比，RSM 模型预测方形分离器分离效率相对较大。同时，模拟结果与他人试验结果和模拟计算结果进行了比较，表明模拟预测方形分离器的分离效率与试验测量和数值模拟结果基本吻合。

同时对不同进口结构对方形分离器性能的影响进行了数值模拟。通过改变进口通道的收缩角分析方形分离器内气体和颗粒速度和浓度以及分离器压降的影响。发现收缩角的增大，方形分离器压降增大，分离器分离效率降低。

第五章：分别 RNG k- $\epsilon$  模型和 RSM 模型，结合颗粒动力学模型，数值模拟卧式分离器内气固两相流动过程。卧式分离器的结构布置见图 13 所示，中心管插入筒体内。气体和颗粒混合物通过进口进入卧式分离器，颗粒被离心力所分离。分离下来的颗粒通过排料口排出。气体通过中心管排出。

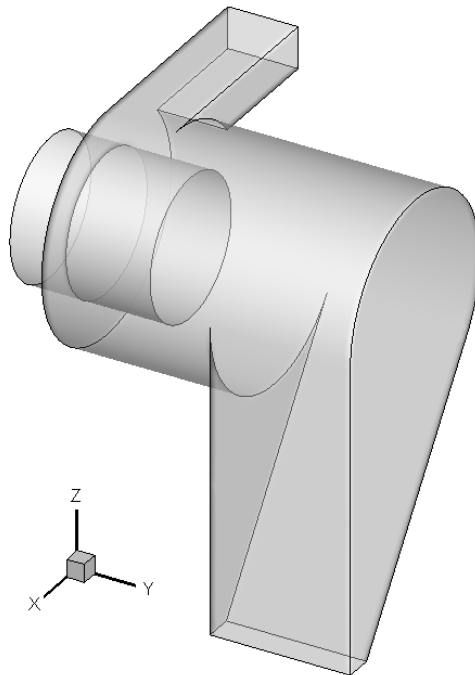


图 13 卧式分离器的结构布置



图 14 表示气体速度流线在卧式分离器内的分布。气体由进口通道切向进入分离器筒体，形成旋转运动。在入口区域，气体形成漩涡，这是由于进口气体与筒体内旋转气体相互作用和干涉作用，两股不同流动方向的气流相互作用引起碰撞，产生漩涡流动。气体进入筒体后，部分气体将通过中心管排出，使得气体速度在做旋转运动的同时，速度逐渐降低。

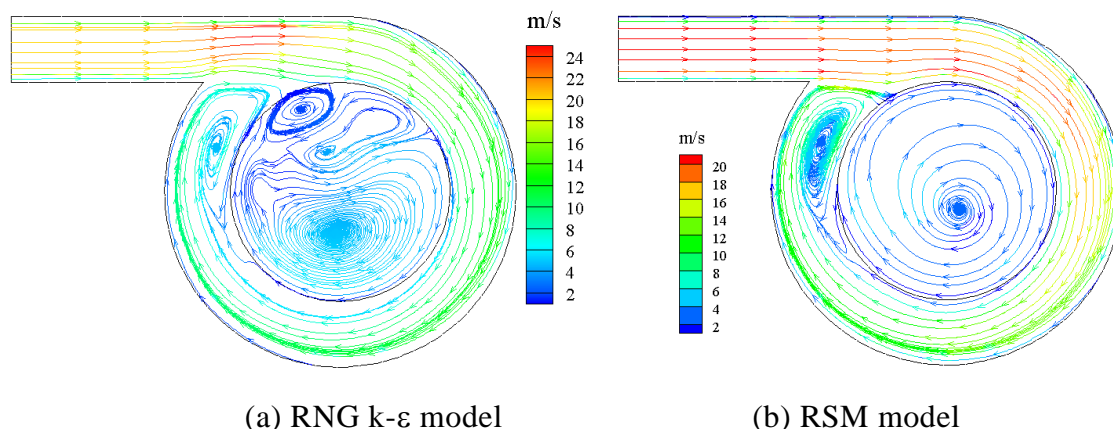


图 14 卧式分离器气体速度流线分布

数值模拟结果表明气体从分离器入口以切向方向进入卧式旋风筒后，在旋风筒体内形成强烈的旋转运动；一部分靠近旋风筒体边壁的气体通过分离隔室入口进入分离隔室，先沿侧壁向下，后沿壁面向上，再回到旋风筒体。沿旋风筒体的轴线方向，气流的旋转中心先是在旋风筒体内左上方，然后旋转中心急剧移向中心稍偏右下侧。在分离器出口，旋转中心又移向旋风筒体的几何中心。出口插入分离器后，使得静压最低处在出口的中心。在旋风筒体内，右侧静压大于左侧静压。

采用 RNG k-ε模型和 RSM 模型预测的气体流动基本相同，但是，存在一定的差异。特别在中心管气体流动，采用 RNG k-ε 模型预测到漩涡流动的出现，相反，RSM 模型预测并未出现气体漩涡流动，表明 RNG k-ε 模型和 RSM 模型对预测结果有一定的影响。

图 15 表示在筒体轴向方向 3 个不同位置处气体切向速度分布规律。在不同位置处气体切向速度分布基本相同。沿筒体径向方向，当  $x$  为负值的区域内，气体切向速度由壁面处的零速度，迅速增加，达到最大值后，再逐渐降低。而

在  $x$  为负值的区域内，切向速度减小，达到最小值（最大负值）后，逐渐增大，在壁面处切向速度为零。切向速度为正值，表明气体向上方向流动，而负值表明气体向下流动。由此可见，在筒体内气体形成旋转流动，产生离心力，有利于气固的分离。

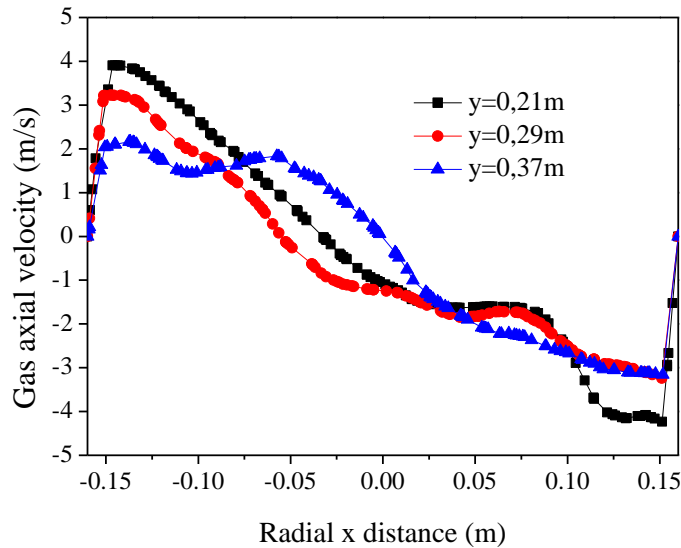


图 15 沿筒体不同位置处气体切向速度的分布规律

数值模拟给出气体压力分布表明：在筒体入口上部的压力梯度明显大于另一侧，也就是这一侧气流的旋转强度要明显大于另一侧。这有利于固体颗粒获得较大的离心力。由于出口的影响，气流在旋风筒内总体的轴向速度还是向外的。但在轴向速度的相反处，势必形成回流。

图 16 表示卧式分离器压降随进口速度的变化。计算结果表明随着进口速度的增加，卧式分离器压降增大。采用 RNG  $k-\varepsilon$  模型和 RSM 模型预测分离器压降有一定的差异。按 RNG  $k-\varepsilon$  模型预测的分离器压降大于 RSM 模型预测的分离器压降。由 RNG  $k-\varepsilon$  模型和 RSM 模型预测分离器压降均随进口速度增大而增加，压降的变化趋势是相同的。

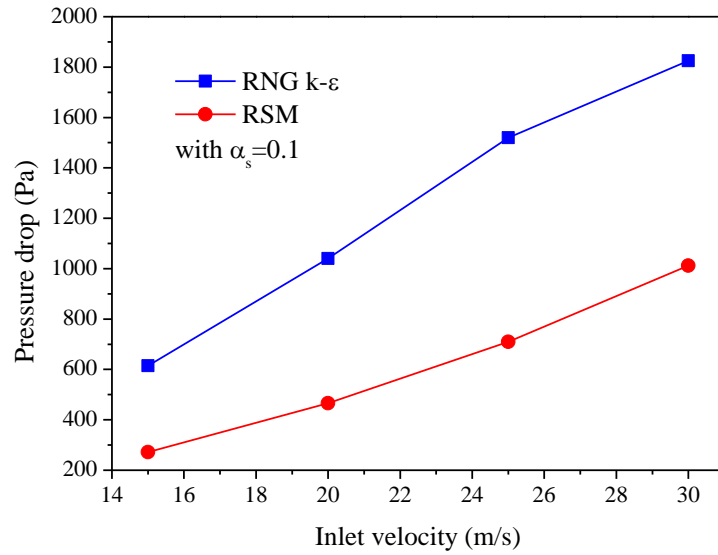


图 16 不同进口速度对卧式分离器压降的影响

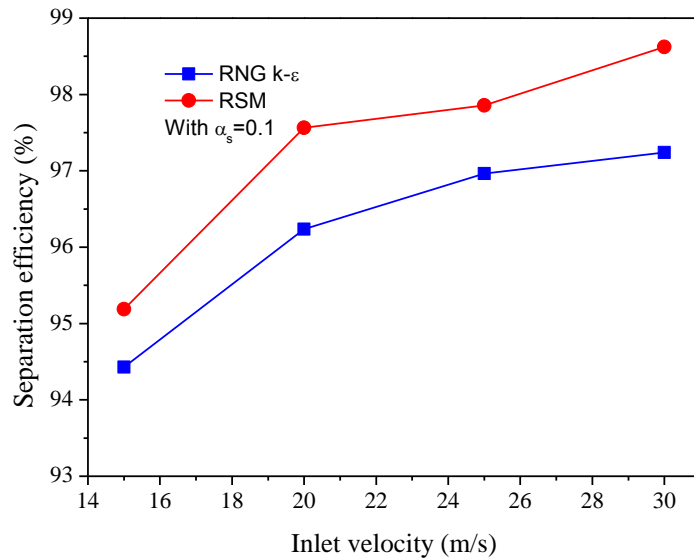


图 17 进口速度对分离器分离效率的影响

图 17 表示卧式分离器分离效率与进口速度的变化规律。计算结果表明随着进口速度的增加，卧式分离器分离效率增大。随着进口速度的增加，形成的离心力就越大，气固分离效果增强，分离效率提高。采用 RNG k-ε 模型和 RSM 模型预测分离效率有一定的差异。按 RNG k-ε 模型预测的分离效率低于 RSM 模

型预测的分离器分离效率。由 RNG  $k-\varepsilon$  模型和 RSM 模型预测分离器分离效率均随进口速度增大而增加，分离效率的变化趋势是相同的。

采用 RNG  $k-\varepsilon$ 模型和 RSM 模型，结合颗粒动理学方法，对“筒锥式”旋风分离器、方形分离器和卧式分离器内气固两相流动和分离特性进行数值模拟，分析不同因素对流动和分离效率的影响。全文总结如下：

1. 采用 RSM 模型预测分离器流场具有良好的对称性，RNG  $k-\varepsilon$ 模型的流场具有非对称特征，但两者模型预测的速度和浓度变化趋势是一致的。RSM 模型预测分离器压降和分离器效率接近于试验结果。表明对于三种不同结构的分离器，优先采用 RSM 模型预测分离器的性能。

2. 在立式“筒锥式”旋风分离器内存在内外双涡旋结构，锥顶内流场则为单涡结构。在中心管的入口区域二次流动出现了两个旋涡中心的现象。在方形分离器角部诱发漩涡，切向速度衰减明显，降低气体和颗粒旋转流动以及速度和浓度场分布。在卧式分离器筒体与颗粒收集斗连接区域，由于流动方向的改变和筒体壁面的共同作用，诱发漩涡，引起颗粒的二次携带，影响卧式分离器分离效率。

3. 卧式分离器进口的非对称性与分离器筒体本身的非对称性决定了其流场的三维性；旋风筒内的强旋运动与分离器筒体内的相对低速可有效地分离气流中的固体颗粒；旋风筒内的旋转中心轨迹并非与轴线重合，而是一条空间曲线；在分离筒体内存在着滞留与回流。旋风筒体的灰室两边相切不仅有利于颗粒的分离，而且产生的二次漩涡最小，提高分离效率和减小流动损失。灰室内漩涡过大，会影响颗粒的分离和引起二次携带。

## Chapter 1 Introduction

### 1.1 Background of the research

Multiphase flow is a fundamental physical phenomenon prevalent in nature and industrial processes, and has a very wide range of application, such as dust air in cement plants, debris flows, sandstorms flow, powder pneumatic conveying, separation and collection of coal during combustion and conversion, other applications where multiphase flow problems occur include the fluidized bed reactor in the petroleum processing industry, spray combustion, solid propellant rocket nozzle flow and materials industry[1-3]. The multiphase flows studied in this work are composed of gas and particle two phase flow.

In the industry, we often encounter the phenomenon of separation of multiphase flow. Many industrial processes, such as mineral processing, food processing, soil remediation, waste treatment, oil refining, apply the phenomenon of particle separation.

Several technologies, including fabric filters, dust collectors and cyclone separators can be used for gas-solid separation. The different separators are suitably used in many different industrial applications. Among them, cyclones play a critical role in separation of solid particles in a flowing fluid. Cyclone separators are widely used in many industrial sectors such as in the petrochemical and process industries to separate dust from gas steams or for product recovery[4-6]. The different geometrical cyclones, including horizontal cyclone and square cyclone, are used in coal combustion and solids treatment[7-9]. Their geometrical simplicity, relative economy in power, and flexibility with respect to high temperature and pressure explain their suitability in industrial application.

In the last decade, cyclones separators have been the subject of several experimental and numerical researches to improve its properties[8-14]. Also different commercial codes for simulations of separators are emerged, including FLUENT, CFX, BARACUDA, ANSYS, TRANSAT. These codes are very efficient at predicting the behavior of cyclone separators. This involves trying to treat several parameters involved by modifying the behavior of their efficacy.

However, there are numerous factors, that affect the performance of cyclones and the gas-solid two-phase flow is extremely complex and then involves many of the basic disciplines of fluid mechanics, thermodynamics, heat and mass transfer, combustion and rheology.

Until now the parameters that affect the performance of cyclone separators and under which conditions, the appropriate approach of study to most of these types of devices such as experiments, theoretical models, numerical simulation, and the possibility of using these devices in new applications are still important issues to be studied further.

Industrial development has greatly promoted the development of cyclones, and has resulted in rapid advancement in recent years. The cyclone has penetrated into many industrial sectors; gas-solid flow related to engineering design has remained mostly based on the experience level in the past. With the rapid development of computing technology and numerical simulation methods, numerical study of gas-solid flow in cyclone separators has reached a new level and has become the focus of much international academic research.

For a numerical simulation, the simulation codes have become an indispensable tool for the study of physical phenomena of very complex geometry. It requires a short time to find out some details that can be very expensive in experimental cases. There are codes widely used by the researchers and in industry.

## **1.2 State of the art of gas-solid cyclone separators**

### **1.2.1 Cyclone separators: A state of the art review**

Several investigations have been carried out in the last decade to improve the cyclone performance. Among these, Stairmand presented one of the most popular design guides which suggested that for the design of a high efficiency cyclone, the cylinder height and exit tube length be, respectively 1.5 and 0.5 times the length of the cyclone body diameter and several researches have been done in a Stairmand high efficiency cyclone[6, 15-21].

Bhattachary et al.[18] developed a systematic approach for building numerical relationships, accurate to engineering requirement, between the

geometrical and flow parameters of an industrial cyclone and the misplacements that quantify its field performance. Firstly, CFD solution using multi-phase Large Eddy Simulations of the complex flow within the cyclone is obtained, followed by Monte-Carlo simulations of particle trajectories on this baseline CFD solution under stochastically varying flow and particle parameters, to functionally relate the misplacements to these parameters and by antecedence to the cyclone geometry. This coupled CFD-Monte Carlo approach can be used to arrive at improved designs of cyclone geometry and optimal operating process parameters through numerical experimentation, leading to greater efficiency of separation and throughput.

Oshitan et al.[19] applied the dry density-segregation in a gas–solid fluidized bed to separate particulate iron ore. They founded that the density and size-segregation is dependent on the air velocity, and the density-segregation results in an iron concentration dependence on the height. Also the dry density-segregation has a potential for the upgrade of the particulate iron ore.

Safikhani, Akhavan-Behabadi, Shams, and Rahimyan [20] obtained detailed flow information by CFD simulation within three standard cyclone separators with different geometries. They discussed the effects of different geometrical parameters on pressure drop and cut-point.

Lim, Kwon and Lee[21]study the characteristics of the collection efficiency for double inlet cyclone with clean air. They conceived and deisgn a double inlet cyclone to evaluate the performance of double inlet cylone at various clean air flow rates. In their study, the collection efficiency of the double inlet cyclone was found to be 5-15% greater than that of the single inlet cyclone. Their study represents the firs trial examining the effects of clean air introduction to a cyclone and they ecvaluate.

Cyclone is a key part for the circulating fluidized bed (CFB) boiler which has great effects on the combustion efficiency, the circulation rate and the desulfurization efficiency by the circulation of the solid particles in the furnace. The traditional circular cross-section cyclone was commonly use as conventional cyclone separator for the CFB boiler. With the development of large CFB boiler, the huge body of the conventional cyclone became a major shortcoming because of the thick refractory wall that needs a long period to start the boiler.

Compared with the traditional circular cross-section cyclone, a Square cyclone has more advantages over the conventional cyclone, due to several reasons such as convenience in construction, easier membrane wall arrangement, shorter start-stop time, and easy integration into the boiler (Lim Jwon and Lee)[21]. Several experimental investigations and numerical simulation have been made to improve the square cyclone performance.

Among these, Darling[23] reports that Ahlstrom Pyropower Company developed a square water-cooled cyclone separator with upward exhaust exit for high temperature separation and applied to its compact CFB boiler design. Lu et al.[24] developed and patented a water-cooled square cyclone separator and applied it to CFB boiler design successfully in China. Su and Mao [25]investigated another type of water-cooler square cyclone separator by PDA experiment, which paces the gas exhaust at the bottom of the separator instead of at the top.

A new kind of cyclone with symmetrical spiral inlet including (SSI) direct symmetrical spiral inlet (DSSI) and converging simmterival spiral single inlet (CSSI) was developed by Zhao et al.[26], and the effects of these inlet types on cyclone performance were tested and compared. Experimental results show the overall efficiency the DSSI cyclone and CSSI is greater by 0.15-1.15% and 0.40–2.40% than that for CTSI cyclone, and the grade efficiency is greater by 2–10% and 5–20%. In addition, the pressure drop coefficient is 5.63 for DSSI cyclone, 5.67 for CSSI, and 5.55 for CTSI cyclone. Despite that the multiple inlet increases the complicity and the cost of the cyclone separators, the cyclones with SSI, especially CSSI, can yield a better collection efficiency, obviously with a minor increase in pressure drop. This presents the possibility of obtaining a better performance cyclone by means of improving its inlet geometry design.

Other authors reported the application such a separator to commercial CFB boiler[27]. A square separator with particle accelerating inlet was developed by Tsinghua University. The author recently designed and patented a cooling type of square cyclone separator with double inlets[28] and have provided some improvements of both higher separation efficiency and lower pressure drop by experiment[29]. Other authors find that the shape and structure of cyclone determine its performance.



The effect of the cylinder shape and size influence the shape of the core-annulus interface inside the cyclone was numerically studied by Lee et al.[30] which then determine the overall flow and collection characteristics. Bernado et al.[31] calculated by CFD method the effect of inlet section angles in relation to the cyclone body on the separation efficiency and found that the efficiency is improved when the inlet section angle is  $45^\circ$  compared with the normal inlet. Qian et al.[3] studied the experimental and numerical study of a prolonged cyclone with an attached vertical tube at the bottom of the dust outlet and found that the length of the vertical tube influenced the efficiency and pressure drop.

A type of square cyclone separator with downward-exhaust exit was developed and granted a Chinese patent. Its separation efficiency was shown as good as that of the traditional cyclone of circular cross-section separator and its particle cut-diameter was around  $15\text{ }\mu\text{m}$ [32]. The gas-solid suspension flow in a lab-scale square cyclone separator with downward gas-exit was measured by Su and Mao[25]. All of the above mentioned research results indicate that the square cyclone separator used in CFB boiler has high collection efficiency[34].

### **1.2.2 Description and geometry of cyclone**

Traditional cyclone separator has a circular cross section and tangential or helical inlet and has been widely studied by many authors both experimentally and numerically[22, 33-37]. Fig.1-1 shows the basic principle of cyclone separator is forcing of the particle-laden gas into a vortex, where inertia and gravitation forces effect particle separation. Among existing cyclones and diverse cyclonic equipment, there is a basic model that at once has been used by industry exhaustively: The inverse flow cyclone.

In this device, the fluid enters tangentially into the cylindrical chamber with high rotational component. The flow descends rotating near the wall, until a certain axial location where the axial velocity component reverses itself, thus making the flow to ascend. This is referred to as the vortex end position. The ascension proceeds near the cyclone axis and, since the flow rotation continues, a double vortex structure is formed, as shown in the figure. The inner vortex finally leads the flow to exit through a central duct, called the vortex finder. The vortex

finder protrudes within the cyclone body, which serves to both shield the inner vortex from the high inlet velocity and stabilize it. It also worth to mention that inversion leading to this peculiar flow structure is apparently originated to the pressure field inside the cyclone, and not directly influenced by the conical shape or the geometrical length.

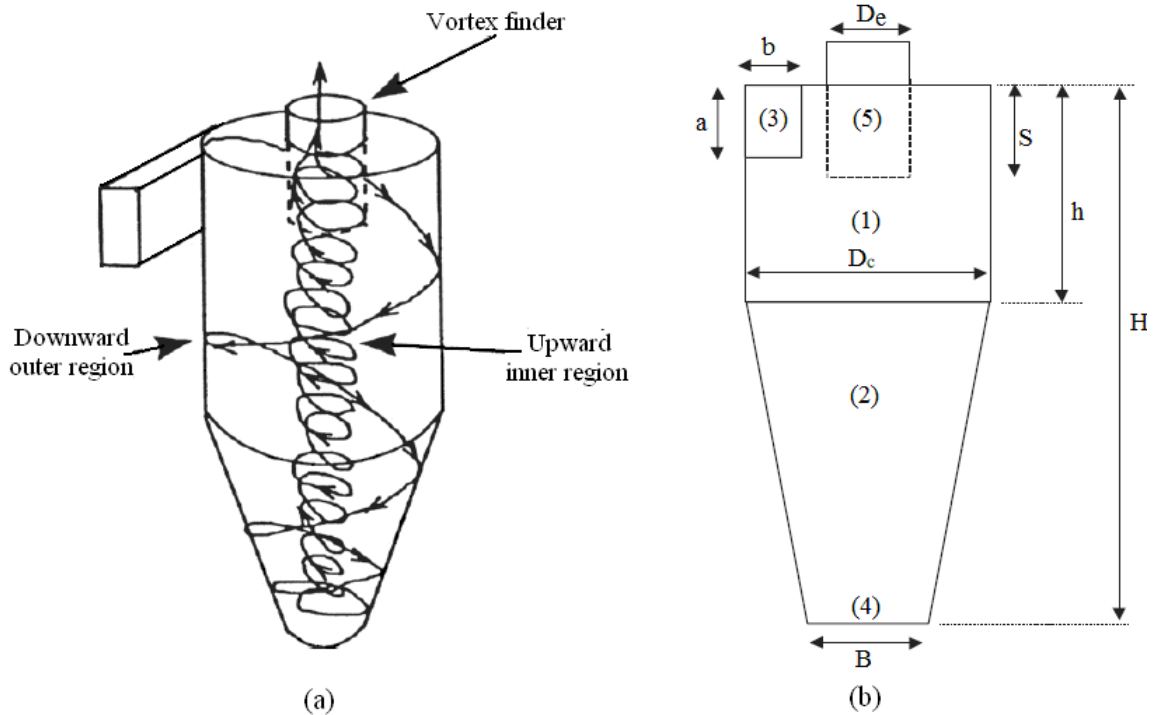


Fig.1-1: (a) Qualitative drawing of the principle of operation and flow patterns in cyclone. (b) Main parts and dimensions of an inverse-flow cyclone: (1) cyclone body, (2) conical part, (3) inlet duct, (4) exit duct, (5) vortex finder[36, 37]

In the gas-solid separation in cyclone, the solid particles, denser than the gas, are subjected to a high centrifugal force, which directs them to the walls, where they collide, lose momentum and become disengaged from the flow[36, 37]. The solids thus separated descend sliding on the conical wall and are collected or extracted at the lower part. This mechanism obviously suffers from a number of imperfections: small particles that follow the gas, particles that rebound and are re-entrained and direct re-entrainment or by-pass at lowest conical section, near the inversion zone, at the vortex finder lip, and all along the inner/outer vortex boundary. All these factors add up to the variables that affect the centrifugal force (mainly geometry and inlet velocity), to make the collection efficiency of cyclone highly variable.

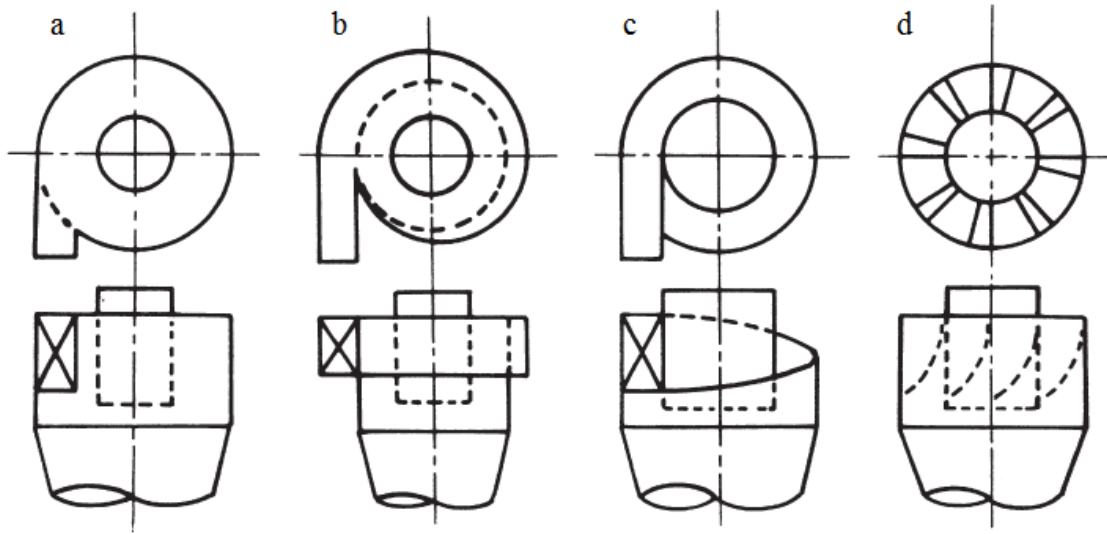


Fig.1-2 Main inlet arrangements: (a) tangential, (b) scroll, (c) helicoidal, (d) axial[40]

Table 1-1 Relevant geometric dimensions of several standard cyclone designs[42]

Name/type	Dc	De	S	H	h	a	b	B
Muschelknautz E	680	170	311	934	173	173	58	228
Muschelknautz D	357	119	318	863	262	187	54	195
Storch 4	260	117	176	1616	909	260	38	91
Storch 3	192	107	200	821	462	167	60	92
Storch 2	225	108	239	1097	464	188	53	84
Storch 1	365	123	142	1943	548	100	100	64
Tengbergen C	337	112	145	930	187	100	100	112
Tengbergen B	210	112	224	604	324	179	56	112
Tengbergen A	277	112	157	647	180	135	74	202
TSN-11	348	136	242	959	219	184	54	154
TSN-15	266	158	350	1124	589	166	60	119
Stairmand high efficiency	316	158	158	1265	474	158	63	119
Stairmand high flow	190	141	165	755	283	141	71	71
Van Tongeren AC	325	100	325	1231	436	149	67	130
Vibco	286	11	124	720	228	111	90	66
Lapple GP	283	141	177	1131	566	141	71	71

Actually, the centrifugal force (or any other parameter of the gas dynamics) can only explain the separation of solids in dilute flows. It is well known that above a certain solids loading, particles are collected as soon as they enter in the device, forming dust strands that descend helicoidally along the walls. The centrifugal force only acts upon the remaining dust, usually a small fraction of the total solids mass flux[38-40].

There are several systems to insert the flow into the cyclone with a high tangential velocity component; some inlet designs are shown in Fig.1-2. Most frequent are the tangential and the scroll configurations. The scroll inlet is usually designed to wrap around up to  $180^\circ$  of the cylindrical cross-section.

Higher arcs are not used, because they are ineffective and unnecessarily increase pressure drop[43], although shorter ones are not unusual. Depending on their use and particular properties of the dusts, many different cyclone designs have been developed over the years. As an example, Table 1-1 shows sixteen different designs of the same inlet area ( $0.01\text{m}^2$ ) performing the same duty at given inlet velocity, as compiled in the monograph by Hoffmann and Stein[42].

### 1.2.3 Performance characteristics of cyclone separators

From an engineering point of view, cyclone performance is measured by collection efficiency (the fraction of solids separated) and pressure drop. Those two parameters are the direct outcome of the development inside the device, in turn described by the velocity, solids concentration and pressure fields. Given the wide range of solids loadings that cyclones are suitable to handle, the flow is generically biphasic; interaction between particles and two-way coupling can only be neglected for low concentrations of solids. In spite of this, traditional cyclone models proceeded from clean-gas velocity measurements, through explanation and correlation of the observed profiles, to arrive at relatively simple formulations of measured efficiency and pressure drop.

A large amount of literature is available describing various theories related to cyclone separator. Numerous scientists explore various methods in order to describe theories of particle collection in cyclone separators, but it is generally agreed that separator efficiency and pressure drop are the two main performance characteristics of a cyclone separator.

The separation efficiency  $\{\eta\}$  is the ratio of the mass fraction of solid particles separated at the bottom of the cyclone and the total fraction of particle

has its entrance. Its complement, based on the particle mass fraction at the outlet, can also be used. This approach allows evaluation of separation efficiency based on the overall mass flow[42]

$$\eta = \frac{m_c}{m_f} = 1 - \frac{m_e}{m_f} = \frac{m_c}{m_c + m_e} \quad (1-1)$$

where  $m_c$  and  $m_e$  are the masses of the lost and collected particles fraction respectively, and where  $m_f = m_c + m_e$ , the mass balance for particles over the cyclone.

A more significant parameter is the partial separation efficiency. It can detect the contribution of each particle group of different sizes. The global separation efficiency here is the cumulative distribution function of the partial efficiencies. It allows assigning a probability of particles separation according to their sizes, by defining a cutoff diameter  $d_{50}$  as the particle size assigns equal probabilities to be separated or carried by the fluid stream, we can judge the separation efficiency of cyclone. Cyclones assigns diameters smaller cutoff are considered more effective.

The pressure drop is one of the two important parameters in the cyclone separator. Many researchers[43-49] have developed different procedures to estimate the pressure drop of cyclone. Most of the procedures, however, are empirical and suitable only for pure gases, low solids mass and not very satisfactory in generality applications. Additionally, the pressure drop of a cyclone under the condition of dust-laden gases or high temperature gases is of importance, and it is much different from that under the condition of normal and pure gases.

Briggs[50] found that the pressure drop decreases with an increase of the dust loading. Muschelknautz et al.[48], Yuu et al.[51], Hoffmann et al.[52] and Luo et al.[55], not only verified Briggs' findings but also discovered other interesting phenomena from experiments. For example, Muschelknautz et al.[48] and Luo et al.[53] found that pressure drops with the rise of the dust loading until one turning point is reached at which the pressure begins to increase. For the determination of the pressure drop of cyclones working at elevated temperature, only very little experimental data have been reported, which are insufficient for a correct evaluation of the temperature effect on the pressure drop. Bohnet et al.[54]

that either the pressure drop or drag coefficient decrease with an increase of gas temperature. Xu et al.[55] and Chen et al.[56] also confirmed such an observation.

Generally, the pressure drop over a cyclone is the difference of static pressure between the inlet and outlet, which can be written as:

$$\Delta P = P_{si} - P_{so} \quad (1-2)$$

The static pressure at inlet cross-section is uniformly distributed because there is no swirling motion. It can be easily measured with a pressure tapping in the wall. However, the static pressure at the outlet wall is quite different from its cross-sectional average due to the strong swirling flow. The dynamic pressure stored in the swirling motion can be significant. The determination of static pressure downstream of cyclone, hence pressure drop, becomes more complicated and difficult. In the past, this problem has been approached in several ways. Stairmand[46] presumably measured the static pressure at the outlet wall immediately downstream of cyclone as he ignored the influence of swirl. Shepherd and Lapple[43] discharged the gas directly from the cyclone to atmosphere (taking the downstream pressure as the ambient pressure). Meissner and Löffler[57] measured the static pressure after a flow rectifier. Hoffmann et al.[52] observed that the static pressure at outlet wall is close to the static pressure that would be measured after an ideal rectifier. Therefore, the static pressure at the wall of the outlet tube minus the static pressure at the inlet gives the true dissipation loss or the pressure drop of a cyclone. The latter three methods have been widely used in research and engineering practices. In addition, the pressure drop in this study is defined as Eq. (1-2) and taken in way similar to that of Meissner and Löffler[57].

#### 1.2.4 Parameters affecting the performance of cyclone

Various factors are observed to affect the cyclone performance and have been reported in many articles. The geometry, flow regime and fluids properties are three groups of parameters that affect the performance of cyclone separator.

The effect of cyclone inlet dimensions on the flow pattern and performance have been numerical investigated by Khairy Elsayed and Chris Lacor[96] using

the RSM for five cyclone separators studied. The results show that, the maximum tangential velocity in the cyclone decreases with increasing the cyclone inlet dimensions. No acceleration occurs in the cyclone space, the maximum tangential velocity is nearly constant throughout the cyclone. Increasing the cyclone inlet dimensions decreases the pressure drop. The cyclone cut-off diameter increases with increasing cyclone inlet dimension (consequently, the cyclone overall efficiency decreases due to weakness of the vortex strength). They reported that the effect of changing the inlet width is more significant than the inlet height especially for the cut-off diameter. The optimum ratio of inlet width to inlet height  $b/a$  is from 0.5 to 0.7.

Zhao et al.[58] have numerically investigated the effect of cyclone inlet on the performance of cyclone separator. They compared the performance of two types of cyclone with the conventional single inlet and spiral double inlets using Reynolds stress turbulent model. The results show that the new type cyclone separator using adding spiral double inlets can improve the symmetry of gas flow and enhance the particle separation efficiency. While their finding is for double inlets cyclone, but it support the importance of the effect of inlet section dimensions on the performance of cyclone.

The significant effects of the cyclone inlet dimensions on the cyclone performance have been acknowledged by researchers[59]. For two inlets cyclone separators, Zhao et al.[58] reported the possibility of increasing the cyclone efficiency without significantly increasing the pressure drop by improving the inlet geometry of cyclone. Many researchers have tested the effect of inlet section angles Qian and Zhang[60] computationally investigated the effect of the inlet section angles. The pressure drop of the cyclone decrease to 30% lower value than that for conventional cyclone, if the inlet section angle becomes  $45^\circ$ . However, Qian and Wu[61] reported only 15% reduction in the pressure drop for  $45^\circ$ . Moreover, researchers have carried out many investigations on the effect of cylinder height and diameter, the cone opening size, the exhaust diameter, length, insert depth, offset and turbulence intensity and boundary layer on the separation performance.

An account of some important factors presented by Schnell and Brown[62] is presented here. Inlet velocity is prime factor affecting the pressure drop and

the cyclone efficiency. Efficiency increases with increase in velocity as centrifugal force increases but this also increases the pressure drop, which is not favorable. With decrease in viscosity, efficiency increases. This is due to reduction in drag force with reducing in viscosity. Decrease in temperature will increase the gas density. One may be tempted to conclude that this will increase efficiency as viscosity decreases. However, increase in temperature also decreases the volumetric flow rate and thereby decreasing efficiency.

Another important factor affecting the efficiency is particle loading or concentration of particle. The collection efficiency and pressure drop are strongly influence by inlet particle concentration. Guangcai et al.[63] found that there was a small increase of collection efficiency with increasing particle concentration. Sujeet Kumar Shukla et al.[64] correlated data from several literatures and reported an increase in collection efficiency with particle concentration increasing in the range of 2.3 to 228.8g/m<sup>3</sup>. With using optical counting technique to measure particle size on-line, Mothes and L öffer[65] found that the grade efficiency curve remained essentially unchanged at varying particle concentrations even though the overall efficiency increased[66].

### **1.3 Gas-solid two-phase flow modeling: A state of the art review**

Particulate solids are separated from gas streams for a variety of reasons. In some instances, the interest is in the recovery of solids as a product, e.g., following a milling operation for which a combined classification and separation is often required[67]. In other cases, the emission of fine particulate solids and dust from a unit operation may be excessive and, therefore, a reduction and control of particulate level is required for the protection of subsequent process equipment or for the environmental emission[68-69]. Typical particulate effluent from a pilot-scale fluidized bed combustor is shown, together with upper limits of allowable emission to atmosphere, and of the inlet dust tolerance of high performance gas turbines, Funk et al.[70]. An overview of the principles of gas-solids separation is given many literature reviews.



### 1.3.1 Turbulence model

For the turbulence flow in cyclones, the key to success of Computational Fluid Dynamic lies with the accurate description of the turbulent behavior of the flow[27]. To model the swirling turbulent flow in a cyclone separator, there are number of turbulence models available in Fluent. These range from the standard k- $\epsilon$  model to more complicated Reynolds stress turbulence model (RSM). Also large eddy simulation (LES) methodology is available as an alternative to the Reynolds average Navier-Stokes approach.

Many researchers have investigated selection of a suitable turbulence model for the highly swirling flows. The standard k- $\epsilon$ , renormalization group k-epsilon (RNG k- $\epsilon$ ) and Realizable k- $\epsilon$  models were not optimized for strongly swirling flows found in cyclone separators[71, 72]. Both the standard k- $\epsilon$  and RNG k- $\epsilon$  turbulence model give unrealistic distribution for the axial velocity profiles (upward flow close to the wall)[33, 34], only the RSM is capable of predicting the combined vortex in accordance with the experimental data. The successful application of the RSM turbulence model for different studies in cyclone separators has been reported by many researchers and has been reported in many articles[8, 14, 58, 71, 73-75].

The RSM requires the solution of transport equations for each of the Reynolds stress components. It yields an accurate prediction on the swirl flow pattern, axial and tangential velocity; cut-off diameter and pressure drop in cyclone simulations[30, 35, 76-77].

### 1.3.2 Gas-solid two phase flow model

Dispersed two-phase flows can be classified according to the importance of interaction mechanism[78, 79]. Fig. 1-3 shows an elementary and practical sketch. Generally, two different regimes are distinguished, depending on the existence of mutual, significant interaction between particles: dilute and dense two-phase flow.

The approximate borderline is a volume fraction  $\alpha_s \approx 10^{-3}$ , which translates generically as an inter-particle spacing  $L/d_s \approx 8$ . Within the dilute regime, all the influence of particles on the gas can be neglected for  $\alpha_s < 10^{-6}$  ( $L/d_s > 80$ ), which

is known as “one-way coupling”; for higher volume fraction, it needs to be accounted for (“two way coupling”). Aside from obvious issues of volume and continuity, the generic flow feature most affected is turbulence. In the dense regime  $\alpha_s > 10^{-3}$ ,  $L/d_s < 8$ , inter-particles become of importance, both physical collisions and indirect influence through the nearby flow field. The collisions can lead to coalescence and break-up, which must be considered too. This regime is called “four-way coupling”.

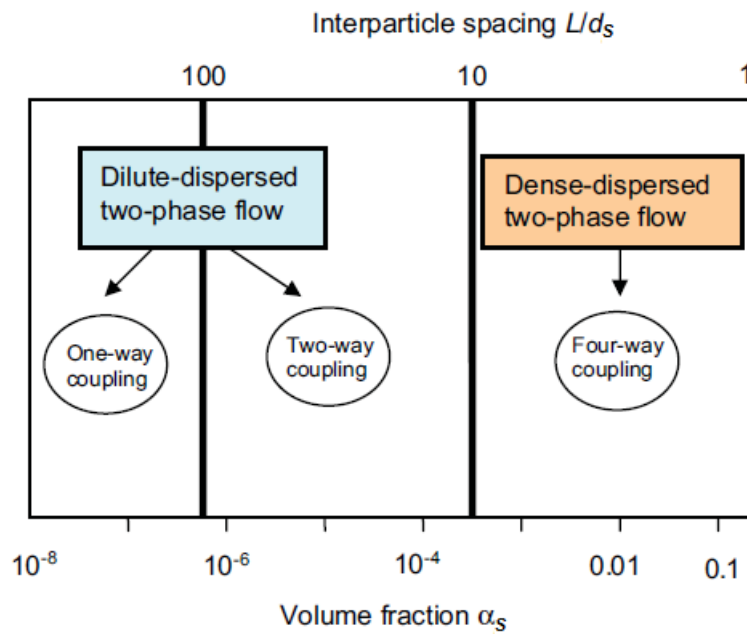


Fig.1-3. Regimes of dispersed two-phase flow as function of the particle volume fraction/inter-particle spacing[81]

Within this framework, numerical models have developed in two parallel paths according to the manner in which the dispersed phase is treated, either by a Lagrangian or by an equivalent Eulerian formulation. In the Lagrangian model, particle trajectories are obtained by integrating the particle equation of motion. In the Eulerian approach, conservation equations are written for the mass, momentum and energy of the particle cloud as a continuum, and integrated to predict volume averaged properties thorough the field.

The suitable choice is often problem-specific, generally speaking, Lagrangian methods are more suited to dilute flows, free of numerical diffusion, less influenced by other errors and more stable for large particle velocity

gradients. Also, the treatment of realistic poly-dispersed particle systems is straightforward. However, for highly loaded flows, limitations related to computer storage, calculation times and convergence arise[80]. In those cases, the Eulerian approach becomes more adequate. It seems also the right framework for modeling particles' mutual interaction[81], although Lagrangian methods have been also applied[79, 82]. Additionally in practice, there are a large amount of particles dispersed in fluid that makes the computational cost for Lagrangian approach extremely expensive. As a result, the Lagrangian approach is limited to only dilute flow typically having particle volume fraction less than 0.01%. The Eulerian approach, which is the model that employ in our simulation, treats the solid phase as a continuous medium where appropriate descriptions for the average solid phase stress are obtained by employing the kinetic theory of granular flow (KTGF).

### **1.3.3 Kinetic theory of granular flow**

Kinetic theory of granular flow has been developed by many authors in last decade[83, 84]. Lun et al.[85] has had some success in describing the momentum and kinetic energy transferred by velocity fluctuation of the particles in the grain inertia regime. In the work of Lun et al. [85], the effect of the interstitial fluid was neglected in deriving the constitutive theory for the solid phase stress and the solid turbulent energy flux from the Maxwell transport equation. Hence, the theory is more appropriately referred to as the kinetic theory of dry granular flow. In their later work, Safikhani [86] included the interstitial fluid effect into the existing kinetic theory of rapid granular flow. Their model introduced a lubrication approximation for modeling interparticle collisions in the presence of an interstitial fluid. The model took into account additional stresses exerted by the fluid on the particle through long-range potential interactions by means of fluid fluctuations.

Liu et al.[87] incorporated the kinetic theory of dry granular flow into a two-fluid model of a laminar gas-particle flow in which they assumed that the random motion of the particles in a fluid-particle system resembled the one predicted for the dry granular flow. Chen et al.[88] were the first to incorporate both the kinetic of dry granular flow and the gas turbulence into the two-fluid

model. The effect of the gas turbulence on the particle fluctuating velocity and the effect of the particle on turbulence modulation of the gas phase were considered in their work. Both are crucial in accurately predicting dilute fluid-particle flow, but are less important in dense fluid-particle flow[89]. A one-equation turbulence model is used to describe the gas turbulence. Chu et al.[90] extended the work of Safikhani et al.[86] and described the gas turbulence as two-equation low Reynolds number  $k$ - $\varepsilon$  turbulence model. The Chu et al.[90] model was originally validated with data[91] for 200  $\mu\text{m}$  polystyrene particles and later validated with the data[92] for 70 and 200  $\mu\text{m}$  glass bead particles. Very good agreement exists between measurements and model predictions for both gas and particle mean velocities. However, Karagoz[92] showed that the model predictions of Chu et al.[90] for 70  $\mu\text{m}$  result in the particle fluctuating velocities that were larger than experimental measurements. Karagoz[92] reasoned that an additional loss of the particle fluctuating kinetic energy due to the lubrication force exerted by the fluid on the particle was significant for smaller particles.

## **1.4 The objectives of this research**

The present contribution aims to add more to existing knowledge on the functioning of cyclones which represents one of the most recent applications in coal fluidized bed combustors.

The fast rate of development of CFD techniques in the past decade has made it possible to conduct detailed simulations of multiphase systems, as reviewed by Arastoopour[93], CFD has been used extensively to study the flow behavior of several multiphase systems. For example, Benyahia et al.[94] and Sun and Gidaspow[95] successfully used CFD codes to predict the flow patterns of the riser. There are several approaches to numerical modeling of multiphase flows, including Eulerian and Lagrangian approaches, which have been reviewed by Sinclair[96]. In the Eulerian or two-fluid model approach, which is used in this study, constitutive relations (closures) are expressed for each phase based on different theories.

This research aims to gain a better understanding of the hydrodynamic characteristics of dense gas-solid two-phase flows in various types of cyclone separators. This thesis consists of five relatively detailed chapters, in which

different topics of engineering interest are considered. A global view of the topics covered is given in the table of contents. Below are a few notes, meant for orientation, about the structure of this thesis.

(1) This first chapter introduces a gas-solid two phase flows state of the art review. A description of the geometry and performance of cyclone separator is presented.

(2) The second chapter describes numerical modeling. Chapter 2 provides a general overview of the two-fluid model employed in the present work. Both the Eulerian approach and Lagrangian approach are discussed and their basic equations for the particle and gas phases as well as their numerical treatment and also the turbulent modeling (RNG k- $\epsilon$  and RSM) are presented in this Chapter.

(3) In the third chapter we analyze gas-solid separation in conventional cylindrical cyclone separators and the modify inlet configuration. The effect of solid inlet concentration and cyclone inlet geometry are also discussed.

(4) The fourth chapter investigates gas-solid separation in a different geometry of square cyclone. In this part, we numerically simulate the separation efficiency and pressure drop by CFD and discuss the effect on geometry of the hydrodynamics of gas solid cyclone separators.

(5) The thesis is concluded in chapter five with separation and pressure drop in horizontal cyclone separator development of cyclone separator. Horizontal cyclone separators are studied and the effect of turbulent model and solid volume fraction are presented in this case.

## Chapter 2 Description of numerical model

### 2.1 Introduction

Numerical modeling has an important factor for investigating gas-solid two phases flow in cyclone separator, and have been investigated in last decade. Additional details can be seen in the literature[97-109]. This chapter discusses the numerical model of gas-solid two phase, the various approaches to modeling these gas-solid two-phase flows in cyclone separator are then presented. Basically governing equation for gas phase and two basic approaches to modeling gas phase as RNG k- $\epsilon$  model and RSM model are discussed in first section of this chapter. Modeling of solid phases is discussed in more detail because of their importance in separation cyclone in second section. According to solid property some comments are made to guide the selection of an appropriate modeling approach. Two approaches, Euler-Lagrange approach and Euler-Euler approach to predict solid-phase flow, Euler-Euler approaches are discussed and their basic equations for the particles phases as well as their numerical treatment are presented.

### 2.2 Turbulence modeling for the fluid phase

There is a large body of literature on CFD modeling of cyclone separators and many of these studies have used the LDA experiments of Hsieh[98] to validate the modelling. Most recent studies suggest that the turbulence in hydrocyclones is too anisotropic to treat with a k- $\epsilon$  model and at least a differential Reynolds stress turbulence model (DRSM) such as the Launder et al. model[99] is needed to give reasonable velocity predictions (Cullivan et al.[100]; Suasnabar[101]; Slack et al.[77]). However, Suasnabar [101] was able to calibrate the k- $\epsilon$  model to obtain correct velocity predictions in simulations of Hsieh's cyclone. Recent CFD Studies by Delgadillo et al.[102] of Hsieh's 75 mm cyclone however have shown that the Launder et al. DRSM still under-predicts the tangential velocities used in conjunction with the VOF[103] to resolve the air-core. Brennan[104] also found that the Launder et al.[99] DRSM under-predicted the tangential velocities in a CFD study of Hsieh's cyclone used in conjunction with either the VOF or the mixture

model[105], to resolve the air-core. Brennan[104] found that the DRSM velocity predictions using either the Launder et al.[99] linear pressure strain model or the quadratic pressure strain model[106] were essentially the same, but the DRSM predictions using the Launder et al.[99] linear pressure strain model could be improved by increasing the fast pressure strain constant from the default value of 0.6–0.9. Recent advances in computational power have made LES practical for some engineering problems and LES has been applied to model cyclone separators. Slack et al.[77] modeled single phase gas cyclones using LES and found good predictions of the velocities although the LES needed a grid of about 600.000 nodes compared to only 240.000 nodes for a DRSM simulation. Both Delgadillo et al.[102] and Brennan[104] modeled Hsieh's 75 mm cyclone using LES in conjunction with the VOF model for the air-core in the studies referred to above and found that the LES/VOF gave very good velocity predictions. In particular Delgadillo and Rajamani found that the LES/VOF combinations gave the best predictions of the air-core shape.

### 2.2.1 RNG k-ε model

The RNG k-ε turbulence model is derived from the instantaneous Navier-Stokes equations, using mathematical technique called “renormalization group” (RNG) methods. It presents several advantages that make it possible to use the model in cases generally unsuitable to standard k-ε model as the rotational flow and the confined flow. The dissipation rate ε equation contains an additional term improving the accuracy solution for rapid strain flows. It considers the effect of rotation through a turbulent viscosity changes. The turbulent Prandtl numbers are no longer constant but are calculated by analytical formulas. See Choudhury[110] for a more comprehensive description of RNG theory and its application to turbulence. The transport equations for the RNG k-ε Model are given by:

Turbulent kinetic energy equation

$$\frac{\partial}{\partial t}(\alpha_g \rho_g k) + \nabla(\alpha_g \rho_g k \mathbf{u}_g) = \nabla(\alpha_g \mu_{eff} \nabla k) + \alpha_g G_k - \alpha_g \rho_g \varepsilon \quad (2-1)$$

Turbulent dissipation equation

$$\frac{\partial}{\partial t}(\alpha_g \rho_g \varepsilon) + \nabla(\alpha_g \rho_g \varepsilon \mathbf{u}_g) = \nabla(\alpha_g \mu_{eff} \nabla \varepsilon) + \alpha_g \frac{\varepsilon}{k} [C_{1\varepsilon} G_k - C_{2\varepsilon}^* \rho \varepsilon] \quad (2-2)$$

where  $C_{2\varepsilon}^*$  is given by:

$$C_{2\varepsilon}^* \equiv C_{2\varepsilon} + \frac{C_\mu \eta^3 (1 - \eta/\eta_0)}{1 + \beta \eta^3} \quad (2-3)$$

The model constant were assumed to have the following values,

$$\beta = 0.012, \eta_0 = 4.38, C_{1\varepsilon} = 1.42, C_{2\varepsilon} = 1.68, C_\mu = 0.0845$$

The effective viscosity is calculated through the following equation:

$$d \left( \frac{\rho^2 k}{\sqrt{\varepsilon \mu}} \right) = 1.72 \frac{\hat{v}}{\sqrt{\hat{v} - 1 + C_v}} d\hat{v} \quad (2-4)$$

$$\hat{v} = \frac{\mu_{eff}}{\mu} \quad (2-5)$$

$$C_v \approx 100$$

The turbulent viscosity  $\mu_t$  is characterizes the intensity of energy dissipations by:

$$\mu_t = \rho C_\mu \frac{k^2}{\varepsilon} \quad (2-6)$$

$$\eta = S \frac{k}{\varepsilon} \quad (2-7)$$

S is the strain rate.

### 2.2.2 Reynolds Stress Model

The Reynolds Stress model (RSM) is higher level turbulence model. It is usually called a second order closure. This modeling approach was proposed by Launder et al.[99]. In RSM, the eddy viscosity approach has been discarded and the Reynolds stresses are directly computed. The exact Reynolds stress transport equation accounts for the directional effects of the Reynolds stress tensor components.

The Reynolds stress model involves calculation of the individual Reynolds stresses,  $\overline{u_i u_j}$  using differential transport equations. The individual Reynolds stresses are then used to obtain the closure of Reynolds-average momentum equation.

The exact transport equations for the transport for the Reynolds stresses,  $\overline{\rho u_i u_j}$ ,



may be written as follows:

$$\begin{aligned}
& \frac{\partial}{\partial t} (\alpha_g \rho_g \overline{u_i u_j}) + \underbrace{\frac{\partial}{\partial x_k} (\alpha_g \rho_g \overline{u_k u_i u_j})}_{C_{ij}} = - \underbrace{\frac{\partial}{\partial x_k} [\rho_g \overline{u_i u_j u_k} + p (\delta_{kj} \overline{u_i} + \delta_{ik} \overline{u_j})]}_{D_{T,ij}} \\
& + \underbrace{\frac{\partial}{\partial x_k} \left[ \mu \frac{\partial}{\partial x_k} (\overline{u_i u_j}) \right]}_{D_{L,ij}} - \underbrace{\rho_g \left( \overline{u_i u_k} \frac{\partial \overline{u_j}}{\partial x_k} + \overline{u_j u_k} \frac{\partial \overline{u_i}}{\partial x_k} \right)}_{P_{ij}} - \underbrace{\rho_g \beta (g_i \overline{u_j \theta} + g_j \overline{u_k \theta})}_{G_{ij}} \\
& + \underbrace{p \left( \frac{\partial \overline{u_i}}{\partial x_j} + \frac{\partial \overline{u_j}}{\partial x_i} \right)}_{\Phi_{ij}} - \underbrace{2 \mu \frac{\partial \overline{u_i}}{\partial x_k} \frac{\partial \overline{u_j}}{\partial x_k}}_{\varepsilon_{ij}} - \underbrace{2 \rho_g \Omega_k (\overline{u_j u_m} \varepsilon_{ikm} + \overline{u_j u_m} \varepsilon_{jkm})}_{F_{ij}}
\end{aligned} \tag{2-8}$$

where  $C_{ij}$  is convection term,  $D_{T,ij}$  is turbulent diffusion term,  $D_{L,ij}$  is molecular diffusion,  $P_{ij}$  is the stress production term,  $G_{ij}$  is buoyancy production,  $\Phi_{ij}$  is pressure strain,  $\varepsilon_{ij}$  is the dissipation,  $F_{ij}$  production by system rotation and  $S_{user}$  is user-defined source term.

Of these terms,  $C_{ij}$ ,  $D_{L,ij}$ ,  $P_{ij}$  and  $F_{ij}$  do not require any modeling. However  $D_{T,ij}$ ,  $\Phi_{ij}$ ,  $G_{ij}$  and  $\varepsilon_{ij}$  have to be modeled for closing the equations. And the modeling assumptions required to close the equation set are describe in the following.

The turbulent diffusive can be modeled by the generalized gradient-diffusion model of Daly and Harlow[111]:

$$D_{T,ij} = C_s \frac{\partial}{\partial x_k} \left( \rho \frac{\overline{u_k u_l}}{\varepsilon} \frac{\partial \overline{u_i u_j}}{\partial x_l} \right) \tag{2-9}$$

However, this equation can result in numerical instabilities, so it has been simplified in Fluent to use a scalar turbulent diffusivity], according to Lien and Leschziner[112] an isotropic diffusive term is likely to give good results even for the cases in fact anisotropic.

$$D_{T,ij} = \frac{\partial}{\partial x_k} \left( \frac{\mu_t}{\sigma_k} \frac{\partial \overline{u_i u_j}}{\partial x_k} \right) \tag{2-10}$$

Lien and Leschziner[112] derived a value of  $\sigma_k = 0.82$  by applying the generalized gradient-diffusion, Eq.(2-9), to the case of a planar homogeneous shear flow. Note that this value of  $\sigma_k$  is different from that in the standard and realizable k- $\varepsilon$  models, in which  $\sigma_k = 1.0$ .

According to Gibson and Launder[113], Fu et al.[114] and Launder[115] the

pressure strain term can be modeling using the following decomposition:

$$\Phi_{ij} = \Phi_{ij,1} + \Phi_{ij,2} + \Phi_{ij,w} \quad (2-11)$$

where the first term  $\Phi_{ij,1}$  as known as the return-to-isotropy term. It is the slow pressure-strain term, and is modeled as:

$$\Phi_{ij,1} \equiv -C_1 \rho \frac{\varepsilon}{k} \left( \overline{u_i u_j} - \frac{2}{3} \delta_{ij} k \right) \quad (2-12)$$

with  $C_1 = 1.8$ .

The second term,  $\Phi_{ij,2}$ , is the rapid pressure-strain term, and is modeled as:

$$\Phi_{ij,2} \equiv -C_2 \left[ \left( P_{ij} + F_{ij} + G_{ij} - C_{ij} \right) - \frac{2}{3} \delta_{ij} (P + G - C) \right] \quad (2-13)$$

with  $C_2 = 0.60$ ,  $P = \frac{1}{2} P_{kk}$ ,  $G = \frac{1}{2} G_{kk}$  and  $C = \frac{1}{2} C_{kk}$ .

The last term  $\Phi_{ij,w}$  represent the wall-reflection term, is responsible for the redistribution of normal stress near the wall. It dampens the normal stress perpendicular to the wall, while enhancing the stresses parallel to the wall. This term is modeled as:

$$\begin{aligned} \Phi_{ij,w} \equiv & C'_1 \frac{\varepsilon}{k} \left( \overline{u_k u_m n_k n_m} \delta_{ij} - \frac{3}{2} \overline{u_i u_k n_j n_k} - \frac{3}{2} \overline{u_j u_k n_i n_k} \right) \frac{k^{3/2}}{C_l \varepsilon d} \\ & + C'_2 \left( \Phi_{km,2} n_k n_m \delta_{ij} - \frac{3}{2} \Phi_{ik,2} n_j n_k - \frac{3}{2} \Phi_{jk,2} n_i n_k \right) \frac{k^{3/2}}{C_l \varepsilon d} \end{aligned} \quad (2-14)$$

where  $C'_1 = 0.5$ ,  $C'_2 = 0.3$ ,  $C_l = \frac{C_\mu^{3/4}}{\kappa}$ ,  $C_\mu = 0.09$ ,  $\kappa = 0.4187$  (von Karman constant),  $n_k$  is the  $x_k$  component of the unit normal to the wall, and  $d$  is the normal distance to the wall.

The production terms due to buoyancy are modeled as:

$$G_{ij} = \beta \frac{\mu_t}{\text{Pr}_t} \left( g_i \frac{\partial T}{\partial x_j} + g_j \frac{\partial T}{\partial x_i} \right) \quad (2-15)$$

where  $\text{Pr}_t$  is the turbulent Prandtl number for energy, with a default value of 0.85.

In general, when the turbulence kinetic energy is needed for modeling a specific term, it is obtained by taking the trace of the Reynolds stress tensor:

$$k = \frac{1}{2} \overline{u_i u_i} \quad (2-16)$$

The dissipation tensor,  $\varepsilon_{ij}$ , is modeled as:

$$\varepsilon_{ij} = \frac{2}{3} \delta_{ij} \rho \varepsilon \quad (2-17)$$

The scalar dissipation  $\varepsilon$  is computed with a model transport equation similar to that used in standard k- $\varepsilon$  model:

$$\frac{\partial}{\partial t} (\alpha_g \rho_g \varepsilon) + \nabla (\alpha_g \rho_g \varepsilon u_i) = \nabla \left[ \left( \mu + \frac{\mu_t}{\sigma_\varepsilon} \right) \nabla \varepsilon \right] + \alpha_g C_{\varepsilon 1} \frac{1}{2} [P_{ii} + C_{\varepsilon 3} G_{ii}] \frac{\varepsilon}{k} - C_{\varepsilon 2} \alpha_g \rho_g \frac{\varepsilon^2}{k} \quad (2-18)$$

where  $\sigma_\varepsilon = 1.0$ ,  $C_{\varepsilon 1} = 1.44$ ,  $C_{\varepsilon 2} = 1.92$ .

The turbulent viscosity  $\mu_t$  is computed similarly to the k- $\varepsilon$  models:

$$\mu_t = \rho C_\mu \frac{k^2}{\varepsilon} \quad (2-19)$$

where  $C_\mu = 0.09$ .

Boundary conditions for the Reynolds Stresses are as follows. At the inlet:

$$\begin{aligned} \overline{u_i u_j} &= \frac{2}{3} k \quad \text{for } i = j \\ \overline{u_i u_j} &= 0 \quad \text{for } i \neq j \end{aligned} \quad (2-20)$$

At the wall Fluent applies explicit wall boundary conditions for the Reynolds stresses by using the log-law.

Using a local coordinate system, the Reynolds stresses at the wall-adjacent cells are computed from:

$$\frac{\overline{u_\tau^2}}{k} = 1.098, \quad \frac{\overline{u_\eta^2}}{k} = 0.247, \quad \frac{\overline{u_\lambda^2}}{k} = 0.655, \quad -\frac{\overline{u_\tau u_\eta}}{k} = 0.255 \quad (2-21)$$

where  $\tau$  is tangential coordinate,  $\eta$  is the normal coordinate, and  $\lambda$  the binomial coordinate.

Near the wall  $k$  is obtain by solving the transport equation. In the far field  $k$  is obtained directly from Reynolds stresses using Eq. (2-16).

## 2.3 Gas-solid two phase flow model description

To predict particulate two-phase flows, two approaches are possible. One treats

the fluid phase as a continuum and the particulate second phase as single particles. This approach, which predicts the particle trajectories in the fluid phase as a result of forces acting on particles, is called the Lagrangian approach. Treating the solid as some kind of continuum, and solving the appropriate continuum equations for the fluid and particle phases, is referred to as the Eulerian approach. The Lagrangian approach has some advantages for predicting those particulate flows in which large particle accelerations occur. It can also handle particulate two-phase flows consisting of polydispersed particle size distributions. The Eulerian approach seems to have advantages in all flow cases where high particle concentrations occur and where the high void fraction of the flow becomes a dominating flow controlling parameter. Only Eulerian approach is discussed and their basic equations for the particle are presented.

The Eulerian approach is used for both the gas and particle phase within cyclone separator. For simplicity, it is assumed that the gas phase is incompressible and particles are spherical.

The concept of volume fraction is introduced here heuristically without resorting to a rigorous treatment. With this approach, it is assumed that it is meaningful to conceive a volume fraction of phase  $k$ ,  $\alpha_k$  in any small volume of space at any particular time. If there are  $n$  phases in total, this gives:

$$\sum_{k=1}^n \alpha_k = 1.0 \quad (2-22)$$

In the framework of Eulerian particle modeling the particles are pictured as an additional continuous phase. The Eulerian particle phase consequently obeys to a similar set of conservation equations like as the gas phase. Thus, in an Eulerian particle simulation the conservation equation can be written as followings.

Continuity equations for gas phase and solids phase are shown by:

$$\frac{\partial(\alpha_g \rho_g)}{\partial t} + \nabla \cdot (\alpha_g \rho_g \mathbf{u}_g) = 0 \quad (2-23)$$

$$\frac{\partial(\alpha_s \rho_s)}{\partial t} + \nabla \cdot (\alpha_s \rho_s \mathbf{u}_s) = 0 \quad (2-24)$$

Momentum equation for gas phase and solids phase are expressed by:

$$\frac{\partial}{\partial t}(\alpha_g \rho_g \mathbf{u}_g) + \nabla \cdot (\alpha_g \rho_g \mathbf{u}_g \mathbf{u}_g) = -\alpha_g \nabla p_g + \nabla \cdot (\alpha_g \boldsymbol{\tau}_g) - \beta(\mathbf{u}_g - \mathbf{u}_s) + \alpha_g \rho_g \mathbf{g} \quad (2-25)$$

$$\frac{\partial}{\partial t}(\alpha_s \rho_s \mathbf{u}_s) + \nabla \cdot (\alpha_s \rho_s \mathbf{u}_s \mathbf{u}_s) = -\alpha_s \nabla p_g - \nabla p_s + \nabla \cdot (\alpha_s \boldsymbol{\tau}_s) + \beta(\mathbf{u}_g - \mathbf{u}_s) + \alpha_s \rho_s \mathbf{g} \quad (2-26)$$

In addition to the mass and momentum conservation equations for the solid phase, a fluctuation kinetic energy equation (Eq. 2-27) is solved to account for the conservation of fluctuation of the particle phase through the implementation of the kinetic theories of granular flows[97]:

$$\frac{3}{2} \left[ \frac{\partial}{\partial t}(\alpha_s \rho_s \theta_s) + \nabla \cdot (\alpha_s \rho_s \theta_s \mathbf{u}_s) \right] = (-\nabla p_s \bar{\mathbf{I}} + \boldsymbol{\tau}_s) : \nabla \mathbf{u}_s + \nabla \cdot (k_s \nabla \theta) - \gamma_s + \phi_s \quad (2-27)$$

where  $\phi_s$  is exchange of fluctuating energy between gas and particle and  $\gamma_s$ , the dissipation of energy due to inelastic collisions).

The behavior of solid phases is achieved through the kinetic theory of granular flows (KTGF), which is an extension of the classical kinetic theory of dense gases [116], where the thermodynamic temperature is replaced by the granular temperature,  $\theta$ , defined as:

$$\theta = \frac{1}{3} u^2$$

where  $u$  is the particle fluctuating velocity. The granular temperature expresses the macroscopic kinetic energy. Kinetic theory based models introduce several additional terms in the solids stress and therefore, modify equation momentum conservation equations for solid phase. For a high volume fraction of solid particles in cyclone separators, granular flow becomes incompressible, the frictional interactions between solid particles must be considered. The theories of soil mechanics may be used to estimate such friction contribution. The solid phase stress can be written as:

$$\boldsymbol{\tau}_s = (-p_s + \lambda_s \nabla \cdot \mathbf{u}_s) \mathbf{I} + \mu_s \left\{ \left[ \nabla \mathbf{u}_s + (\nabla \mathbf{u}_s)^T \right] - \frac{2}{3} (\nabla \cdot \mathbf{u}_s) \mathbf{I} \right\} \quad (2-28)$$

where  $p_s$  is solids pressure,  $\mu_s$  is solid viscosity and  $\lambda_s$  is solid bulk viscosity.

Several different expressions have been derived for solids pressure, solids shear viscosity and solids bulk viscosity, employing different approximations and

assumptions while applying the kinetic theory of granular flows. Some of the commonly used equations are described below.

Solids pressure is:

$$p_s = \alpha_s \rho_s \theta_s \left[ 1 + 2 \rho_s g_0 (1 + e_s) \right] \quad (2-29)$$

where  $e_s$  is the restitution coefficient of particles.

Solid shear viscosity is:

$$\mu_s = \frac{4}{5} \alpha_s \rho_s d_s g_0 (1 + e_s) \left( \frac{\theta_s}{\pi} \right)^{1/2} + \frac{10 d_s \rho_s (\theta_s \pi)^{1/2}}{96 (1 + e_s) g_0} \left[ 1 + \frac{4}{5} g_0 \alpha_s (1 + e_s) \right]^2 \quad (2-30)$$

Solid bulk velocity is:

$$\lambda_s = \frac{4}{3} \alpha_s \rho_s d_s g_0 (1 + e) \left( \frac{\theta_s}{\pi} \right)^{1/2} \quad (2-31)$$

Expressions for solids pressure and solids viscosity are depend on the radial distribution function, and it is expressed by:

$$g_0 = \left[ 1 - \left( \frac{\alpha_s}{\alpha_{s,\max}} \right)^{\frac{1}{3}} \right]^{-1} \quad (2-32)$$

Dissipation of energy due to inelastic collisions can be expressed in the form is:

$$\gamma_s = 3(1 - e^2) \alpha_s^2 \rho_s g_0 \theta \left( \frac{4}{d_p} \left( \frac{\theta}{\pi} \right)^{1/2} - \nabla \cdot \mathbf{u}_s \right) \quad (2-33)$$

Energy exchange between the fluid and the solid phase is modeled as:

$$\phi_s = -3\beta_{gs}\theta \quad (2-34)$$

The interface momentum transfer coefficient is expressed as:

$$\beta_{gs} = \frac{3C_d \alpha_g \alpha_s \rho_g |\mathbf{u}_g - \mathbf{u}_s|}{4d_s} \varepsilon_g^{-2.65} \quad (2-35)$$

with

$$C_d = \frac{24}{Re} (1 + 0.15 Re^{0.687}), \quad Re < 1000$$

$$C_d = 0.44, \quad Re \geq 1000$$

## 2.4 Brief summary

This second chapter yields the numerical model of gas-solid two phase flows in cyclone separator. Two approaches are possible to predict particulate two-phase flows, one treats the fluid gas phase as a continuum and the particulate second phase as single particles. This approach, which predicts the particle trajectories in the fluid phase as a result of forces acting on particles, is called the Lagrangian approach. Treating the solid as some kind of continuum, and solving the appropriate continuum equations for the gas and particle phases, is referred to as the Eulerian approach. Both approaches were cited and particular attention is given to Eulerian approach which seems to have advantages in all flow cases where high particle concentrations occur and where the high void fraction of the flow becomes a dominating flow controlling parameter. The basic equations for the gas fluid and particles as well as their numerical treatment were presented.

For strongly swirling flows the standard  $k$ - $\epsilon$  turbulence model is known to have limitations. In order to obtain values for the Reynolds stress terms, a turbulence model, known as the RNG  $k$ - $\epsilon$ , was selected in the following simulations. To compare the results obtained with RNG  $k$ - $\epsilon$ , another turbulence model, known as RSM, was also selected. These two turbulent models have been selected in combination with Euler-Euler on the platform of commercial CFD Software package, FLUENT 6.3.23, to develop the following numerical calculation.

## **Chapter 3 Numerical study of a cylindrical cyclone separators**

### **3.1 Introduction**

Gas cyclone separators are widely used in industries to separate dust from gas or for product recovery because of their geometrical simplicity and relative economy in power consumption. Cyclones may also be adapted for use in extreme operating conditions (high temperature, high pressure, and corrosive gases). Since there are no moving parts, cyclones are relatively maintenance-free. Therefore, cyclones have found increasing utility in the field of air pollution, the petrochemical and process industries to separate dust from gas streams or for product recovery. Until now, a considerable number of experimental and numerical investigations have been performed either on small sampling cyclones or on larger industrial cyclone separators[118-122]. In this chapter, the conventional cylindrical cyclone where used with different inlet geometries of the cyclone separator, to study the effect of turbulence model, solid volume fraction and the cyclone inlet geometry on cyclone performance.

In this part, we used RNG k- $\epsilon$  and RSM model in FLUENT 6.3.26 to study numerical simulation of dense gas and particle flow within cyclone separators. The turbulent model effect is verified by comparing the RNG k- $\epsilon$  and RSM results in term of gas pressure field and gas-solid volume fraction. The effects of inlet geometry are investigated based on the velocity component, pressure drops and separation efficiency.

### **3.2 Description of numerical model**

#### **3.2.1 Configuration of cyclone separators**

The cyclone is a device that separates particles from a carrier air stream by means of centrifugal force acting on the particles. The essential geometry of an air cyclone is depicted in Fig.3-1. Solid particles, initially entrained in the gas flow, enter the tangential inlet near the top of the cyclone, and follow the downward spiral of the air vortex. Centrifugal force and inertial effects act on the solid



particles to move them outward toward the inner wall of the cyclone where they are trapped in the boundary flow. Trapped particles eventually move down the inner wall and are collected at the base of the cyclone while the gas flow reverses direction near the base of the cyclone, and exits through the vortex finder at the top of the cyclone.

The cyclone separator considered in this simulation is the conventional cyclone which consists of an upper cylindrical part, with a tangential inlet and lower part with exit at the apex. A schematic diagram of a cyclone separator and four different inlet configurations with the main dimensions is presented in Figs.3-1(a) and 3-1(b). Table 3-1 shows the dimension of cyclone and the model parameters used for this study.

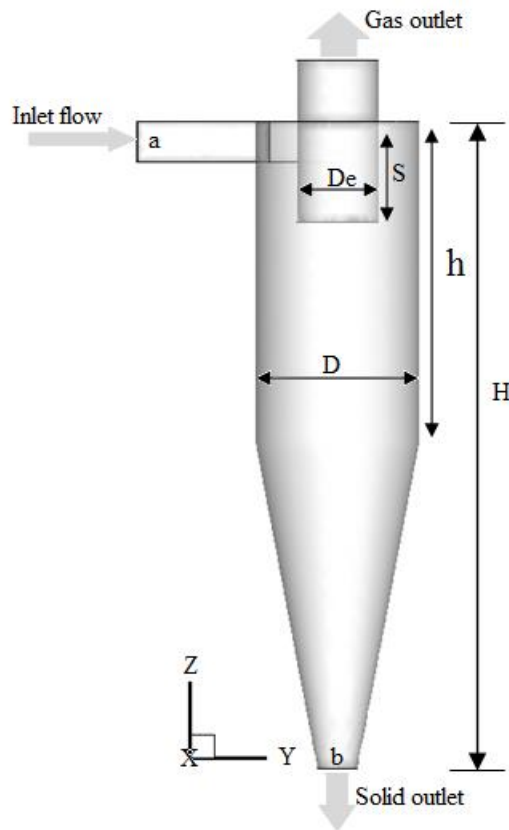


Fig. 3-1(a) Structure scheme of the cyclone

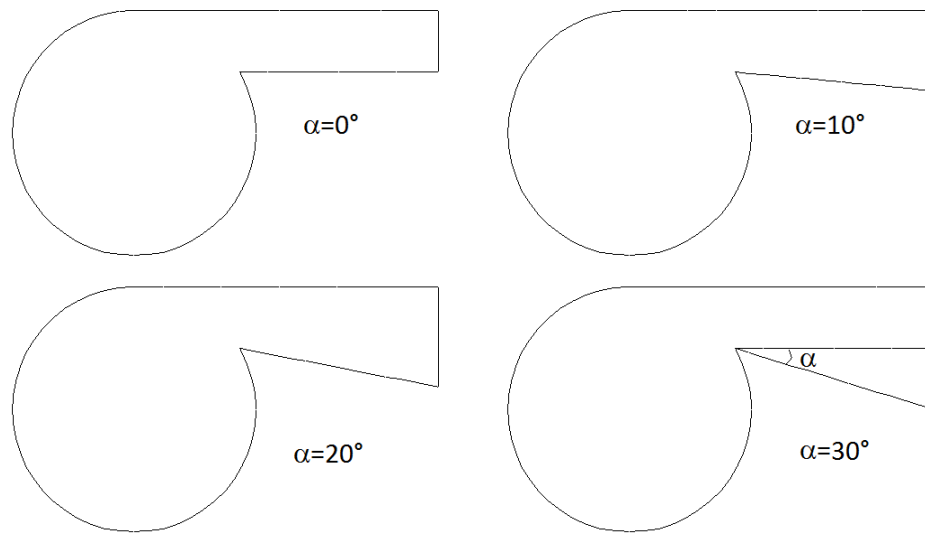


Fig.3-1(b) Four different inlet configurations for cyclone separators

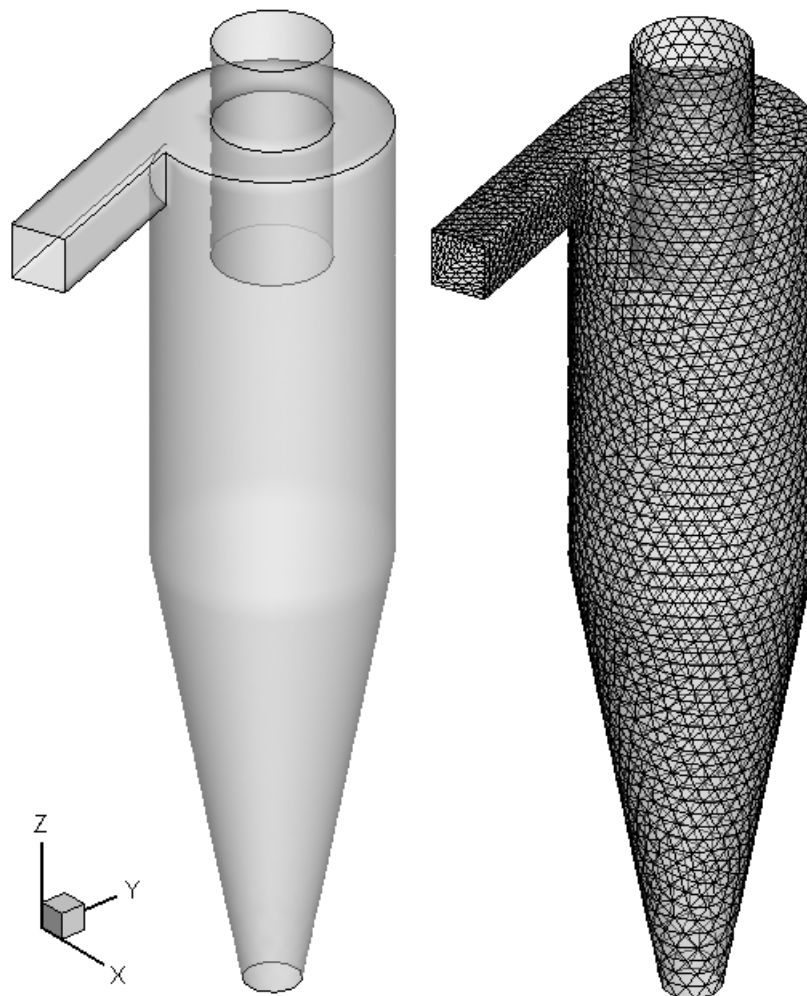


Fig 3-1(c) A schematic and grid representation of the 3D cyclone used in this simulation

Table 3-1 Dimensions of the cyclone and model parameter used in this simulation

Symbol	Units	Parameter	Value
H	m	Cyclone height	0.8
h	m	Cylinder length	0.4
S	m	Exit tube length	0.125
D	m	Cyclone body diameter	0.2
De	m	Gas exit diameter	0.1
a	m	Inlet width	0.05
b	m	Inlet length	0.05
B	m	Solid outlet diameter	0.05
$d_s$	$\mu\text{m}$	Solid diameter	150
$\alpha_s$	--	Solid volume fraction	0.1
$\rho_g$	$\text{kg/m}^3$	Gas density	0.298
$\rho_s$	$\text{kg/m}^3$	Solid density	2400
$\mu_g$	$\text{kg/m-s}$	Gas viscosity	$1.491 \times 10^{-4}$

### 3.2.2 Turbulence model

Numerical methods have been developed to solve the equations presented in previous Chapter, whose complexity is significantly increased due to the Reynolds stress terms on the right-hand side of momentum equations. The RNG k- $\epsilon$  and RSM were used in this part. These models have been described in the Chapter 2.

### 3.2.3 Gas-solid two phase flows

Flows in cyclone separators are multiphase. The flow in conventional cyclone in this study consists of gas and solid two phase flows and can be solved by a number of CFD techniques. These include the full Eulerian multiphase approach, simplified Eulerian approaches such as the Mixture and VOF models and the Lagrangian approach. The full Eulerian multiphase flow approach, where a set of continuity, momentum and turbulence equations for each phase is preferred for systems with very high dispersed phase concentrations, where solid/solid interactions carry a significant amount of the stress. The disadvantage of the full

Eulerian multiphase modeling approach has been its high computational cost. Further implementations in commercial CFD codes have until recently been limited to using the k- $\epsilon$  model for turbulence. In this chapter, the solid volume fraction is 0.1 corresponding to a high dispersed phase concentration and therefore a dense two-phase flow regime. In the case of the dense regime, inter-particles becomes of importance, both physical collisions and indirect influence through the nearby flow field, also limitations related to computer storage, calculation times and convergence arise. In those cases, the Eulerian-Eulerian approach, where a set of continuity, momentum and turbulence equations for each phase are established, therefore becomes more adequate. The gas phase is incompressible and particles are spherical and mono-sized. The governing equations for the conservation of mass and momentum for each phase and the constitutive relations are given in Chapter 2.

### **3.2.4 Boundary conditions**

Computational mesh created in millimeter was scaled to meter using transformation option available in the FLUENT. After checking the grid for quality aspects, material properties and physical models are selected. The velocity inlet boundary condition was used at the inlet and the inlet velocity was set as 20, 22, 25 and 30m/s. The pressure condition is prescribed at exit boundary faces. No slip condition was adopted at the wall. The particle volume fraction was set as 0.1 values at the inlet and it was assumed that the particle had the same inlet velocity of gas.

### **3.2.5 Grid independence**

Fig.3-1(c) show a schematic and the surface grid of the 3D cyclone used in this section. The tetrahedral computational grids were generated using GAMBIT grid generators. The grid independence study has been performed for the test cyclones with RSM turbulent model. Three levels of grid for each cyclone have been tested, to be sure that obtained results are grid independent. Fig.3-2 shows the comparison of static pressure for three different grids (99794 cells, 115327 cells and 126859 cells) with the case of cyclone angle  $\alpha = 0^\circ$ , corresponding to conventional cylindrical. As shown in Fig.3-2 the static pressure for grid with 126859 cells is slightly higher compared to other two grids. However all the results show the same trend, and to eliminate any uncertainty, the following simulations were performed

using the grid with 115327 cells.

The grids used in the RNG k- $\epsilon$  and RSM models have to be conforming to the resolution requirements of the underlying turbulence model. Frequently, the RNG k- $\epsilon$  zone will be connected to the RSM zones by Non-Conformal Interfaces (NCI) to allow a more refined grid in the k- $\epsilon$  zone. A multigrid scheme is used to accelerate the convergence of the solver by computing corrections on a series of coarse grid levels. The use of this multigrid scheme can greatly reduce the number of iterations and the CPU time required to obtain a converged solution, particularly to model a large number of control volumes.

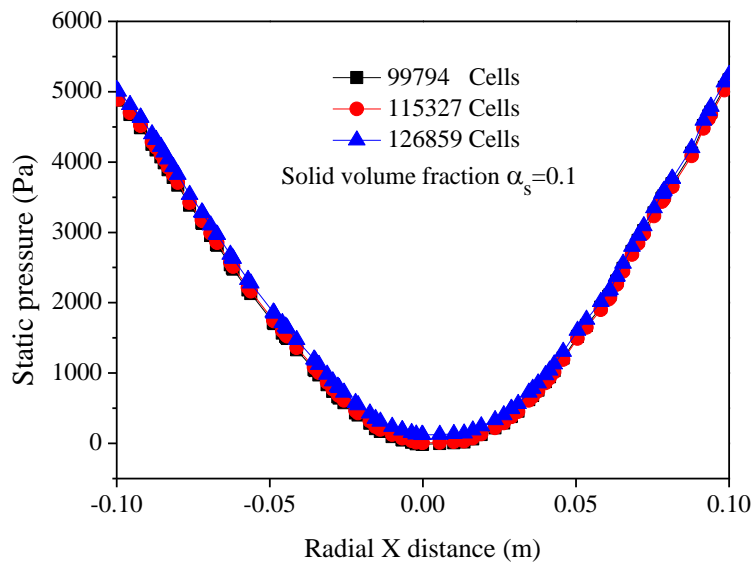


Fig.3-2 Static pressure of three grid levels

### 3.3 Results and discussion

#### 3.3.1 Effect of turbulence model on cyclone separator

##### 3.3.1.1 Effect on the flow field

The tangential velocity distribution is the dominant velocity component in the cyclone. For the same reason the velocity magnitude contours are almost identical to those of tangential velocity. The distribution of tangential velocity and the axial velocity of cyclone separator are shown in following figures respectively. For both the RNG k- $\epsilon$  and RSM models, at different gas and particle inlet velocities the following results were:

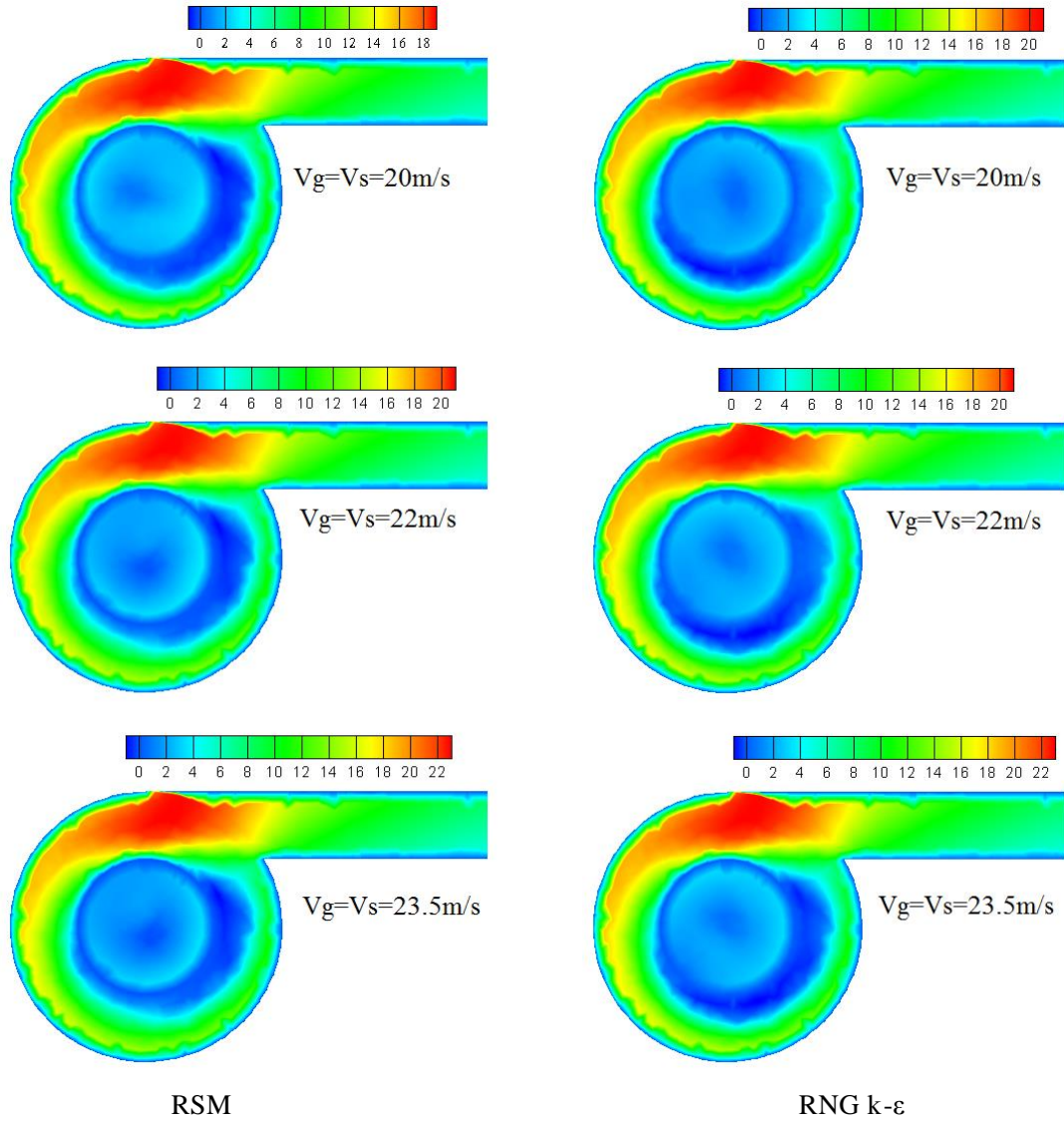


Fig. 3-3 Cross sectional gas tangential velocity for two turbulence model

The value of the tangential velocity equals zero at the wall and at the center of the cyclone. The high speed gas enters the inlet and is accelerated up to 1.5-2.0 times that of the inlet velocity value, the cross sectional gas tangential velocity are showed in Fig.3-3 for Reynolds Stress model and for RNG k- $\epsilon$  model at different inlet gas-particle velocity. Then the velocity decreases as the gas spins down and reaches a minimum at the center of cyclone. There is as chaotic flow just below the entrance of the vortex finder, as the gas flow collides with the follow-up flow, the gas velocity decreases sharply at the outside surface of the vortex finder which causes the short-circuiting flow phenomenon at the entrance of vortex finder, thus

resulting in a higher pressure drop and a decrease in collection efficiency. The main cause of the short-circuiting and which results in a high pressure drop cannot be overcome by the altering gas and particle inlet velocity. Moreover to overcome this problem, it is suggested that the inlet shape should be modified[101].

Furthermore Fig.3-4 shows the profile of gas and particle tangential velocity at different inlet velocities for the RSM model, Fig.3-5 shows the profile of gas and particle tangential velocities at different heights along the axis of the cyclone. The flow field within the cyclone indicates the expected forced free combination of the Rankine vortex. Additionally the axis of the vortex does not coincide with the axis of the cyclone.

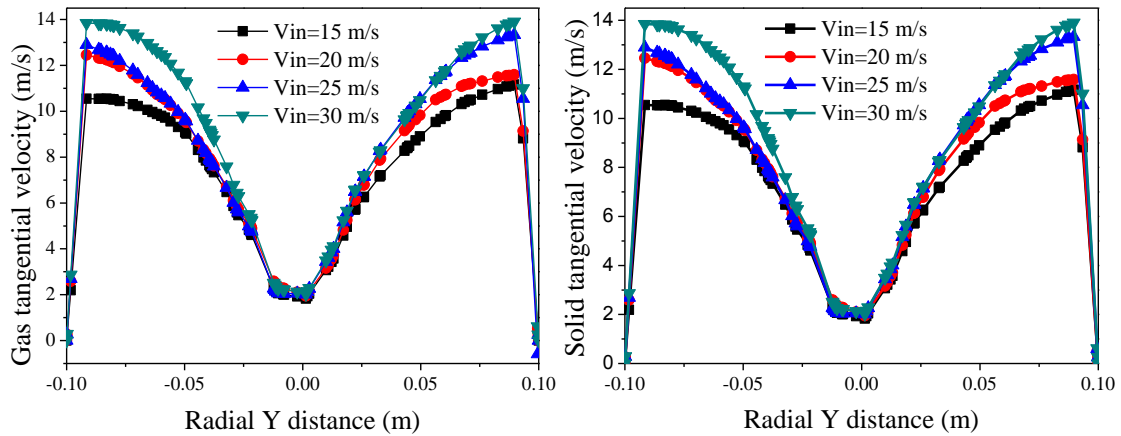


Fig.3-4 Profile of gas and particle tangential velocities at different gas-solid inlet velocities

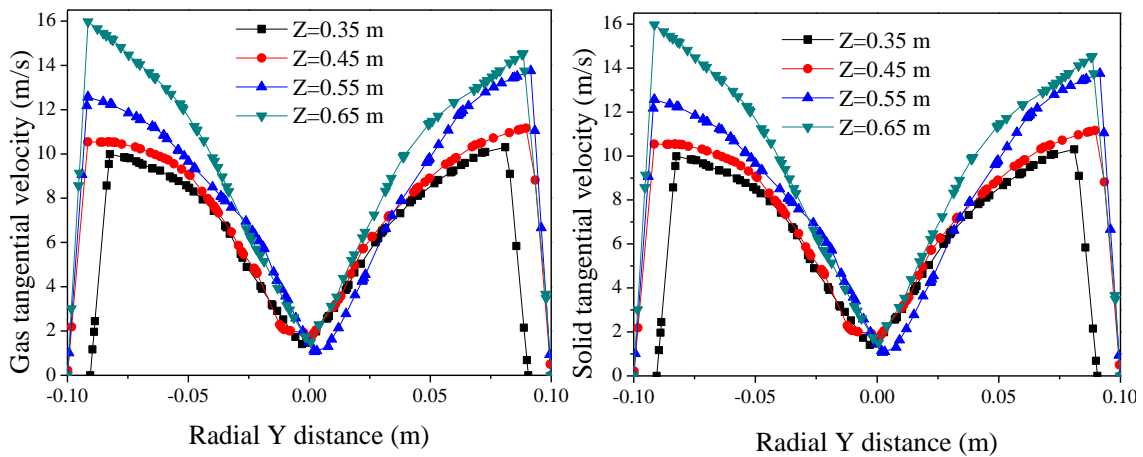


Fig. 3-5 A profile of gas and solid tangential velocities at different heights along the axis of the cyclone

Figs.3-6 and 3-7 present a contour plot of gas axial velocities respectively with different gas and particle inlet velocities (15m/s, 20m/s, 25m/s and 30m/s) and along the axis of the cyclone at four axial locations (from top to bottom  $z = 0.35\text{m}$ ,  $z = 0.45\text{m}$ ,  $z = 0.55\text{m}$  and  $z = 0.65\text{m}$ ). Those figures show that the forced vortex is a twisted cylinder for all models and are not completely in the conical section. The results are qualitatively similar to those obtained by Cullivan et al.[123] for hydrocyclone. The center of the forced vortex does not coincided with the geometrical center of cyclone separators and some modified inlet shapes were proposed[103]. They also show that the diameter of the forced vortex is larger than of the diameter of the vortex finder.

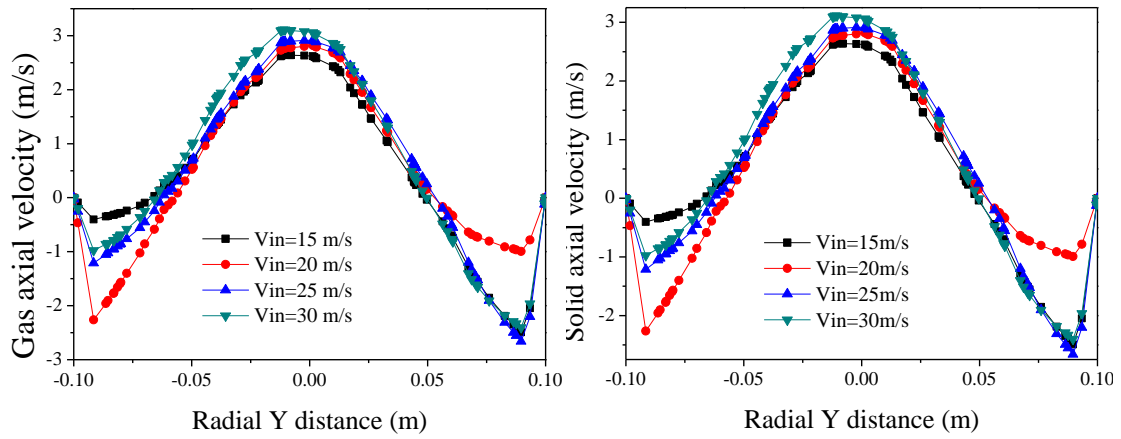


Fig.3-6 A profile of gas and solid axial velocities at different gas-solid inlet velocities

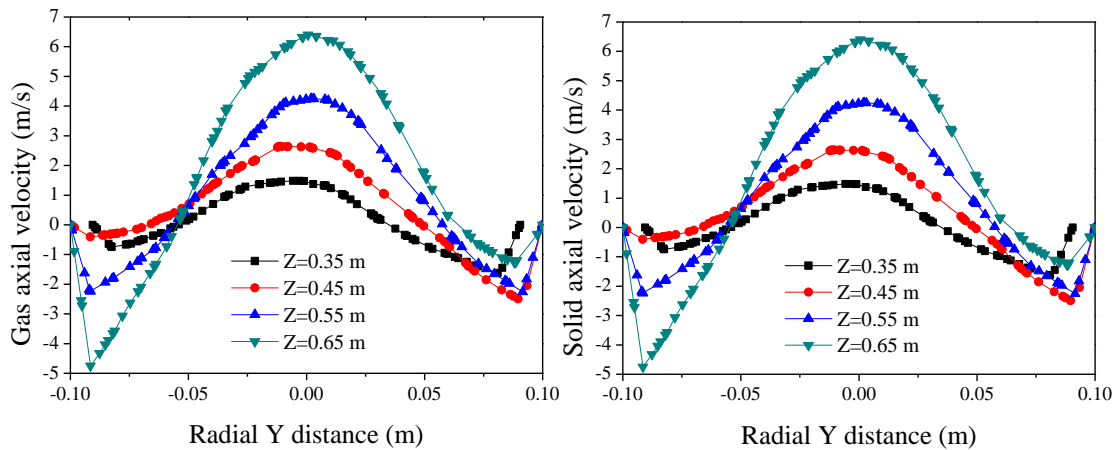


Fig.3-7 A profile of gas and particle axial velocities at different heights along the axis of the cyclone

Moreover the results show that the tangential velocity around the cylindrical section of cyclone (Figs.3-4, 3-5, 3-6 and 3-7) present the RSM model almost



display an axial symmetry for different inlet velocities, while the RNG k- $\epsilon$  model display no axial symmetry.

Simulated results of velocity distributions reveal that the tangential velocity field in a cyclone basically consists of a core of solid body rotation in the central region and a free vortex in the outer region. From Rankine's combined vortex flow model, the flow field comprises the forced vortex region and the free vortex region. We denote  $U$ ,  $V$  and  $W$  as the gas velocity components with respect to the cylindrical coordinate's  $r$ ,  $\theta$  and  $z$ , respectively. The velocity in the forced vortex region ( $0 \leq r \leq r_f$ ) is expressed by

$$V = \omega r \quad (3-1)$$

and that in the free vortex region ( $r > r_f$ ) is given by

$$V_r = \Gamma = \omega r_f^2 \quad (3-2)$$

where  $r_f$  is the radius of the free vortex,  $\omega$  is the angular velocity, and  $\Gamma$  represents the circulation. The corresponding static pressure distribution can also be obtained for the forced vortex region as follows

$$p = p_o + \frac{\rho \Gamma^2}{2r_f^4} \quad (3-3)$$

and for the free vortex region, it shows as follows

$$p = p_o + \frac{\rho \Gamma^2}{2} \left( \frac{2}{r_f^2} - \frac{1}{r^2} \right) \quad (3-3)$$

where  $p_o$  is the static pressure at the center of the cyclone.

In an actual operation, the gas-solid flow in a cyclone is turbulent. The turbulence effects on the distribution of the gas velocity and static pressure in the preceding model is, however, excluded. The strongly swirling turbulent gas-solid flows in tangential inlet cyclones were accounted using RNG k- $\epsilon$  turbulence model. There are an upward flow region in the near-axial core region and a downward flow region in the wall region in the wall region. Also the pressure increase radially in the cyclone. The RNG k- $\epsilon$  turbulence model is seen to predict the velocity and pressure in the wall regime, but not so precisely in the near-axial core region because of the inability of the model to simulate the nonisotropic turbulence of strongly swirling flow.

For the engineering design of tangential inlet cyclone, the variation of the

tangential velocity in the radial direction can be correlated in a form

$$V_r^\beta = C \quad (3-4)$$

where  $C$  is the constant and the vortex exponent  $\beta$  is related to cyclone diameter. For most tangential inlet cyclone,  $\beta$  varies from 0.5 to 0.7 which is in agreement with present simulations.

### 3.3.1.2 Effect on the pressure field

It was the first to detect that the standard  $k-\varepsilon$  turbulent model was not able to accurately simulate this kind of flow. In this part the comparative studies of two turbulence models, the RSM and a variation of the  $k-\varepsilon$  model based on RNG was evaluated. Simulations were compared with pressure fields. For all runs, the RNG  $k-\varepsilon$  model showed great improvement over. However, as expected, the RSM exhibited the best behavior.

Fig. 3-8 shows the profile of static pressure to the radius of the cyclone. It presents the static pressure on the cylindrical part of cyclone, the result show that the airflow causes depression for both RNG  $k-\varepsilon$  and RSM turbulent model, as a swirl was created at the center of cyclone and a slight increase in pressure of the RSM model compared to the RNG  $k-\varepsilon$  model.

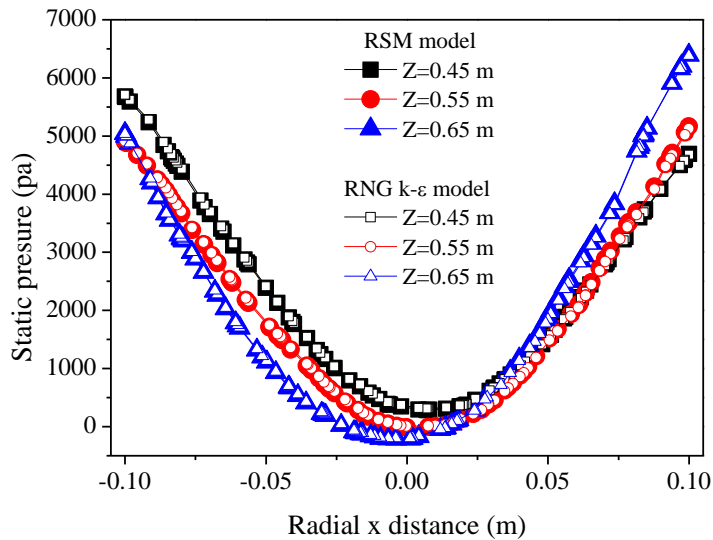


Fig.3-8 Profiles of static pressure for two turbulence models

Additionally, the static pressure decrease radially from wall to axis of the cyclone, the pressure are increase by well for the RSM model near the walls. A contour plot of static pressure shown in Fig.3-9 gives a clear illustration. This result

is in good agreement with the investigation of Gimbum et al. [73]. The pressure gradient is the largest along the radial direction, as here exist a highly forced vortex. Although the pressure distribution showed acceptable agreement for the all models, the pressure drop increases with increased inlet velocity and the RSM gives a higher pressure drop compared to the RNG k- $\epsilon$  model. Considering the RSM and RNG k- $\epsilon$  turbulence models (Fig.3-10), it can be seen that the RSM model is more precise than the RNG k- $\epsilon$  model.

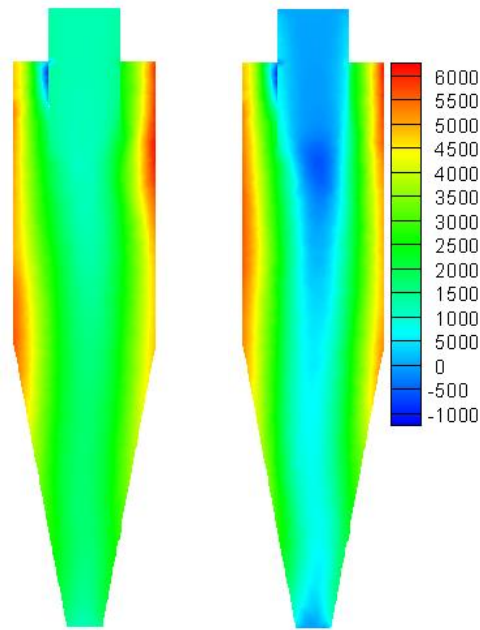


Fig.3-9 Contour plot of static pressure for (left) RNG k- $\epsilon$  model and (right) RSM model

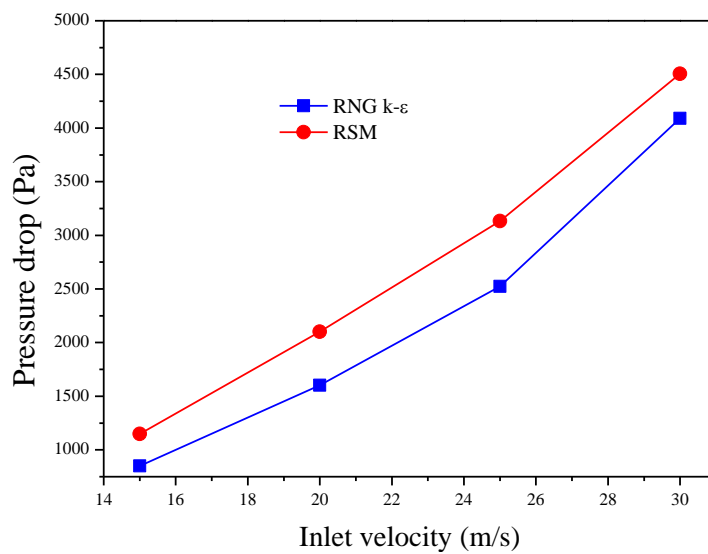


Fig.3-10 Profile of pressure drop as function of gas inlet velocity

### 3.3.1.3 Contour Plot of Volume Fraction

Simulation results showed that the particle volume fraction increased and reached annular bed condition instantly after startup under the action of gravitational force. Figs. 3-11 and 3-12 present the contour of volume fraction of gas and particle for (a) RSM and (b) RNG k- $\epsilon$  model respectively at different cross sectional height of cyclone (Fig.3-11) and at y-plane (Fig. 3-12).

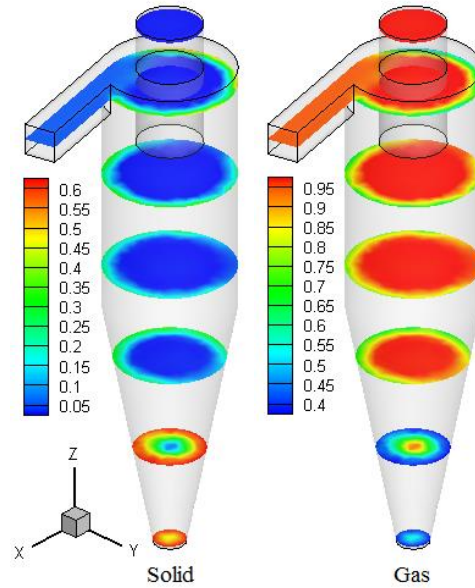


Fig. 3-11 (a) Contour plot of gas and particle volume fraction at different heights of the cyclone for RSM

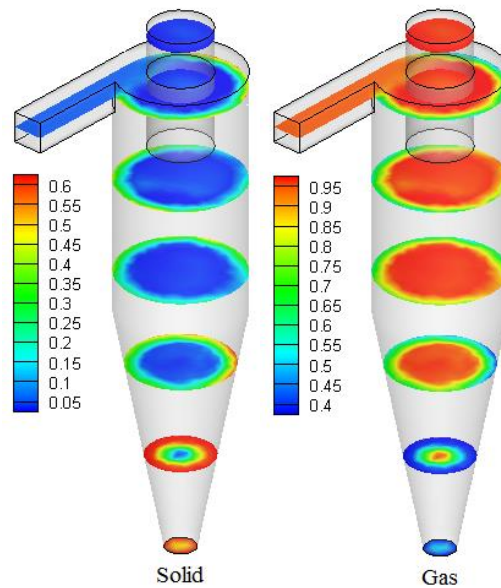


Fig. 3-11(b) Contour plot of gas and particle volume fraction at different heights of the cyclone for RNG k- $\epsilon$  model

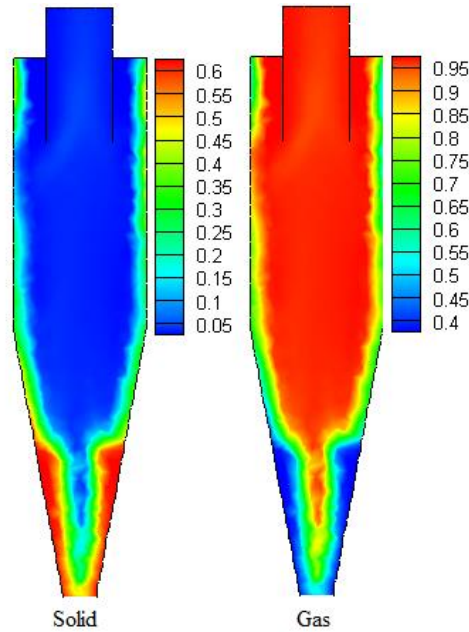
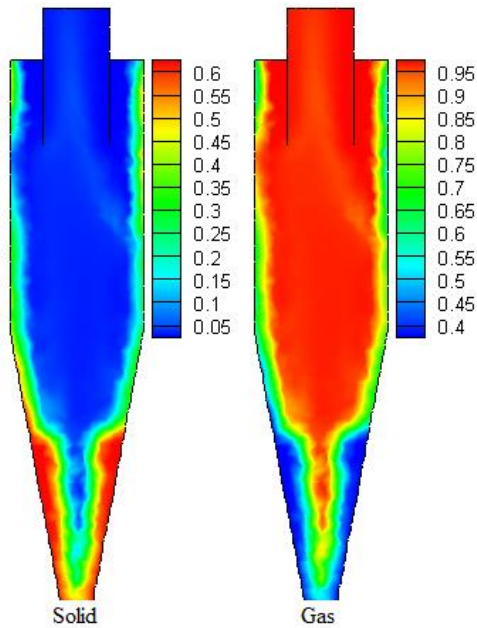


Fig. 3-12 (a) Particle and gas volume fraction for RSM as y-plan of cyclone

Fig. 3-12 (b) Particle and gas volume fraction for RNG k- $\epsilon$  y-plan of cyclone

These figures show the gas volume fraction increases in the top and the particle increases in the bottom under the gravitational force. Also the results show that the particle concentration along the radial direction of cyclone can be divided into two regions: central region of cyclone area with low particle concentration and the wall region with high particle concentration. The gas and particle flow to the wall, leading to increased particle concentration near the wall and in the bottom of

cyclone. Moreover the Fig.3-13 shows the particle volume fraction at the conical and cylindrical part of cyclone for all turbulence models.

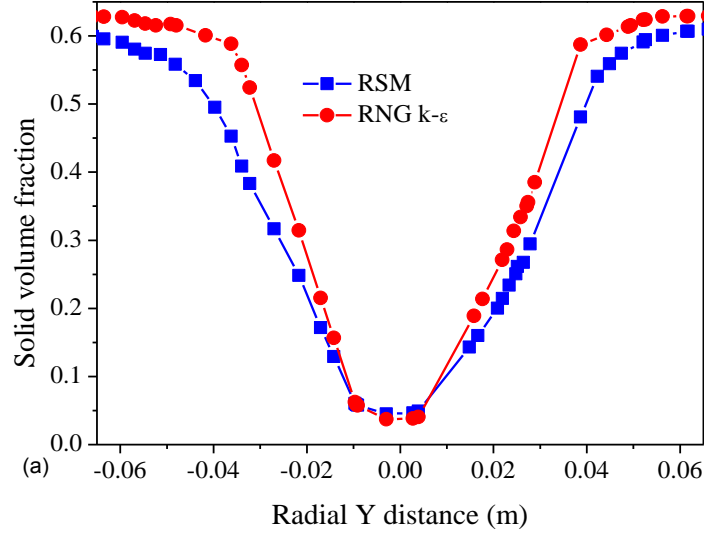


Fig.3-13(a) Profile of solid volume fraction at the conical part of cyclone.

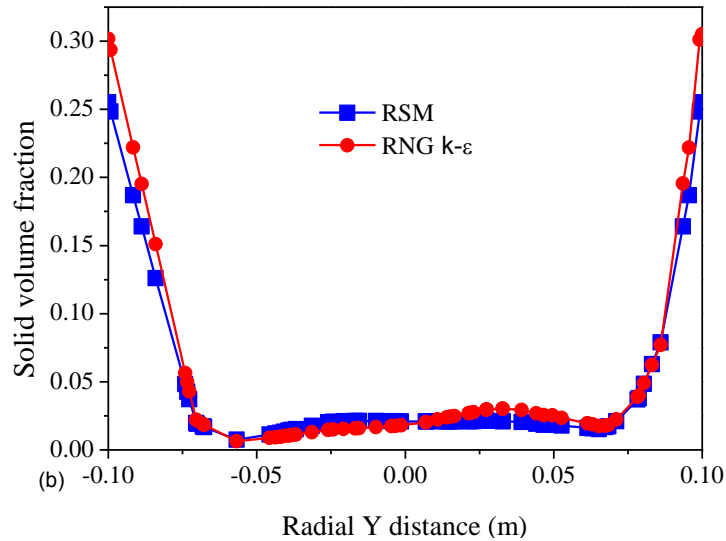


Fig.3-13(b) Profile of solid volume fraction at the cylindrical part of cyclone.

### 3.3.2 Effect of inlet geometry on the flow pattern and performance

#### 3.3.2.1 Effect on the tangential and axial velocity

To evaluate the effect of increasing the cyclone inlet angle  $\alpha$  on the tangential and axial velocity profiles, the axial and tangential velocity profiles at different sections and different inlet velocity for the four different inlet configurations of cyclones are compared in Figs. 3-14, 3-15, 3-16 and 3-17, respectively. Two different cases were considered for comparison of different inlet configurations. Figs. 3-14 and 3-16

show a comparison among four different inlet configurations with different inlet velocity. For this case, the gas and solid inlet velocity are 15, 20, 25 and 30m/s and RSM is used as turbulent model. The second case is about the comparisons with three different heights along axis of the cyclone (Figs. 3-14 and 3-16), for this case, the heights are 0.45, 0.55 and 0.65m. Results are given for both axial (Figs. 3-14 and 3-15) and tangential velocity (Figs. 3-16 and 3-17).

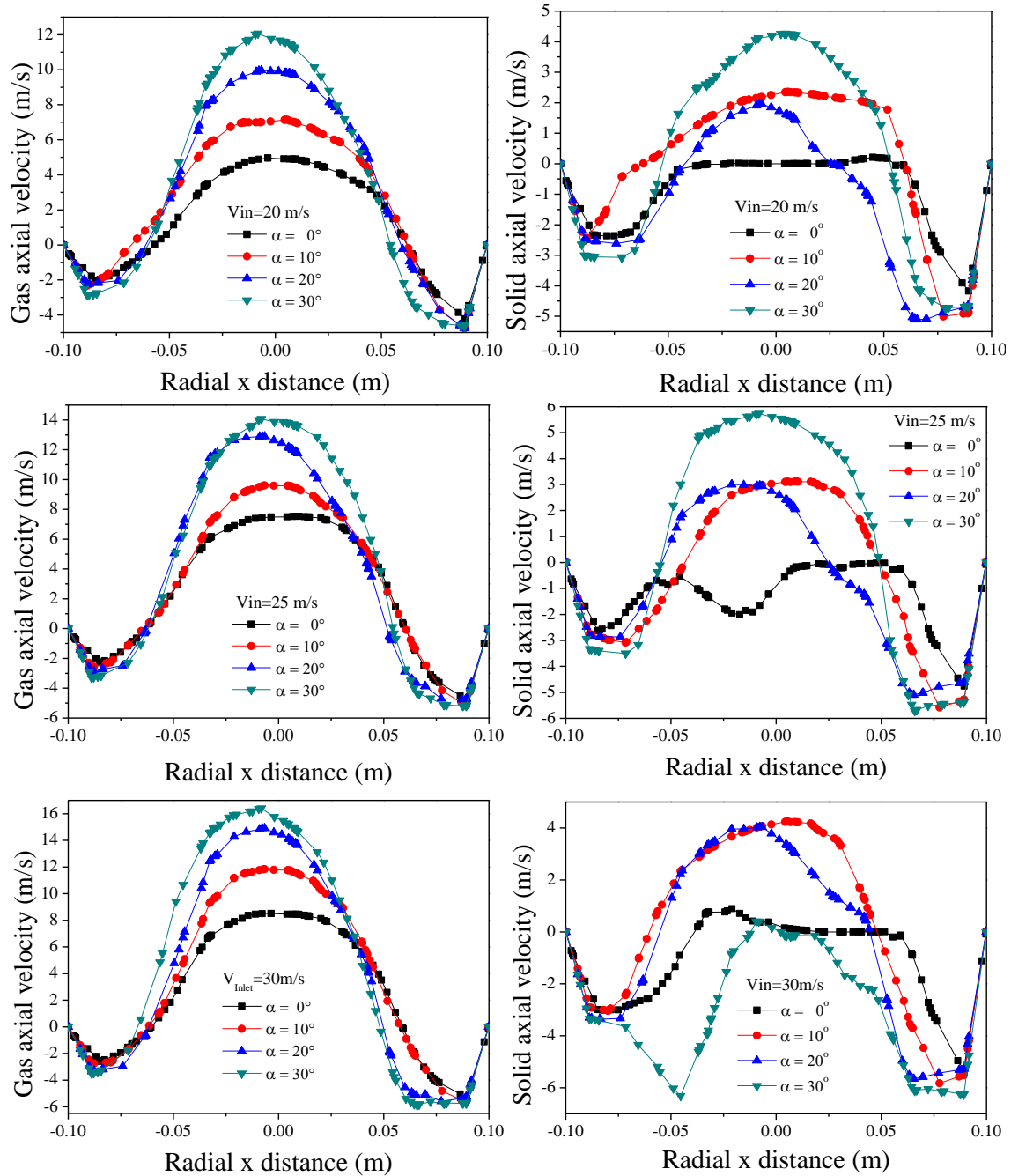


Fig. 3-14 Gas and particle axial velocities with different inlet velocity for four different inlet geometries

Figs. 3-14 and 3-15 present the profile of axial velocity for gas (left) and solid (right) respectively at different inlet velocities and at different heights along the axis of the cyclone. As is clear from Figs 3-14 and 3-15 the variation of axial velocity is limited close to the wall with changing the inlet configuration angle  $\alpha$ . The axial velocity profiles for the four inlet configurations  $\alpha$  are very similar except at the central region which the magnitude peak increases with increase inlet configuration angle  $\alpha$ .

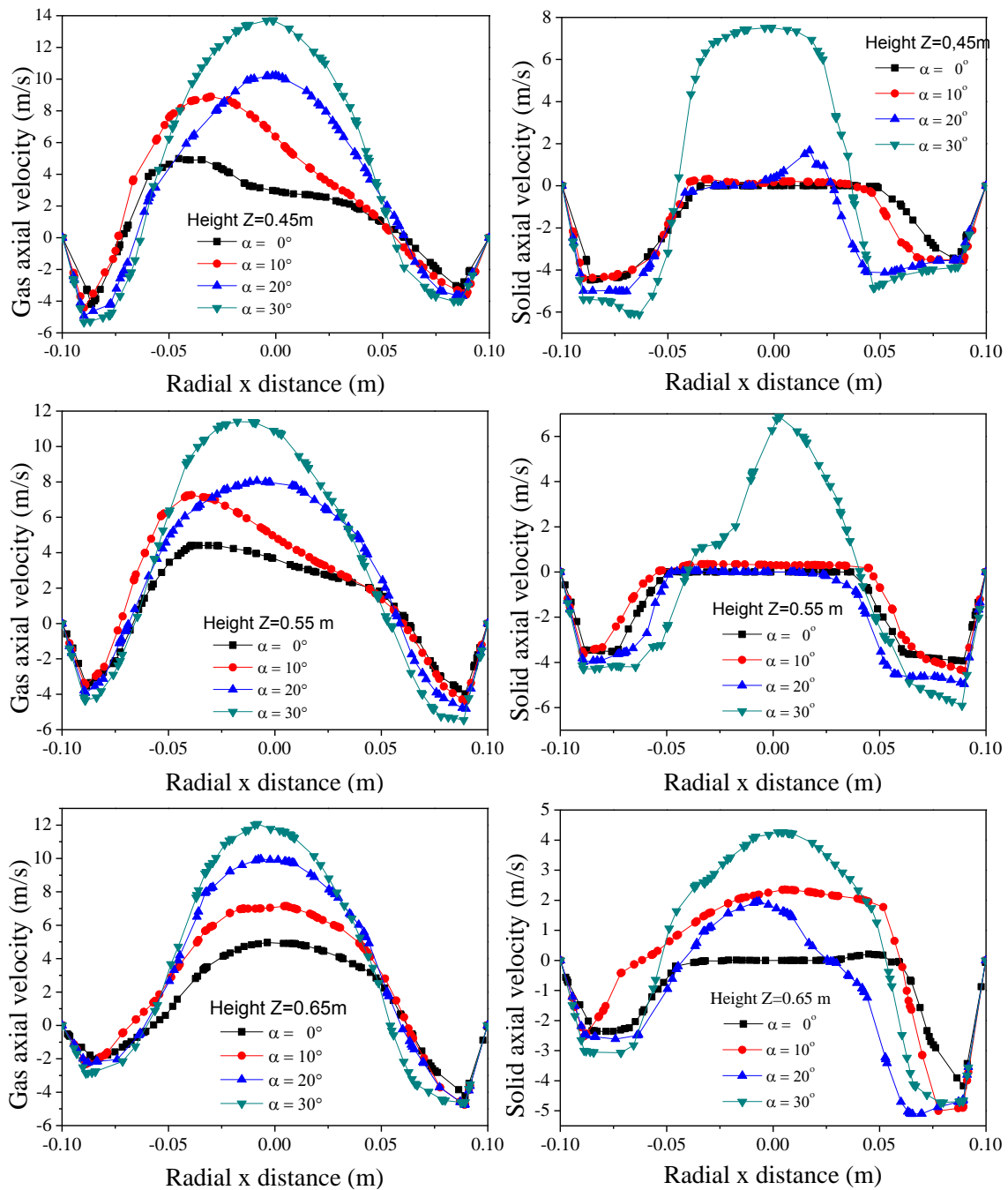


Fig. 3-15 Gas and particle axial velocities with different heights along the axis of cyclone



The most important is the effect of cyclone inlet configuration on the tangential velocity (proportional to the centrifugal force, which is the main force in the separation process). Figs. 3-16 and 3-17 show the gas and solid tangential velocities in cyclone separators. As shown in Figs. 3-16 and 3-17 increasing the cyclone inlet configuration angle can increase the maximum tangential velocity.

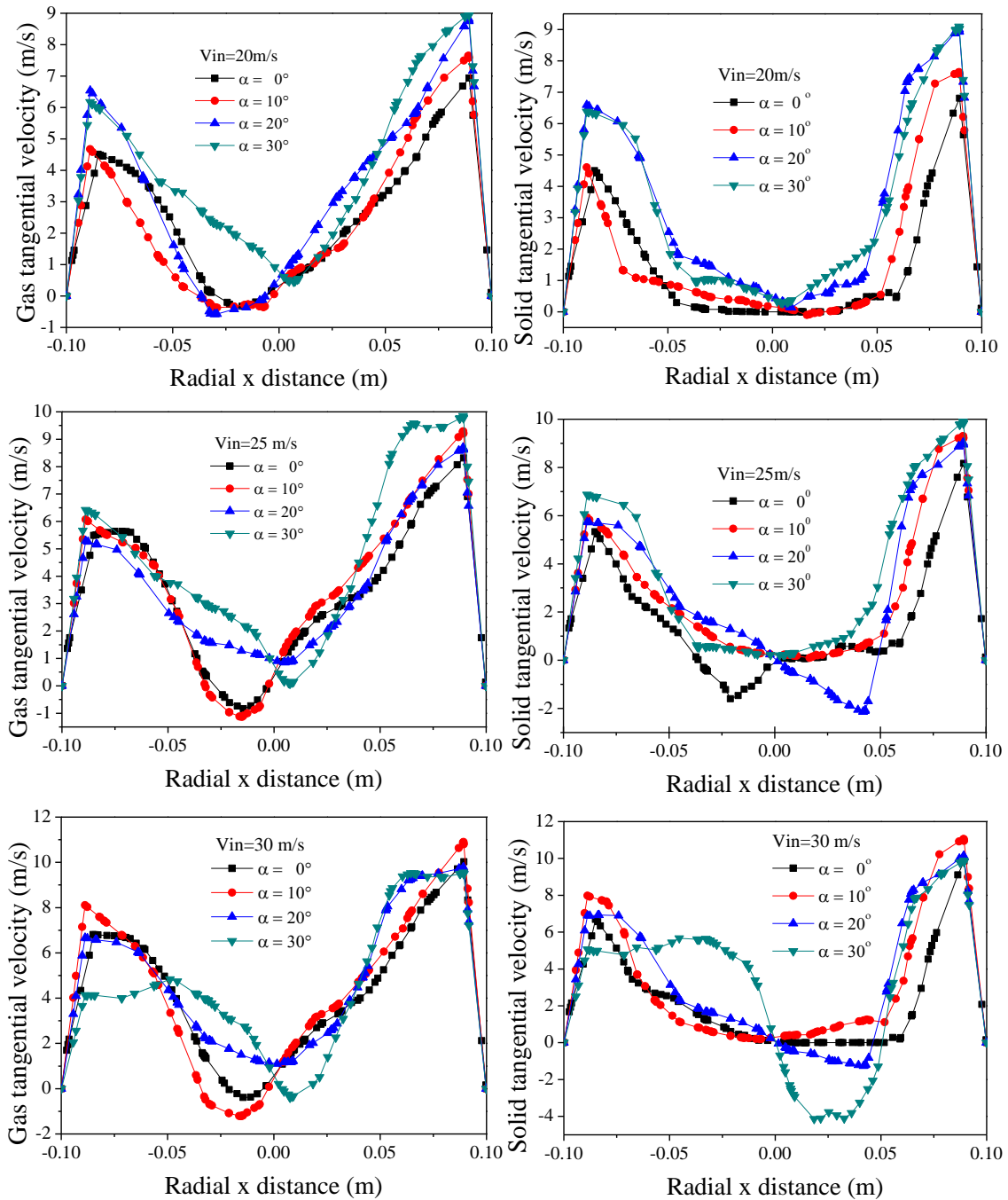


Fig. 3-16 Gas and solid tangential velocity with different inlet velocity

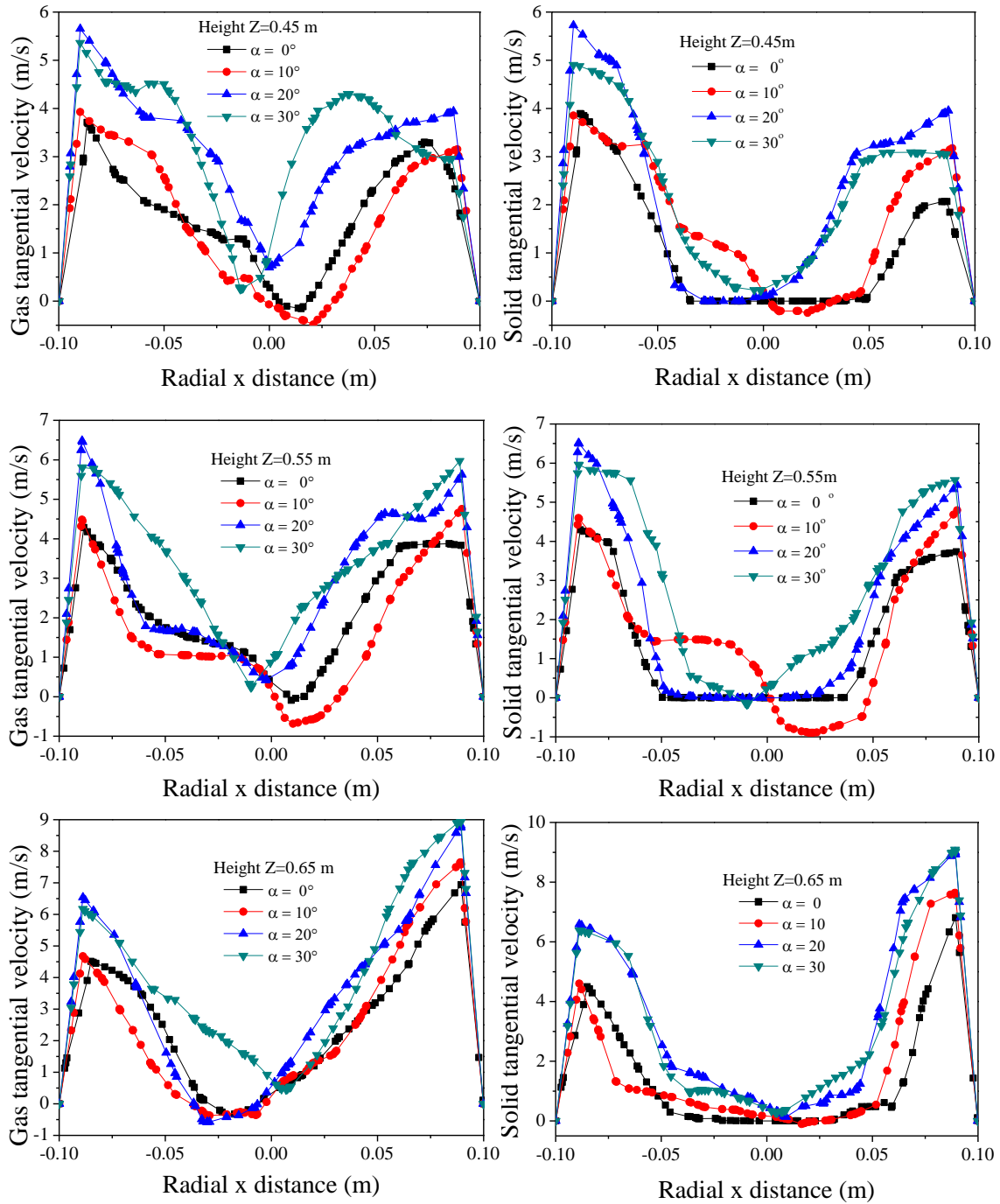


Fig. 3-17 Gas and solid tangential velocity distribution along the axis of cyclone with different heights

As shown in Figs. 3-14 and 3-17 this aspect seems to be irregular for high inlet velocity and also for the section not close to inlet cyclone. Cyclone with inlet configuration angle  $\alpha$  has the maximum tangential velocity in comparison with other cyclones. This means that increasing the cyclone inlet angle will enhance the

collection efficiency. Additionally with different inlet gas-solid inlet velocity the value of the tangential velocity is zero at the wall and at the center of the flow field

### 3.3.2.2 Effect on the Pressure Drop of Cyclone

Accordingly, in order to examine the effect of the inlet geometry on cyclone performance, Fig. 3-18 shows the results comparison of different inlet configuration pressure drop curves as function of inlet velocity. The calculation of pressure drop is made by the difference between exit and inlet area-weighted static pressure. RSM model was used as turbulence model. As shown in the Fig.3-18, the comparison shows fairly good agreement over the entire inlet angle  $\alpha$  there are no experimental data available for direct comparison. But there is some visible difference observed for the case of high inlet angle  $\alpha = 30^\circ$ . The explanation of this difference is not clear at this stage but is considered possibly due to the inlet geometry. As might be expected, for a given inlet flow velocity, the pressure drop generally increases with increase of inlet velocity.

To validate the simulations and test the reliability of the cyclone inlet angle  $\alpha$ , some detailed simulations and experiments literature for comparison with our numerical simulations were selected. This requires the full recuperation information about the geometry of the cyclone on the physical parameters and numerical simulations. The results obtained in this numerical simulation for different inlet angle are then compared with available data for dilute phase. This available data was performed by Wang et al.[10].

Wang et al.[10] used the RSM and stochastic Lagrangian model in the commercial software package Fluent to study the gas-solid flow in a typical Lapple cyclone separator. Physical experiments have also been conducted to validate their numerical model. In such an experiment, air was blown into the inlet of the cyclone. The inlet gas velocity and particle velocity were both 20m/s. the exit tube was open to the air and the gas pressure at the top of the vortex finder was 1 atm. The solid particle phase volume fraction was less than 10%. The material used was a typical cement raw material. Its particle size distribution can be well described by the Rosin-Rammler equation:

$$R(d) = \exp \left[ - \left( d / \bar{d} \right)^n \right] \quad (3-4)$$

where  $d$  is particle diameter, and  $R(d)$  means the mass fraction of droplets with diameter greater than  $d$ . The characteristic diameter  $\bar{d}$  equals 29.90  $\mu\text{m}$  and the

distribution parameter  $n$  is 0.806. The particle density is  $\rho_s=3320 \text{ kg/m}^3$ .

Fig.3-18 show the comparison between the simulation result and data from B. Wang et al.[10], despite the high values of pressure drop due to the different parameter (dilute and dense phase for example), as might be expected, for a given inlet flow velocity, the pressure drop increases with increase of inlet velocity.

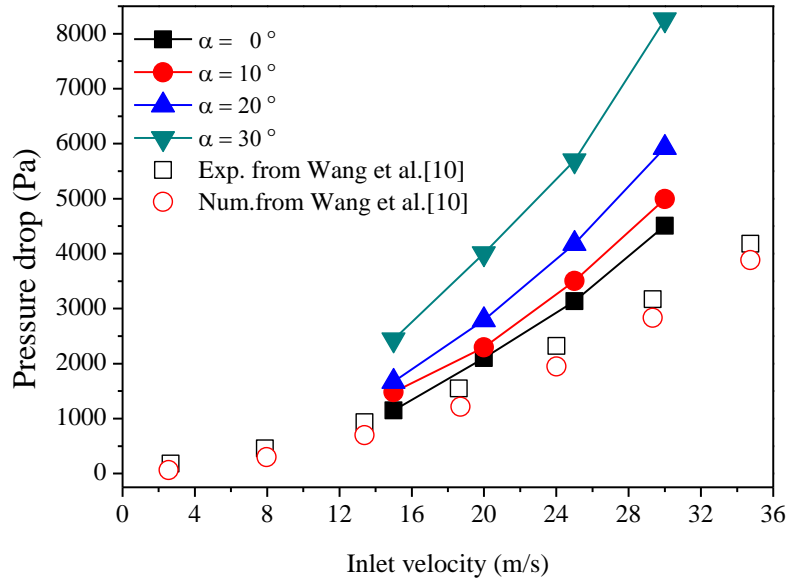


Fig.3-18 Comparison within four inlet configuration and the numerical and experimental data[10] with cyclone pressure drop

### 3.3.2.3 Effect on separation efficiency of cyclones

Cyclone designers have long known that the separation efficiency of tangential inlet cyclones improves with increasing solids loading. Even so, the exact mechanism for this improvement is still not established beyond doubt, in spite of many investigations of the topic.

In order to examine the effect of inlet geometry on the separator efficiency, Fig.3-19 shows the comparison results of separator efficiency as a function of inlet velocity, with the RSM turbulence model and solid volume fraction of 0.1. The overall efficiency can be seen to increase substantially with increasing inlet velocity for all case. The separation efficiency of cyclone with inlet configuration angle  $\alpha=0^\circ$  present high separation efficiency compare to  $10^\circ$ ,  $20^\circ$  and  $30^\circ$ . This indicates that the inlet configuration of the cyclone plays an important role in the collection efficiency similar to that in conventional cyclone separator for dilute flow.

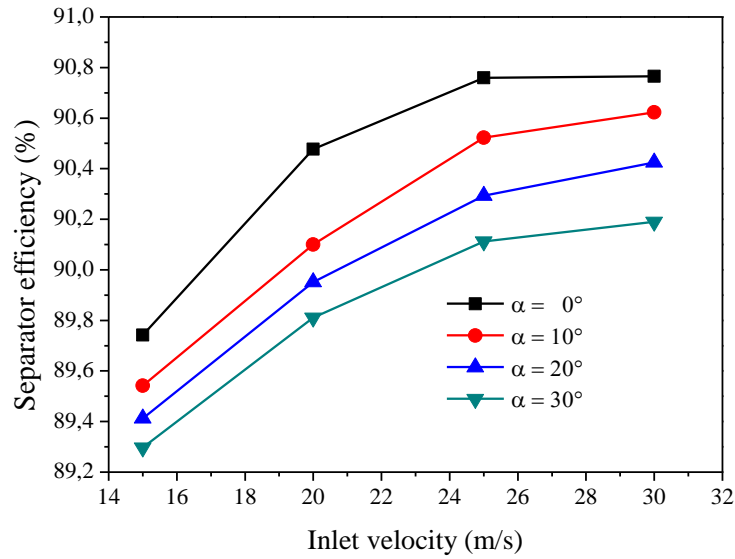


Fig.3-19 Separator efficiency for different inlet geometries as function of inlet velocity

### 3.4 Brief summary

The flow behavior of gas and particles has been simulated based on the Eulerian–Eulerian two-fluid modeling approach with KTGF in the conventional cyclone separator. A numerical simulation using CFD, based on the RSM and RNG k- $\epsilon$  model was studied in this chapter. Comparison of the results given by the velocity component, pressure fields and volume fraction can describe the turbulent flow.

Four cyclones of different inlet configuration have been simulated using RSM, to study the effect of cyclone inlet configuration on the cyclone separator performance and the field flow.

Based on the presented numerical simulation, results of this part are summarized as follows:

The tangential and axial velocities around the cylindrical section of the cyclone show that the RSM almost have an axial symmetry for different inlet velocities. However, the RNG k- $\epsilon$  model displays no axial symmetry.

High pressure near the wall of the cyclone due to centrifugal force creates a depression on the axis of the cyclone. The results of this study indicate that the pressure drop increases with increasing inlet velocities for both the RSM and RNG k- $\epsilon$  models, moreover the RSM gives a higher pressure drop compared to the RNG

k- $\epsilon$  model. Additionally, the RSM model provides well for the simulations of both the forced and free vortex.

The magnitude peak of tangential velocity in cyclone and pressure drop increase with increasing the cyclone inlet configuration angle. The separation efficiency of cyclone increases with inlet velocity, decreases with increase of inlet angle configuration, and it is significantly influenced by the inlet angle. This indicates that the inlet configuration of the cyclone plays an important role in the collection efficiency similar to that in conventional cyclone separator for dilute flow.

## **Chapter 4 Numerical study of square cyclone separators**

### **4.1 Introduction**

The cyclone separator is a key component in the operation of the circulating fluidized bed (CFB) boiler, which has great effects on the combustion efficiency, the circulation rate and the desulfurization efficiency, by the circulation of the solid particles of the furnace. The traditional circular cross-section cyclone was commonly used as a conventional cyclone separator for the CFB boiler. With the development of large CFB boilers, the huge body of the conventional cyclone became a major shortcoming because of the thick refractory wall that leads to the requirement for a long period to start the boiler.

Compared with the traditional circular cross-section cyclone, a square cyclone has many advantages over the conventional cyclone, due to convenience in construction, easier membrane wall arrangement, shorter start-stop time, and easy integration with the boiler[21].

All of the above mentioned researches results indicate that the square cyclone separators used in CFB boilers have high collection efficiency. However, the present contribution in this chapter aims to add more to existing knowledge on the functioning of square cyclones which represents one of the most recent applications of the technique of separation by centrifugal force.

CFD has a great potential to predict the flow field characteristics and particle trajectories inside the cyclone as well as the pressure drop[28]. The complicated swirling turbulent flow in a cyclone places great demand on the numerical techniques and the turbulence models employed in the CFD codes. CFD was widely used to investigate flow field inside conventional cyclones. Raoufi et al.[124] used computational fluid dynamics to simulate and optimize vortex of conventional cyclones. Although many numerical works have been conducted on conventional cyclones, there is a little numerical study of square cyclones.

As numerical investigations of square cyclones could have an important role in the better understanding of their flow parameters, this Chapter is intended to obtain

detailed flow information by CFD simulation within square cyclones in the case of downward gas-exit without a vortex. The square cyclones are modeled at different flow rates and flow fields are evaluated inside these square cyclones. Contours of pressure profiles and solid volume fraction within the cyclone are shown. Tangential velocity components profiles in different sections and different inlet flow are also investigated.

In the following sections the dense flow behavior of gas and particles within a square cyclone separator is simulated by means of computational fluid dynamics will be treated in detail. The RNG k- $\epsilon$  model and the RSM were used to model gas turbulence. The dispersed two phase flow behavior of gas and particles has been simulated based on the Eulerian-Eulerian two-fluid modeling approach with KTGF in the square cyclone separator. The flow behavior is examined in the term of tangential velocity components, static pressure and pressure drop contour plots for flow field and solid volume fraction. The effects of the turbulence model, solid volume fraction and the inlet geometry on the square cyclone will be discussed.

## **4.2 Numerical simulation methods**

### **4.2.1 Geometry configuration of four squares cyclones**

Traditional cyclone separators have a circular cross section and a tangential or helical inlet and have been widely studied by many authors both experimentally and numerically. Fig.4-1 shows the geometry of the square cyclone used in the studied cases, which is close to that of Su and Mao[25] without vortex finder. The dimensions of square cyclone and the model parameters are shown in Table 4-1. As seen in the figure the cyclone separator model, which has a square cross-section, and was made up of a square body without vortex finder a rectangular inlet connected to the cyclone body and cylindrical downward gas-exit.

Note that in this present chapter the simulation were performed with 5 different square cyclones. Fig. 4-1 and Table 4-1 show only the square cyclone used in this section, the four other cyclone have more detail in Section 4.3.4 of this Chapter.



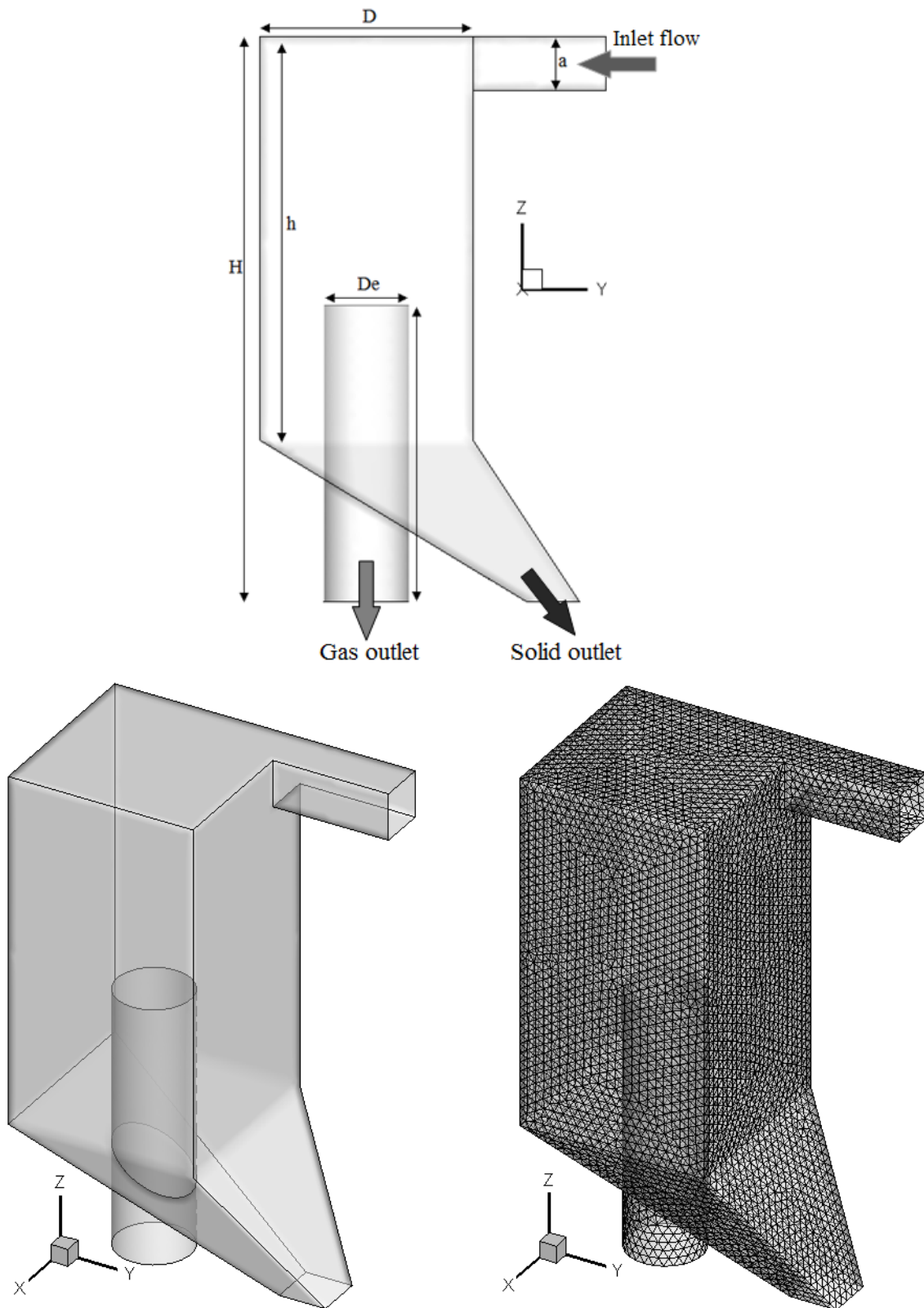


Fig. 4-1 Geometry dimension 3D geometry and grid of the square cyclone use in the first section of this chapter

Table 4-1 Dimensions of the cyclone and the models parameter used in the simulation

Notation	Parameter	Value(s)	Units
H	Cyclone height	1.05	m
h	Square body height	0.75	m
D	Square body width	0.40	m
S	Gas exit tube length	0.55	m
De	Gas exit diameter	0.16	m
a	Inlet height	0.06	m
b	Inlet width	0.06	m
$d_s$	Solid diameter	150	$\mu\text{m}$
$\rho_s$	Solid density	2400	$\text{kg/m}^3$
$\alpha_s$	Solid volume fraction	0.1, 0.01 and 0.05	--

#### 4.2.2 Turbulence model

For the turbulent flow in cyclones, the key to success of CFD lies with the accurate description of the turbulent behavior of the flow[28]. To model the swirling turbulent flow in a cyclone separator, there are number of turbulence models available in Fluent. These range from the standard k- $\varepsilon$  model to more complicated RSM. Also LES methodology is available as an alternative to the Reynolds average Navier-Stokes approach. In this part RNG k- $\varepsilon$  and RSM were used to model gas turbulent flow.

#### 4.2.3 Gas-solid two phase flow model

Flows in cyclone separators are multiphase. The flow in square cyclone in this study consists of gas and solid particles. Two phase flows can be solved by a number of CFD techniques. These include the Eulerian Approach, simplified Eulerian approaches and the Lagrangian approach. In this study, the inlet solid volume fractions  $\varepsilon_s$  are 0.1 and 0.01 corresponding to a high dispersed phase concentration and therefore a dense two-phase flow regime. In the case of the dense regime, interparticles becomes of importance, both physical collisions and indirect influence through the nearby flow field, also limitations related to computer storage,

calculation times and convergence arise. In those cases, the Eulerian approach where a set of continuity, momentum and turbulence equation for each phase is therefore becomes more adequate. The conservation and transport equations for phase were developed in Chapter 2.

#### 4.2.4 Boundary condition

The velocity inlet boundary condition prescribed at inlet boundary faces. At the inlet, all velocities and volume fractions of both phases were specified. The pressure was not specified at the inlet because of the incompressible gas phase assumption. At the outlet, only the pressure was specified atmospheric. No slip condition was adopted at the wall.

#### 4.2.5 Grid independence studies

The tetrahedral computational grids were generated using GAMBIT grid generator. The grid independence study has been performed for the square cyclone. Three levels of grid have been tested, to be sure that the obtained results are not grid dependent.

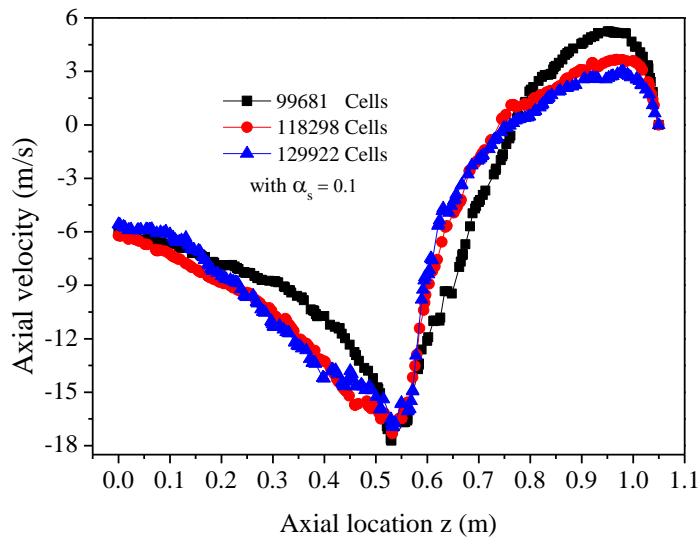


Fig.4-2 Axial velocity of gas distribution along z-axial direction at the three different grid sizes

Three levels of mesh 99681, 118298 and 129922 cells have been used. As shown in Fig.4-2, the grid with 99681 cells gives a high axial velocity near the inlet and a low axial velocity close at the bottom in the axial direction, while the grid with 118298 and 129922 show the same trends in the axial direction. Thus, for

excluding any uncertainty, computations have been performed using the 118298 cells grid.

### 4.3. Validation of the numerical model

In order to validate the obtained results, it is necessary to compare the prediction with experimental data. The comparison performed with the experimentally measurements of Su and Mao [25] and CFD model of Shams et al. [125] are present as follow.

Su and Mao employed a three-dimensional Particle Dynamic Analyzer (3D-PDA) to measure the gas–solid two-phase flow in a lab-scale square cyclone separator with downward gas-exit under several cases. The separator used by Su and Mao was a square one and its edge length its edge length was 120mm, body height 180 mm. The diameter of the vortex finder and the exhaust exit were both 60mm. The height of the vortex finder was 90mm. The distance between the bottom of the vortex finder and the top of the exhaust was 60mm. The separated particles were collected by a discharge bin. The exhaust gas went through the downward exit to open air by an induced blower. The particle used was glass beads of mean diameter 30–40  $\mu\text{m}$  and of density 2400  $\text{kg/m}^3$ . The data use there is the velocity distribution at the plane located at 120mm from the top of cyclone.

Shams et al used a CFD method to predict and evaluate the flow field inside a square cyclone. In their study, the RSTM is used to simulate the Reynolds stresses, the Eulerian-Lagrangian computational procedure is implemented to predict particle trajectory in the cyclone. The simulations are performed for two cyclone types with different geometries have been studied experimentally by Su and Mao [25] and Wang [10]. The second case study by Shams is present there, this case studied has exhaust gas through downward exit, and the particle used was glass beds of mean diameter of 30-40  $\mu\text{m}$  and density of 2400  $\text{kg/m}^3$ . The simulations are performed at inlet velocities of 20, 25.3 and 28.32m/s.

The present simulations are compared with measured and CFD simulation of z-velocity distribution of Su and Mao and Shams et al.[125] at the cross-section located at 0.7m from the bottom of cyclone and at 120mm from the top for two available data. As shown in Fig. 4-3, the present simulation matches the experimental velocity profile with overestimation of the z-velocity in left side of

cyclone, and underestimation of the z-velocity in right side. Considering the complexity of the turbulent swirling flow in the square, the agreement between the present simulation and measurements is considered to be quite acceptable.

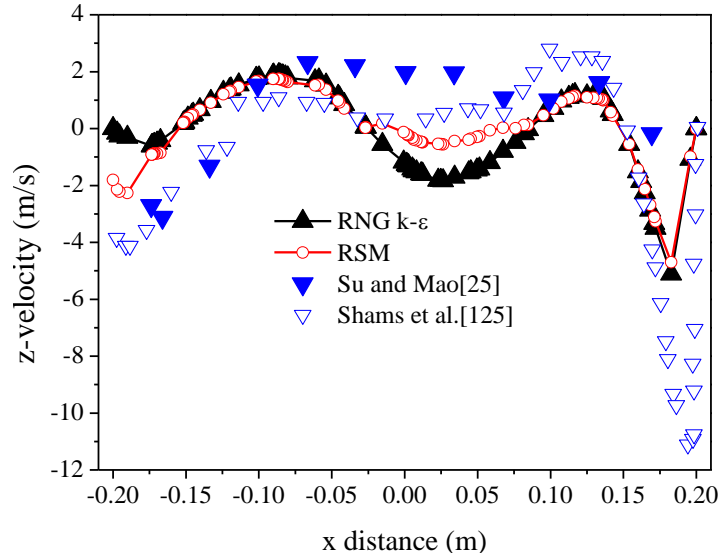


Fig. 4-3 Comparison of the z-velocity between the experimental data from Su and Mao [25], the numerical data from Shams et al. [125] and the current model result at 0.7 m from the cyclone bottom, the inlet velocity is 22m/s and solid volume fraction  $\alpha_s = 0.1$ .

## 4.4 Results and discussions

### 4.4.1 Comparison of turbulence model

In the first step of this chapter, the simulations are performed for the square cyclone without angle ( $\alpha = 0^\circ$ ). A schematic of the geometry of a square cyclone separator and its corresponding numerical grid is shown in Fig. 4-1. As indicated in Fig.4-1 the exhaust gas through a downward exit open to the air, and the surrounding pressure is at 1 atm. To solve the equations listed in Chapter 2, we need appropriate boundary conditions for the velocities of the gas and the solids phases, pressure, and the granular temperature. Initially, the volume fraction of particles in the square cyclone separator is provided and the gas velocity inside the square cyclone separator is set to zero. At the inlet, a uniform distribution is assumed for the velocity components, kinetic energy of turbulence, and energy dissipation rate of the gas phase. All velocities and volume fractions of the gas and solid phase are specified. The particulate material has a density and diameter of  $\rho_s = 2400 \text{ kg/m}^3$  and  $d_s = 0.150 \mu\text{m}$  respectively and solid volume fraction of  $\alpha_s = 0.1$  was used.

The simulations are performed at inlet velocity of 14, 18, 20, 22, 24 and 28 m/s and the RNG  $k-\epsilon$  model and RSM are selected as turbulent model to simulation gas-solid two-phase flow in square cyclone separator.

#### 4.4.1.1 Velocity distribution

The gas and particle phase velocities vectors at the cyclone cross-section  $z=0.85\text{m}$  are shown in Figs. 4-4 and 4-5 for RNG  $k-\epsilon$  and RSM model respectively.

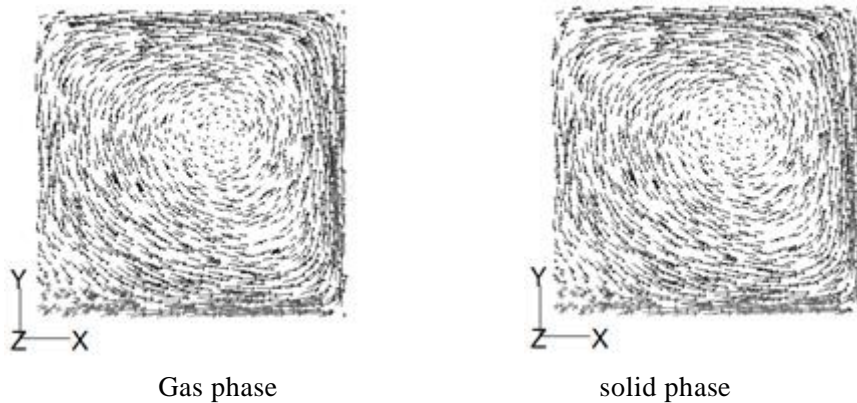


Fig. 4-4 Velocity Vector for gas and particle at the cross section at  $z = 0.85\text{ m}$  for RNG  $k-\epsilon$  model

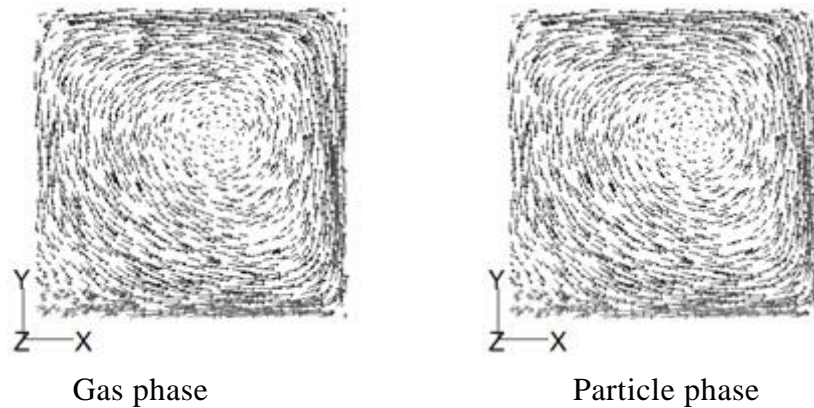


Fig. 4-5 Velocity vector for gas and particle at the cross section at  $z = 0.85\text{ m}$  for RSM model

For both two model the gas-solid flow entered the square cyclone at inlet velocity and directly impinged on the corner wall facing the inlet. There was an eddy at the corner facing the inlet. The flow turned its direction sharply and the particles impacted the wall strongly. Some of the impacting particles rebounded from the corner wall and were carried away by the gas flow. Some of them were deposited and fell down along corner surface. Moreover the corner is one of the

major regions to cause pressure drop and was found to be beneficial to particle separation mainly because the strong fluctuating flow consumed much of the kinetic energy of both the particle and gas.

#### 4.4.1.2 Pressure fields

In this part the comparative studies of two turbulence models, the RSM and a variation of the k- $\epsilon$  model based on RNG k- $\epsilon$  was evaluated. Simulations were compared with pressure fields.

Fig. 4-6 and Fig.4-7 show the profiles of pressure drop and static pressure respectively. Fig. 4-6 shows that the pressure drop increase with increasing inlet velocity and a slight increase in pressure of the RSM model compared to the RNG k- $\epsilon$  model.

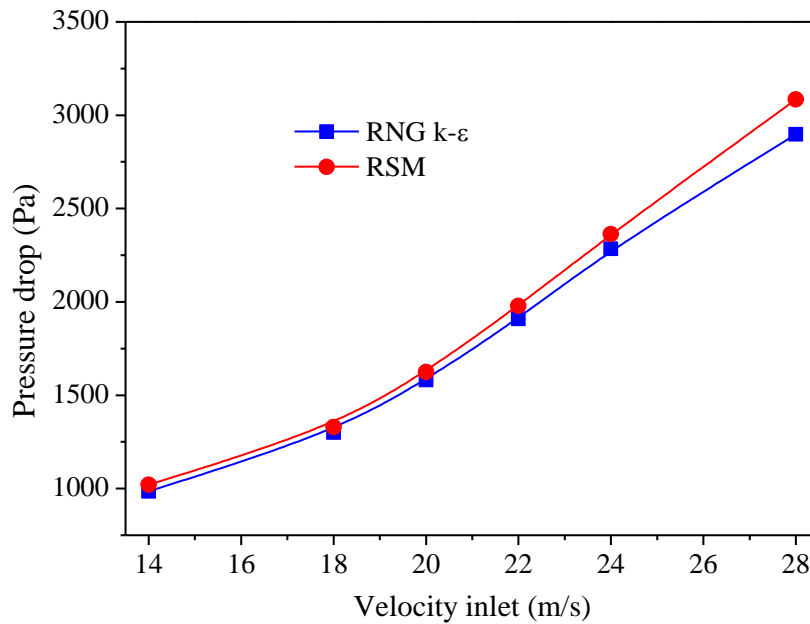


Fig. 4-6 Profile of Pressure drop

Fig. 4-7 shows the profile of static pressure according to the height of cyclone at part of cyclone  $z = 0.60$  m. The results show that the airflow causes depression as a swirl at the center of cyclone, similar to the conventional cyclone. Also the static pressure decreases radial from wall to axis of the cyclone and the pressure is increased for the RSM model near the walls, Fig.4-8 contours of static pressure gives a clear illustration of this phenomenon. Although the pressure distribution showed acceptable agreement for all models the RSM gives a higher-pressure drop compared to the RNG k- $\epsilon$  model.

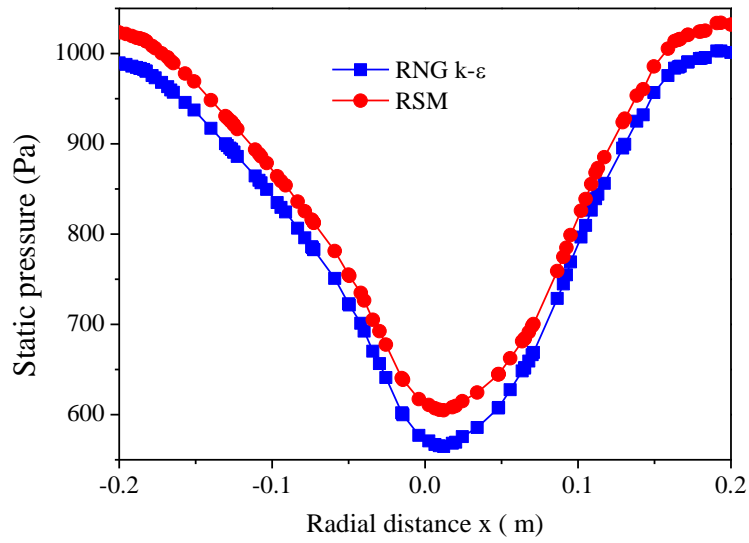


Fig.4-7 profile of static pressure in x-coordinate

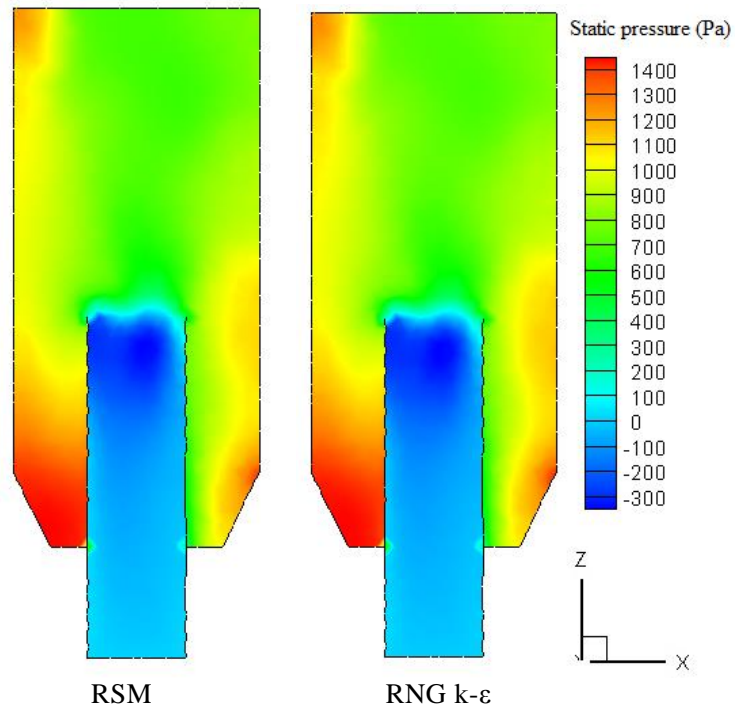


Fig.4-8 Contour plot of static pressure with two different turbulence models at x-plane of cyclone

#### 4.4.1.3 Solid volume fraction

Simulation results showed that the particle volume fraction increased and reached annular bed condition instantly after startup under the action of gravitational force.



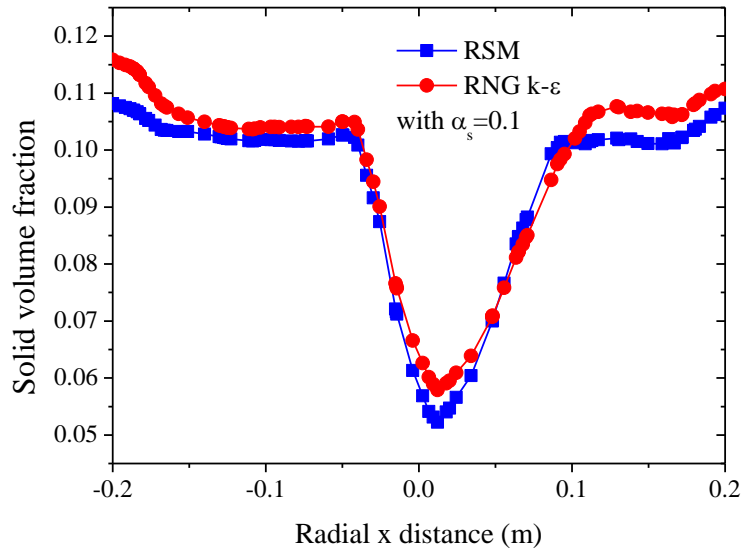


Fig.4-9 Profile of solid volume fraction with x-coordinate

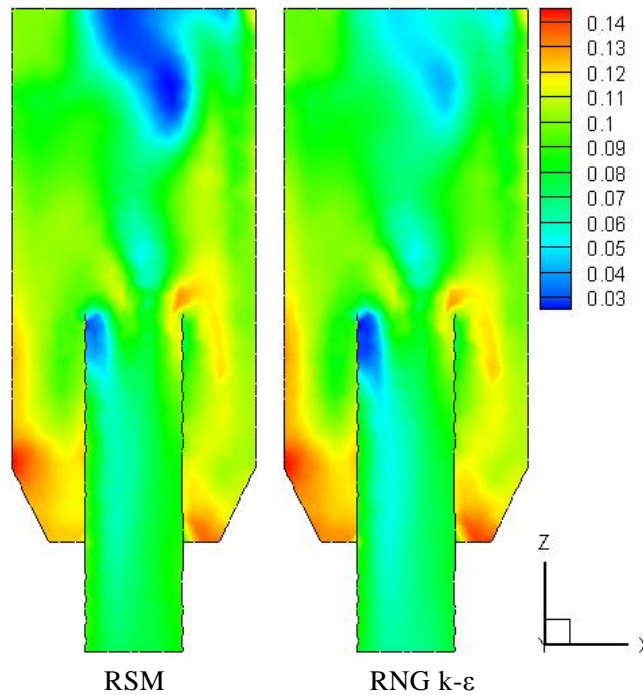


Fig. 4-10 Contour plot of solid volume fraction at x-plane of cyclone

Fig. 4-9 present the profile of particle volume fraction for RSM and RNG k- $\epsilon$  model at  $H=0.65\text{m}$  height of cyclone along the x-radial direction. The results show that particle concentration along the radial direction of cyclone can be divided into two regions: the central region of the cyclone area with low particle concentration and the wall region with high particle concentration. The gas and particle flow to the wall, leading to increased particle concentration near the wall of cyclone.

Fig.4-10 shows the particle volume fraction at the x-z plan section of cyclone for all turbulence models, moreover these figure show that volume fraction distribution is not symmetrical.

#### **4.4.1.4 Separation efficiency**

In addition to pressure drop, separation efficiency is also considered an important parameter in the evaluation cyclone performance. Generally, an increase in inlet velocity will increase the separation efficiency of the cyclone; this will also increase the pressure drop. Some available data in literature review were selected to compare the obtain results, experimental computing conditions should be mentioned.

As mentioned earlier in the literature review, the new inlet type, which is different type of inlet from that used by former researchers was developed and experimental study by Zhao et al.[26]. Zhao et al. research were performed under the following conditions: the solid particle used were talcum powder obeyed by log-normal size distribution with skeletal density of  $2700\text{kg/m}^3$ , with a concentration of  $50\text{g/m}^3$ , mass-mean diameter of  $5.97\mu\text{m}$  and geometric deviation of 2.08. The mean atmospheric pressure, ambient temperature, and relative humidity during the tests were 99.93kPa, 293K and less than 75%, respectively. Noted that the cyclone with conventional single inlet Model A, with inlet velocity of 12, 16, 20 and 24 m/s were selected and presented there in the term of collection efficiency for our comparison.

The data from Wang et al.[10] has been presented above in Section 3.3.2.2, in this section were are interested in the collection efficiency both numerical and experimentally studied by Wang et al.[10].

As shown in Fig.4-6, the pressure drop increases with the inlet velocity. Fig.4-11 shows the comparative measured separation efficiency of the square cyclone as a function of inlet velocities compared to the results of Wang el al.[10] and Zhao et al.[26] for a conventional cyclone. As can be seen in Fig.4-11, the influence of inlet velocity on separation efficiency for dense particle concentration is apparent. In a conventional cyclone it is usually expected that an increase in inlet velocity will increase separation efficiency. This has been found by both experimental and numerical studies to be the case by Zhao et al. [26] and Wang et al.

[10]. The results presented here demonstrate that with an increase in inlet velocity a square cyclone will have an increased separation efficiency in a similar manner to a conventional cyclone. The results presented here also demonstrate that the collection efficiency of the square cyclone differs depending on the model used. The collection efficiency of a cyclone modeled with the RSM model is higher than that modeled with RNG k- $\epsilon$  model.

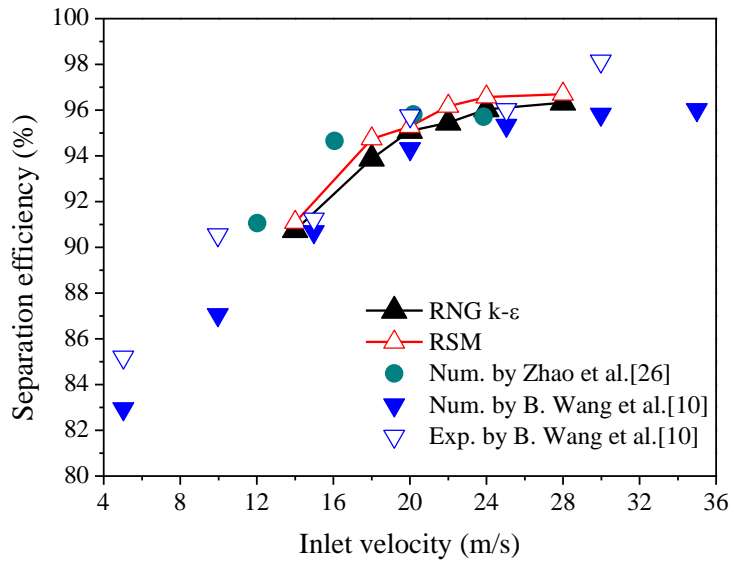


Fig.4-11 Separation efficiency of the cyclone at different inlet velocity

#### 4.4.2 Effect of solid concentration on square cyclones

The following section examines simulations performed in three cases with different solid volume fractions: Case A with solid volume fraction 0.01; Case B with solid volume fraction 0.05 and Case C with solid volume fraction 0.1. RSM is selected in these cases as turbulent model to simulation gas-solid two-phase flow in square cyclone separator with three different inlet volume fractions.

##### 4.4.2.1 Flow fields

Experimental measurements of the velocities in square cyclone separator without a vortex finder do not exist to validate the velocity prediction at present, but the predicted velocity field is seen to be similar to the conventional cyclone separators. Only the tangential velocity components are presented here since the contour of the velocity magnitude within the cyclone are almost identical with those of tangential velocity. Additionally within the cyclone the tangential velocity is the dominant velocity component. It should be noted that the tangential velocity

distribution inside a square cyclone basically agrees with the rotational flow that consists of inner forced and outer free vortexes. In this part the tangential velocity is investigated in the different heights of cyclone and different inlet velocities.

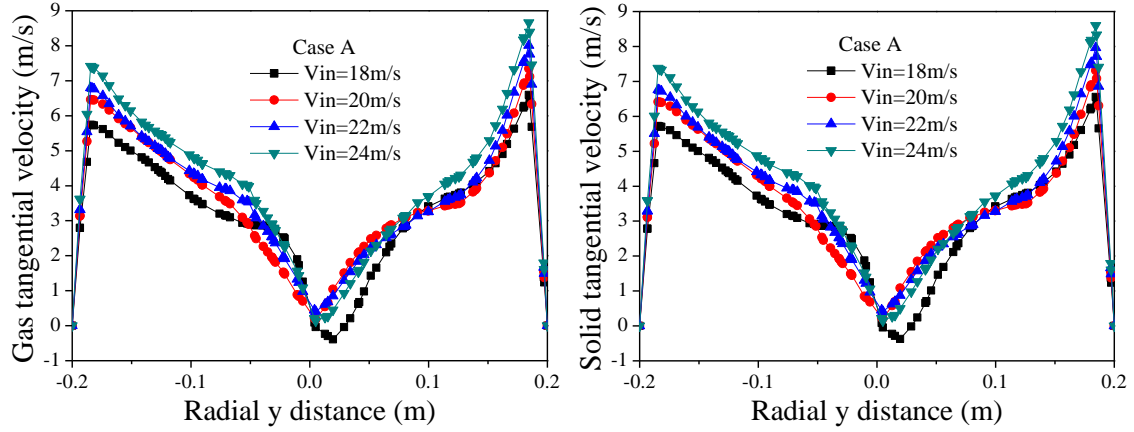


Fig.4-12 (a) Gas and solid tangential velocities with different inlet velocities for Case A

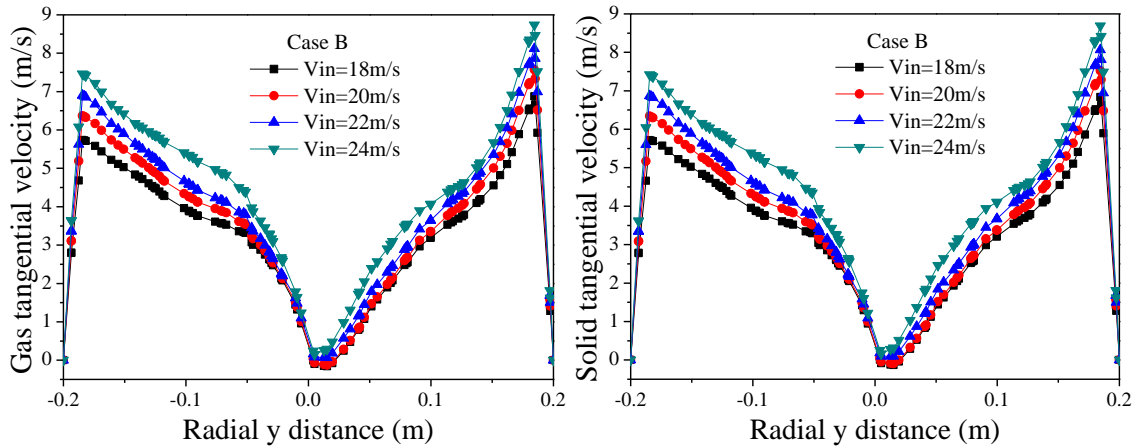


Fig.4-12(b) Gas and solid tangential velocities with different inlet velocity for Case B

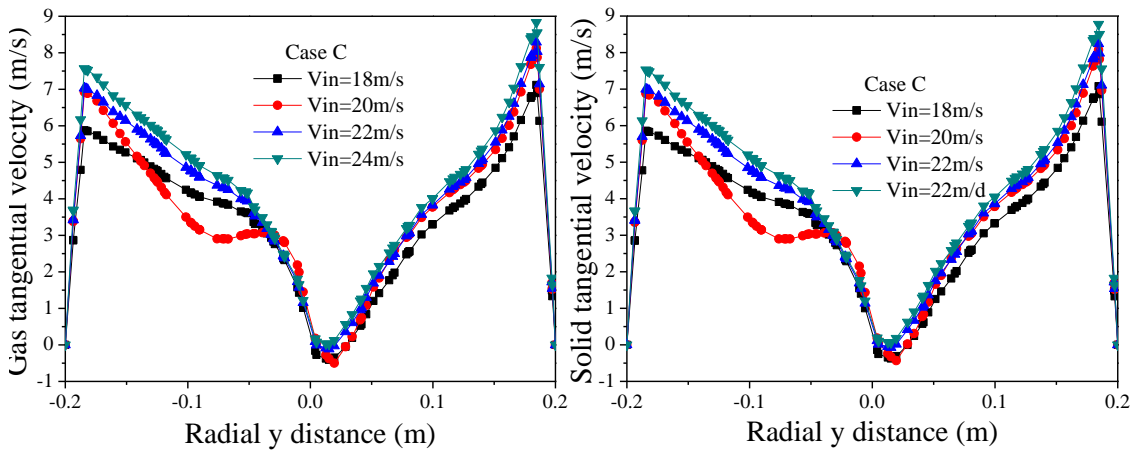


Fig.4-12(c) Gas and solid tangential velocities with different inlet velocity for Case C

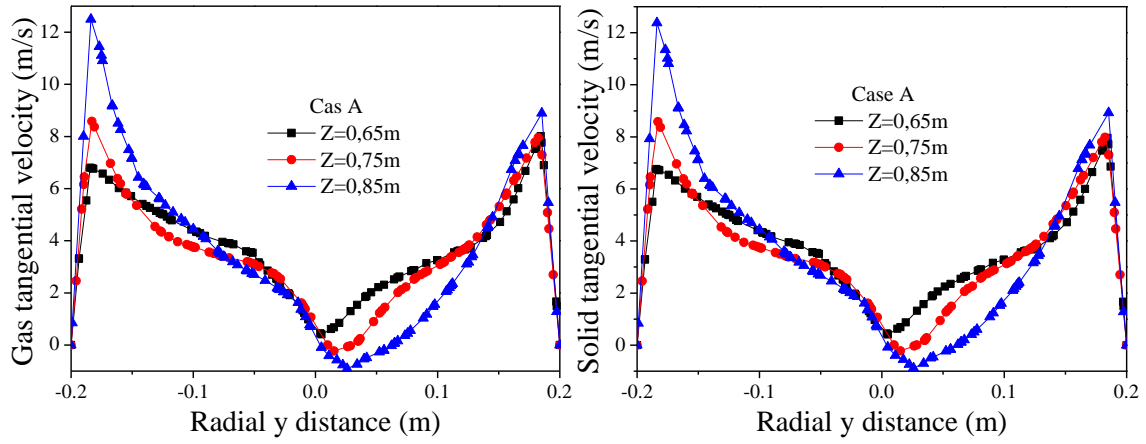


Fig. 4-13(a) Gas and solid tangential velocities at three axial locations of cyclone: Case A

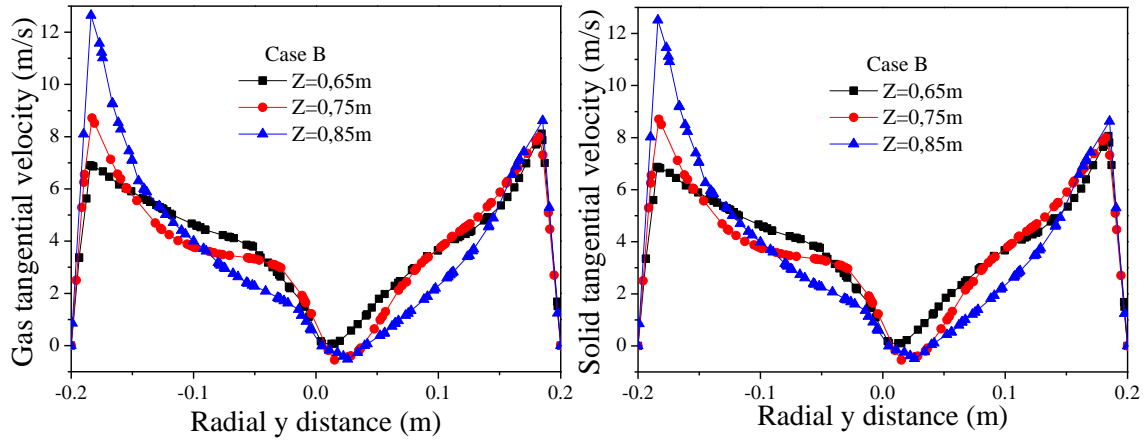


Fig. 4-13(b) Gas and solid tangential velocities at three axial locations of cyclone: Case B

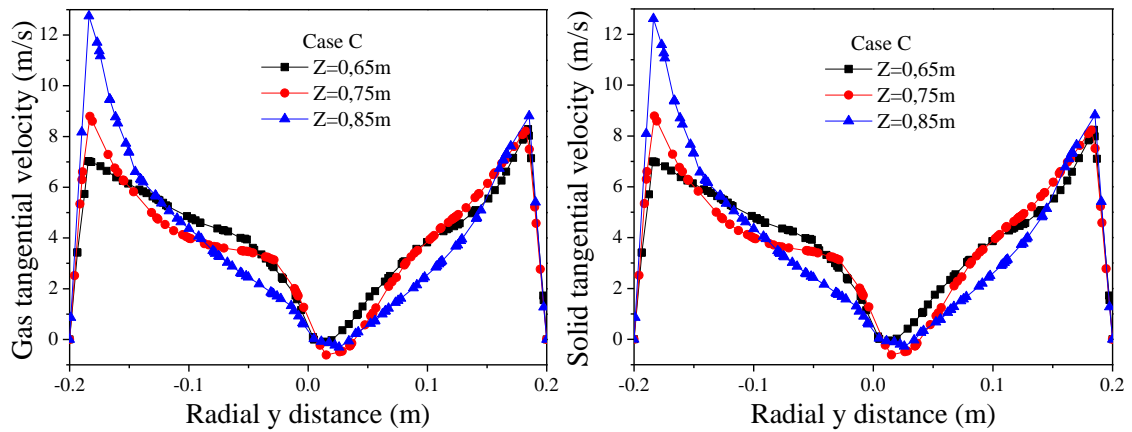


Fig 4-13(c) Gas and solid tangential velocities at three axial location of cyclone: Case C

Fig.4-12 presents the gas and solid tangential velocities at different inlet

velocities (a) Case A and (b) case B and (b) Case C respectively. The results show that the tangential velocity magnitude increased by increasing the inlet velocity for three cases studied, the values of tangential velocity equals zero on the wall and at the center of the cyclone and have negative value for low inlet velocity for all cases. Additionally, for all cases the tangential velocity distributions are not symmetrical.

Figs. 4-13 show the profiles of the tangential velocity along the radial orientation at different heights of the square cyclone for all cases. For different volume fractions the tangential profiles show that inside the square cyclone the swirling flow consist of an outer free vortex and inner forced vortex close to center, these results are seen to be similar to those in conventional cyclones. Moreover, in the inner region the tangential velocity is relatively similar at different heights of square cyclone for both two cases. The tangential velocity distribution in the outer region is rather similar at different height of square cyclone for Fig.4-13(a) and is completely different for those in Fig.4-13(b). Note that increases of solid inlet volume fraction also effect the tangential velocity distribution.

#### 4.4.2.2 Pressure fields

One of the most important parameters in the investigation of cyclone performance is the pressure drop in the cyclone. Figs. 4-14 present the radial profiles of static pressure at  $z = 0.60$  m from the bottom of cyclone for different cases studied. The static pressure shows the low pressure zone in the center of the cyclone for each inlet velocity and for different cases studied.

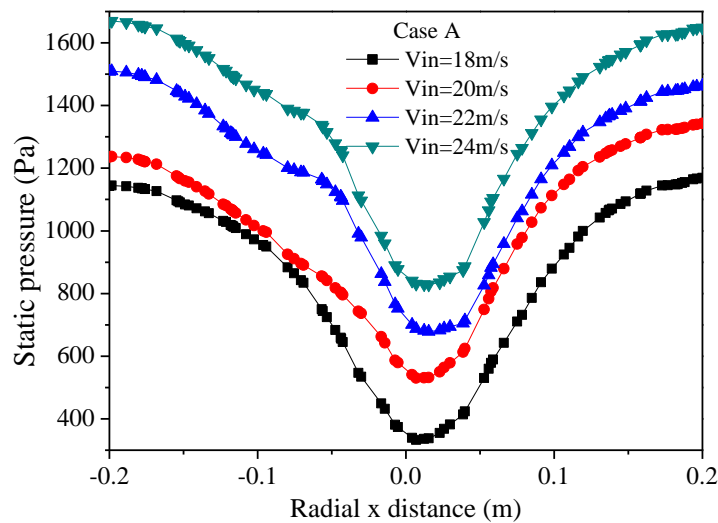


Fig. 4-14 (a) Profile of static pressure with different solid volume fractions as function of different inlet velocity: Case A

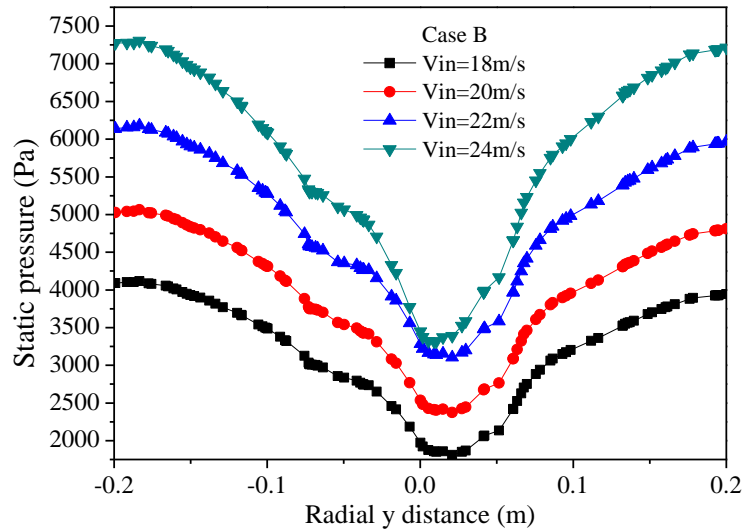


Fig. 4-14 (b) Profile of static pressure with different solid volume fractions as function of different inlet velocity: Case B

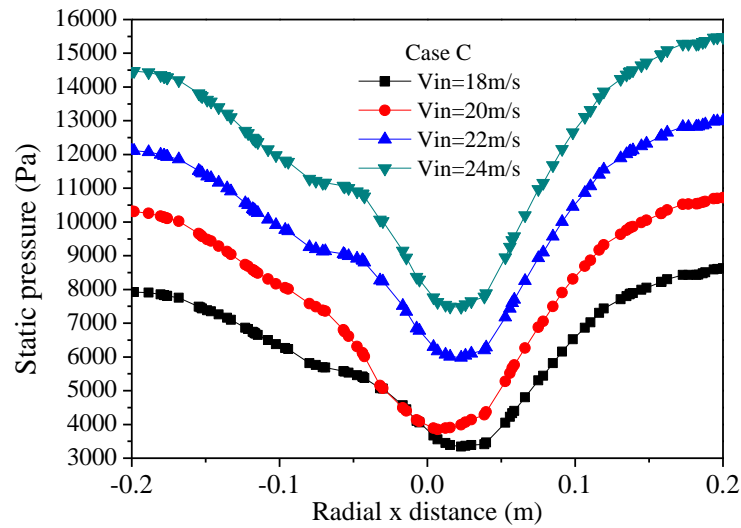


Fig. 4-14 (c) Profile of static pressure with different solid volume fractions as function of different inlet velocity: Case C

As seen in the Fig. 4-14, within the square cyclone the static pressure decreases radially from wall to axis. Moreover, the Figure of Case C gives higher static pressure compared to the Cases A and B. Comparison between pressures drops of the square cyclone in three cases are presented in Fig.4-15 respectively with different cases studied. The pressure drop increases with increased inlet velocity and for high solid volume fraction the results gives a higher-pressure drop compared

to those in low solid volume fraction. The pressure drop increase proportionally with inlet solid volume fraction.

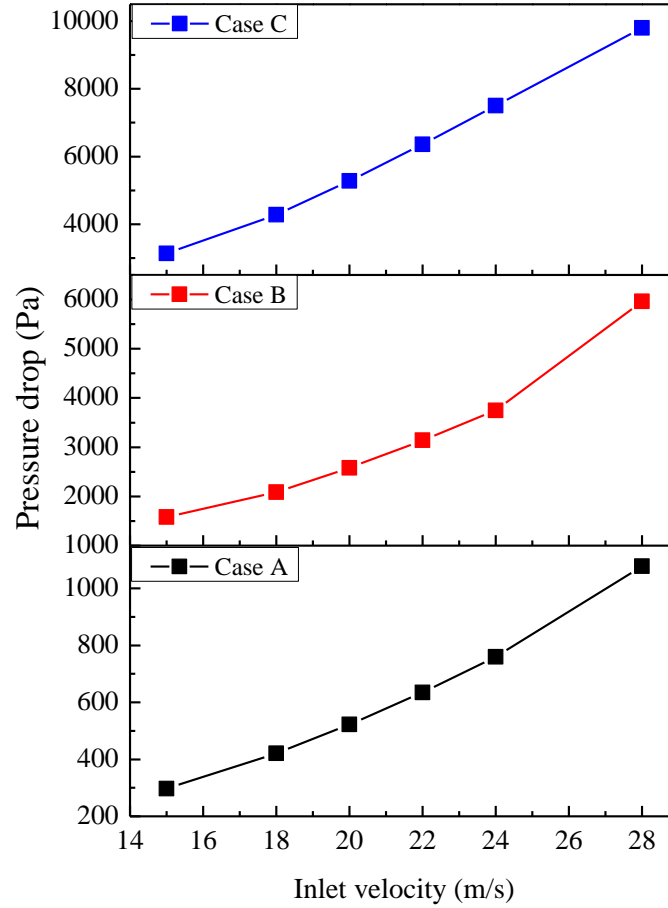


Fig. 4-15 Profile of pressure drop with different inlet velocity

#### 4.4.2.3 Collection efficiency

The results of collection efficiency with three different inlet solid volume fractions are present in Fig.4-16 as function of gas inlet velocity. For a different inlet solid volume fraction, a tendency of collection efficiency increase with increasing with inlet velocity is observed. Because the tangential velocity inside the square cyclone separator increases with the increasing inlet gas and solid velocities, which leads to the increase of centrifugal forces, therefore, the collection efficiency increases accordingly. As can be seen from Fig.4-16, the influence of inlet solid volume fraction on collection efficiency is obvious; the collection efficiency for Case C which is higher than other cases.



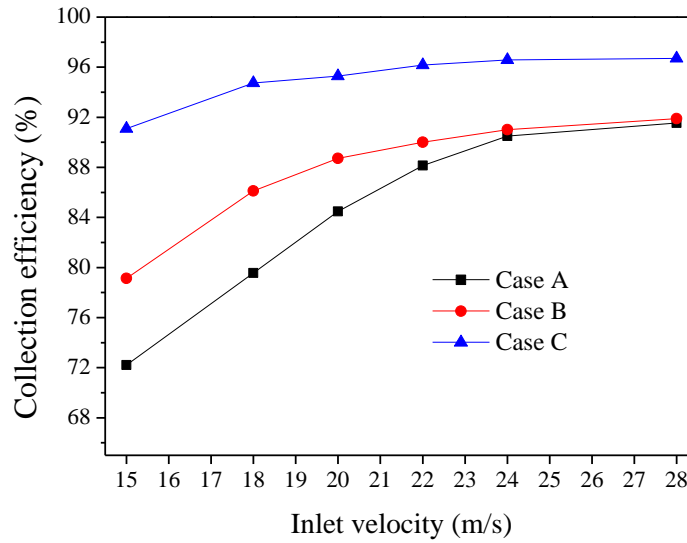


Fig.4-16 Cyclone collection efficiency for different cases studied

#### 4.4.3 Effect of inlet configuration on square cyclone separators

As numerical investigations of square cyclones could have an important role to better understanding of the flow parameters, this part is intended to obtain detailed flow information by CFD simulation within square cyclones. A square cyclone investigated by Su and Mao [25] is simulated numerically, with the variation of different inlet geometries. The square cyclones are modeled at different flow inlet velocity and flow fields are evaluated inside these cyclones. Profiles of pressure and collection efficiency within the square cyclones are shown. Tangential velocity profiles and velocity vectors in different sections are investigated.

Three dimensional CFD simulation was carried out for the square cyclone separator with the above four types of inlet configurations. Equations were solved numerically by the finite volume method using the commercial CFD code Fluent 6.3.23, in which the control volume method was used to discretize the transport equations.

As mentioned earlier in Section 4-2, the simulations were performed on five square cyclones separator with different geometries, which four have been simulate there with different inlet geometries configuration angle  $\alpha$ . These cyclones had a reversed flow tangential inlet. The geometry and dimensions of cyclones are shown in Fig.4-17 and Table 4-2.

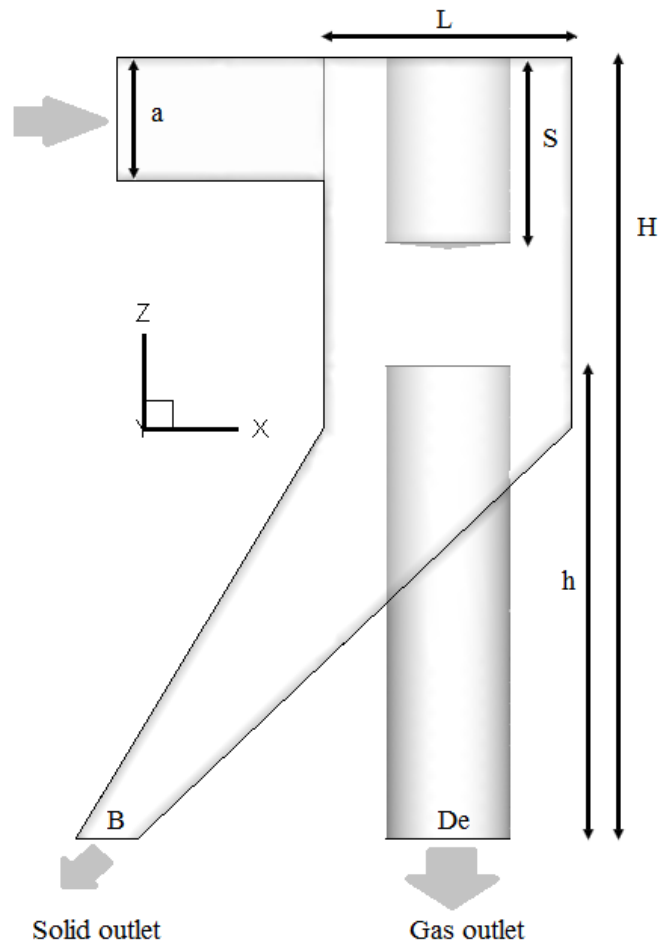


Fig.4-17-(a) Geometry of cyclone with different inlet configuration

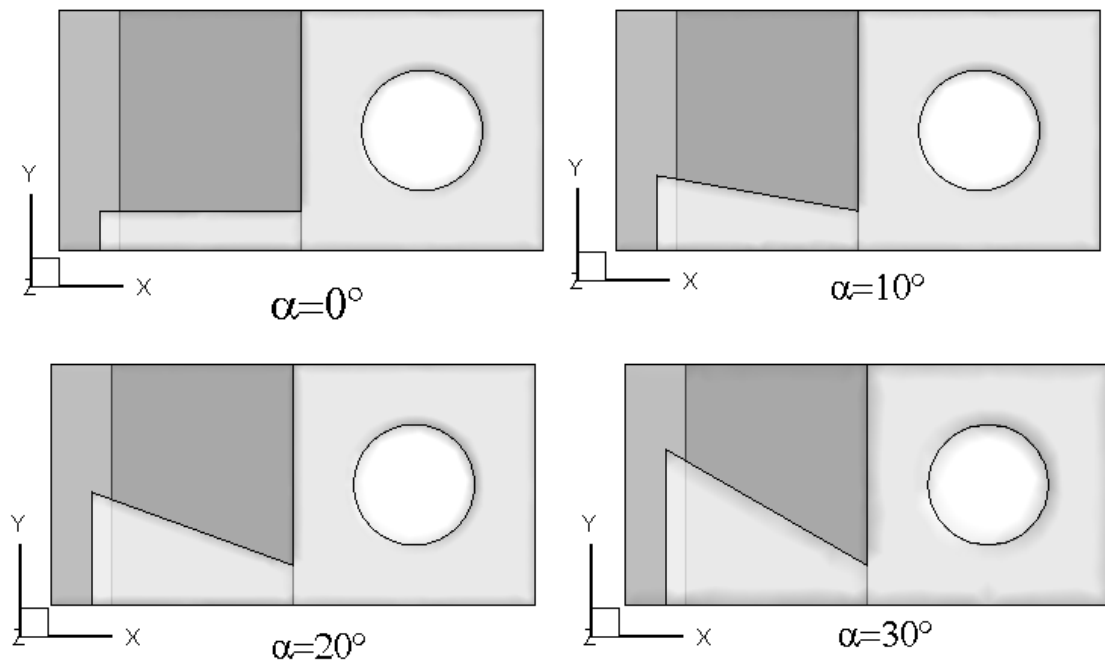


Fig. 4-17 (b) yx-plane geometry for four types of inlet configurations of square separator

Table 4-2 the dimensions of the cyclone used in the simulations.

Notation	Units	Parameters	Values
H	m	Square cyclone length	0.38
h	m	Exit tube length exit gas	0.23
S	m	Vortex finder length	0.09
D	m	Square cyclone width	0.12
De	m	Gas exit diameter	0.06
a	m	Inlet height	0.06
b	m	Inlet width	0.02
$\alpha$	°	Inlet angle	0, 10, 20 and 30

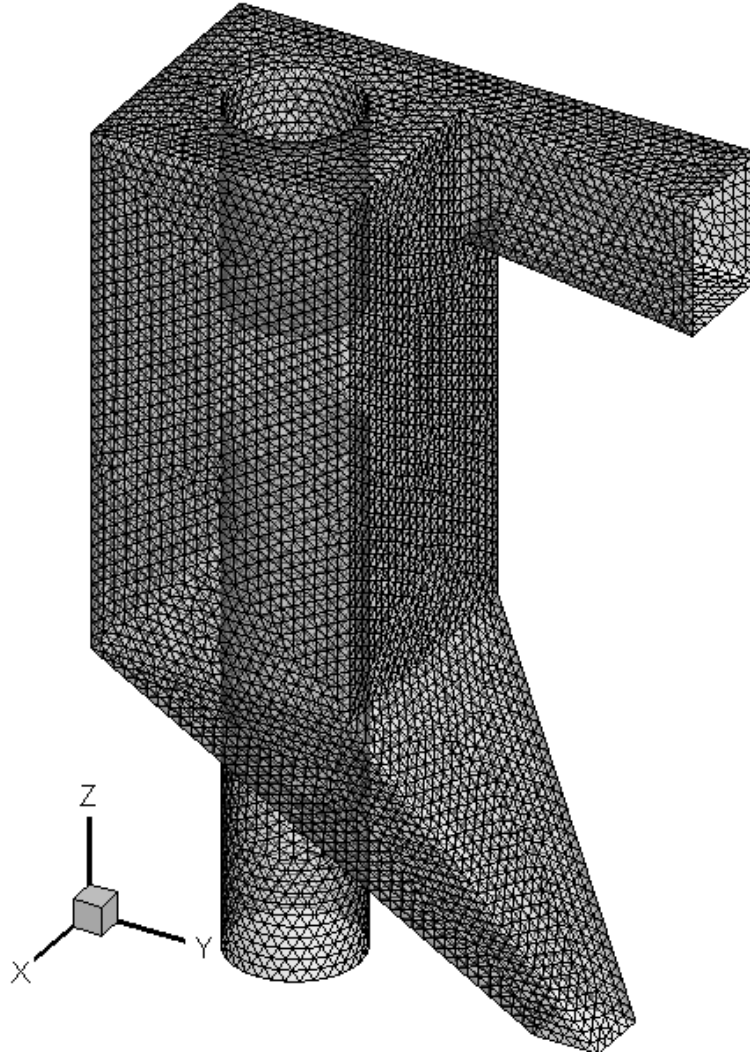
Table 4-3 Models parameters used in the simulations.

Notation	Units	Property	Value(s)
$d_s$	$\mu\text{m}$	Solid diameter	150
$\rho_s$	$\text{kg/m}^3$	Solid density	2400
$\varepsilon_s$	/	Solid volume fraction	0.1
$\rho_g$	$\text{kg/m}^3$	Gas density	1.225
$\mu_g$	$\text{kg/m-s}$	Gas viscosity	$1.789 \times 10^{-5}$
$V_{in}$	m/s	Inlet velocity	15, 20, 25 and 30

The gas-solid turbulent flow and separation processes in square cyclone separators are numerically modeled by the CFD method. The RSM is used to simulate the gas flow and the flow behavior of gas–solid phases was predicted using the Eulerian–Eulerian two-fluid model approach with kinetic theory of granular flow to obtain the flow patterns in square cyclone separator.

The velocity inlet boundary condition was used at the inlet and the inlet velocity was specified as the experimental value. The pressure outlet boundary condition was used at the outlet. The standard wall function was adopted.

Different grid meshes were tested before the final simulation and the four square cyclones have total number of 150214 cells for  $\alpha = 0^\circ$ , 152322 cells for  $\alpha = 10^\circ$ , 154189 cells for  $\alpha = 20^\circ$ , and 154914 cells for  $\alpha = 30^\circ$ , respectively. For all four square cyclone the tetrahedral grid was used, Fig.4-16(c) show a generated mesh in 3D grid. Model parameter uses in this section are shown in Table 4-3.

Fig.4-17 (c) CFD mesh of cyclone case with inlet angle  $\alpha = 20^\circ$ 

#### 4.4.3.1 Flow fields

Fig.4-18 shows the profile of gas and solid z-velocity for different inlet geometries at heights along axis of the cyclone.

In the square cyclone separator, the vertical velocity is important for the particle collection in a cyclone. The z-velocity distribution in near wall region is downward and has a greater amount in the right side. In the center of the cyclone, upward z-velocity distribution is observed in the numerical result, as shown in Fig. 4-18 the largest downward velocity was not near the wall of the separator, For different inlet configurations angle  $\alpha$  the z-velocity distribution at the wall facing the inlet, was much larger than that toward the inlet, as shown by Fig.4-18 with different height along of square cyclone, and the square with inlet angle  $\alpha = 30^\circ$

was also more larger than other angle  $\alpha$ . But at height fare from inlet cyclone (0.11 and 0.12 m of height) the distribution of the z-velocity was different, where both gas and particles had upward velocity close to the center part of the cyclone. The re-circulation flow was due to the change of the pressure distribution.

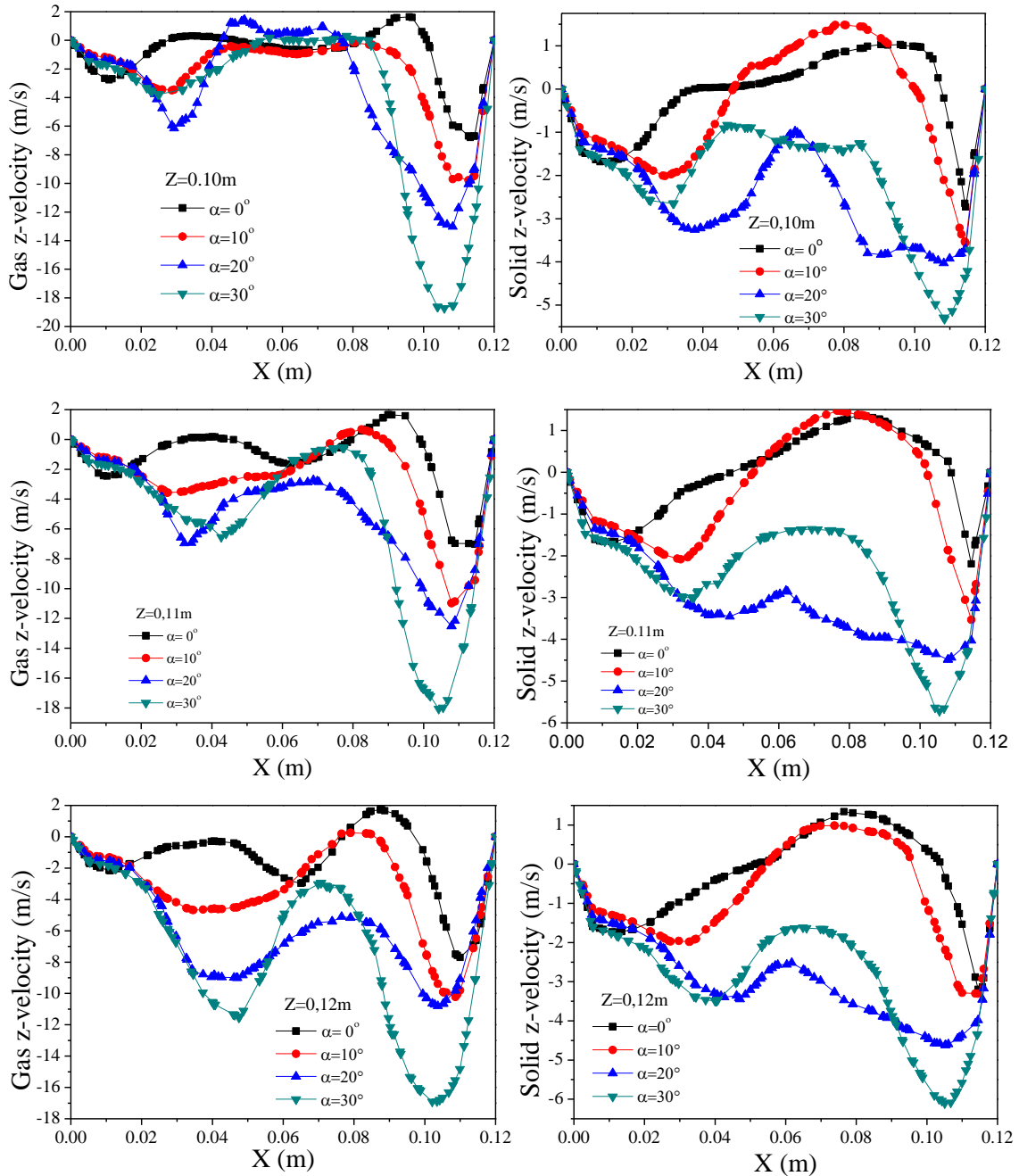


Fig. 4-18 Profile of gas and solid velocity along the axis of the cyclone at three axial locations for different inlet geometries at, inlet velocity is 20m/s

The largest downward  $z$ -velocity was at the right wall of the square separator at height  $z=0.110\text{m}$  and  $z=0.120\text{m}$ . The velocity at the left wall was relatively much smaller for four different angles  $\alpha$ . This implied the right wall gave more contribution for particle collection than the left wall did, especially the front corner at the right wall.

#### 4.4.3.2 Pressure fields

It is difficult to understand the cyclone separation behavior without some information about the flow field. CFD is a very useful tool to obtain details of the flow inside a cyclone.

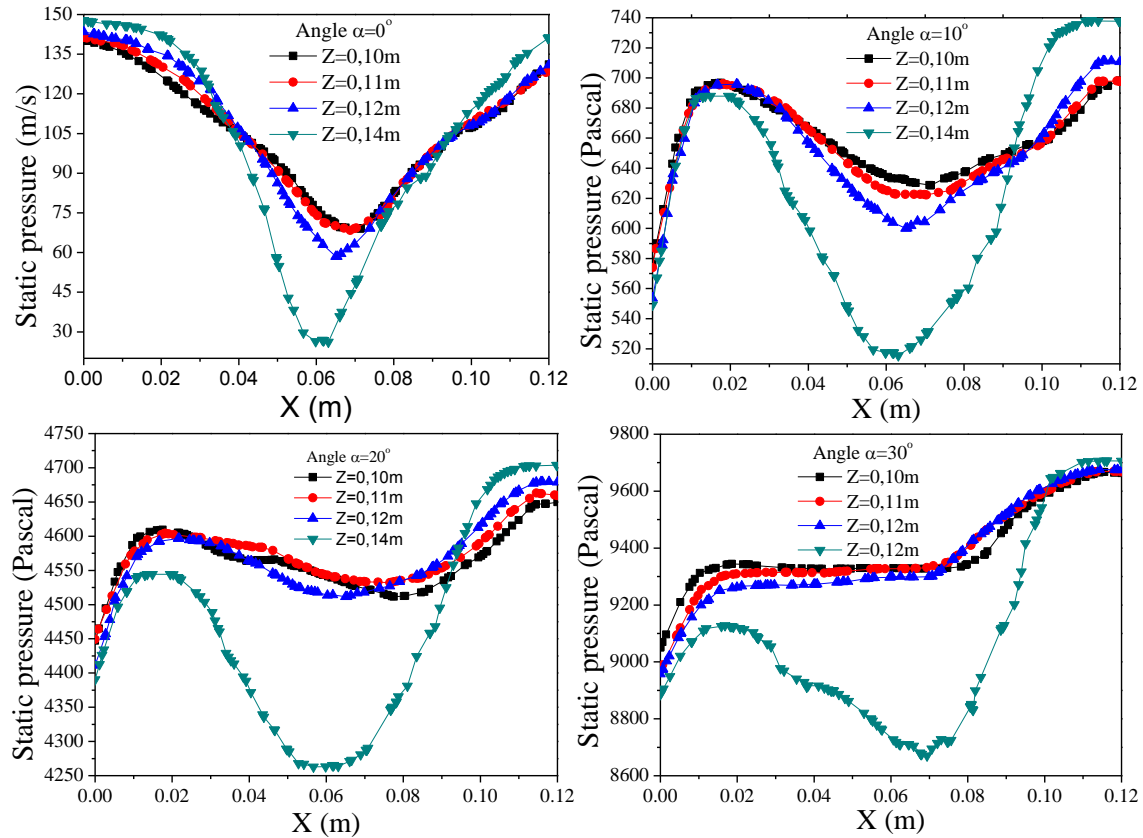


Fig. 4-19 Profile of static pressure for different inlet angle at different height along axis of square cyclone

The profiles of static pressure in square are shown in Fig.4-19 for four inlet configuration angle and with different height along the axis of cyclone, a low pressure. For all the cases the low pressure zone in the centre of the square cyclone is seen to be similar to the conventional cyclones. One of the most important parameters in the investigation of a cyclone performance is the pressure drop in the cyclone. But for angle more than  $0^\circ$  the static pressure is as lower in the center of

the square as in section close to inlet.

Fig.4-20 shows the comparison of pressure drop in on the square cyclone with the four different inlet configurations angle  $\alpha$  as function of inlet velocity. For four different inlet configurations angle  $\alpha$ , the CFD predicts the effect of the inlet velocity on the cyclone collection efficiency with an acceptable deviation. Comparison between the different inlet configurations angle  $\alpha$  shows that the pressure drop in square cyclone increase with increased inlet angle  $\alpha$  of cyclone geometry, as shown in Fig.4-20, the cyclone with inlet  $\alpha=30^\circ$  have high pressure than other angle the numerical simulation has better agreement with experimental data.

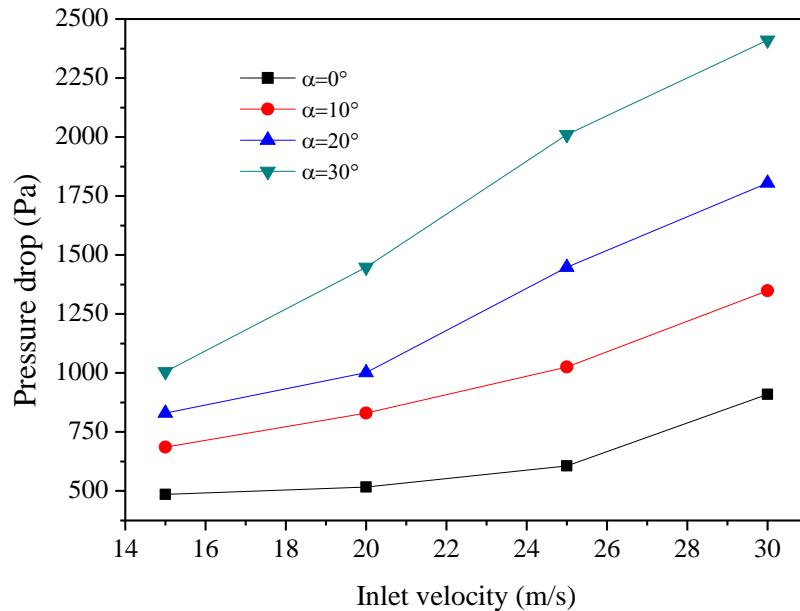


Fig.4-20 Pressure drop for four different inlet configurations

#### 4.4.3.3 Separation efficiency

In order to examine the effect of inlet geometry on square cyclone efficiency characteristics, Fig.4-21 shows the comparison results of separation efficiency with four different inlet configuration, as a function of the inlet velocities ( $V_{in}=15, 20, 25$  and  $30$  m/s). For the four different inlet configurations, a tendency of overall collection efficiency inlet velocity is observed. Obviously, the separation efficiency of the square cyclone with inlet angle  $\alpha=0^\circ$  is greater than that of square cyclone with angle  $\alpha>0^\circ$ . This indicates that the inlet configuration type plays an important role in the collection efficiency. As shown in Fig.4-21 the collection efficiency

decreases with increase inlet section. The effects of the cyclone inlet configuration angle  $\alpha$  on pressure drop (Fig.4-19) and collection efficiency are opposite. Increasing the inlet width will save more driving power but leads to reduced collection efficiency.

Moreover, the collection efficiency from Fig.4-16 and Fig.4-21 show that given two different cyclone geometries and being processed under the same conditions, it will yield different collection efficiency curves. This demonstrates the influence of the geometry especially the vortex finder on the efficiency of the cyclone. As can be seen from Figs.4-16 and 4-21, the collection efficiency of square cyclone with vortex finder (Fig.4-21) is higher comparing to the square cyclone without vortex finder presented in section 4.4.2.3(Fig.4-16) especially for high inlet velocity.

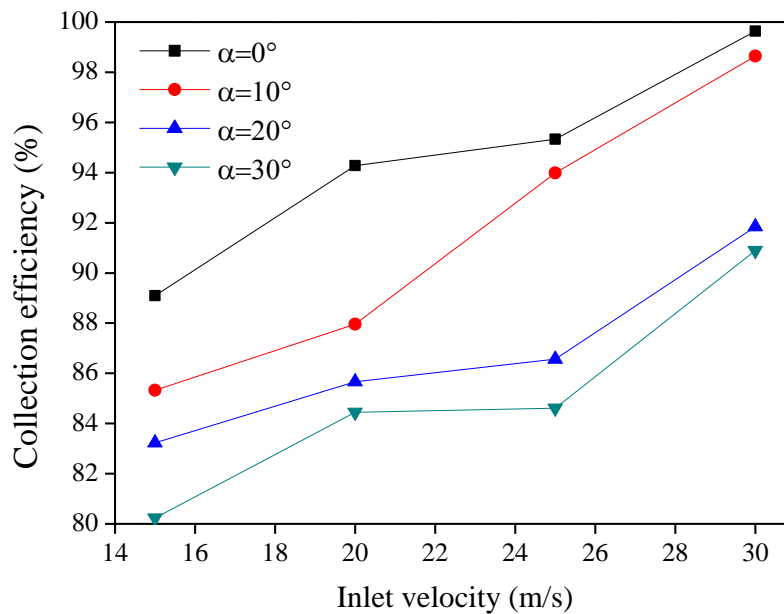


Fig.4-21 Cyclone collection efficiency as a function of inlet velocity

## 4.5 Brief summary

A numerical simulation by CFD, based on the RSM and RNG k- $\epsilon$  model was used to study the flow in square cyclone separators with a downward gas-exit within two cases. The case where a square cyclone have not vortex finder were initially performed and other case that has four types of cyclones with different inlet configurations were simulated with the condition similar in first section. Comparison of the results given by tangential velocity component, pressure fields



and volume fraction can describe the turbulent flow within a square cyclone.

Firstly the tangential velocity profiles show that inside the square cyclone without vortex finder, the swirling flow consists of an outer free vortex and inner forced vortex close to center. These results are similar to those seen in a conventional cyclone. Additionally, this study indicates that the pressure drop and separation efficiency increase with increasing inlet velocities for both the Reynolds stress model and the RNG k- $\epsilon$  model. Moreover, the Reynolds stress model gives a higher-pressure drop distribution and high separation efficiency compared to the RNG k- $\epsilon$  model. The Reynolds stress model provides well for the forced vortex and free vortex, and the lower pressure in center of square cyclone is seen to be similar to that of a conventional cyclone. Moreover, comparison of the pressure drop for two cases in a square cyclone show that the pressure increases considerably by increasing the solid volume fraction. However these numerical simulations results need to be validated in future work by the experimental data.

Secondly, the flow in a square cyclone separator is numerically simulated for four types of inlet geometries. The results showed that square cyclone with different inlet geometries would increase the pressure drop and decrease the separation efficiency as function of inlet angle. Note that the effects of the cyclone inlet configuration angle  $\alpha$  on pressure drop and collection efficiency are opposite. Increasing the inlet width will save more driving power but leads to reduced collection efficiency.

## **Chapter 5 Separation and pressure drop in horizontal cyclone separator**

### **5.1. Introduction**

Gas-solid two-phase flows are commonly found in many engineering applications and natural processes and contributions to the understanding of the behavior of such flow systems can significantly enhance the design and, in turn, the productivity of such processes. Numerical studies on gas-solid two-phase flows have become one of the most important approaches recently[129-138].

Cyclone separators are simple inertial separators with no moving parts. The major areas where cyclones have been used include the mining industry, construction materials industry, food industry and power utility industry. The cyclone separator is used by these industries for separation of component that make up a multiphase stream. Examples of the function that cyclone performs include particle classification and separation in the mining and construction industries; hot gas cleaning for chemical feedstock, and fluidized bed combustion system in chemical and power industries; and spray dried products recovery in food industries.

The separators are becoming increasingly popular in the power industry because of the power industry's growing interest in the circulating fluidized bed combustion (CFBC) system and the integrated coal gasification systems. The cyclone is an integral part of CFBC system, and its performance at high operating temperature and pressure attributes to the overall performance of the CFBC system. Cyclones are also used for cleaning gas in the combined coal gasification cycles.

The two most important parameters that determine the overall performance of cyclone separators are the collection efficiency and pressure drop. The collection efficiency determines whether the cyclone can effectively meet the dust removal requirement for the application. In an industrial application both the grade efficiency of the cyclone and overall efficiency are determining factor during the system design, to see if cyclone can be effectively incorporated in the system to handle particle removal. The pressure drop determines whether the cyclone can be economically viable for the application. The two factors that the pressure drop

requirement affects are the energy requirements and the initial capital cost for fluid mover: fan or pump.

Cyclone separators have been used extensively during this century as a major gas cleaning device. The standard designs available now were perfected decades ago on the basis of practical experience and insight but often without quantitative application of the principles of engineering practice. Although these approaches have worked well in certain circumstances, they may not always lead to the best possible designs. Now, increasing demands and competition require the use of good mathematical models describing the operation of cyclones, as well as their use, with modern tools of optimization to give the best designs. In this chapter dense gas-solid two-phase turbulent flow were simulated using Fluent software. The two turbulence model and Eulerian approach with kinetic theory for granular flow will be combined to study and describe the dense gas-solid flow and the performance of cyclone in horizontal cyclone separator. The main objective of this part lies in the implementation of the 3D mesh of the horizontal cyclone and the numerical simulation of the separation of dense gas-solid flow.

## **5.2. Mathematical model and numerical solution method**

### **5.2.1 Gas–solid two-fluid model**

In general, two methods are used to simulate particle in gas–solid two phase flow i.e. discrete element method (DEM) and Eulerian-Eulerian two phase flow model. The DEM approach traces individual particles while the gas-phase flow continuum is described by the Navier–Stokes equation. This method is highly accurate, but requires mesh adaptation and is expensive. The Eulerian approach is used for both the gas and particle phase within horizontal cyclone. For simplicity, it is assumed that flow is isothermal. The gas phase is incompressible and particles are spherical and mono-sized. The governing equations for the conservation of mass and momentum for each phase and the constitutive relations are given in Chapter 2.

### **5.2.2 Turbulence model**

We have seen that the gas solid flow in cyclone is turbulent so many choices of models available to us. Given the anisotropy of the system, the k- $\epsilon$  model standard is not appropriate. There have several turbulent models in FLUENT code and two

models are used in this part that we seemed adapted to our case study. The simulations are performed with the RNG k- $\epsilon$  models with options "swirl dominant flow" and RSM. Indeed, the first simulates the typical flow cyclones and the second takes into account all the Reynolds tensor and thus allows a good analysis of the results. The details of those two models are described in Chapter 2 and see Fluent User guide for more details about a choice of turbulent models.

### 5.2.3 Geometry of horizontal cyclone separator

A schematic of the geometry of a horizontal cyclone separator and its corresponding numerical grid is shown in Figs.5-1, 5-2. The horizontal cyclone separator investigated consists mainly of a cylindrical body, horizontal gas exit and downward solid exit. The set of governing equations presented in Chapter 2 is solved by a CFD code (FLUENT 6.3.23). Table 5-1 lists the parameters used in these simulations.

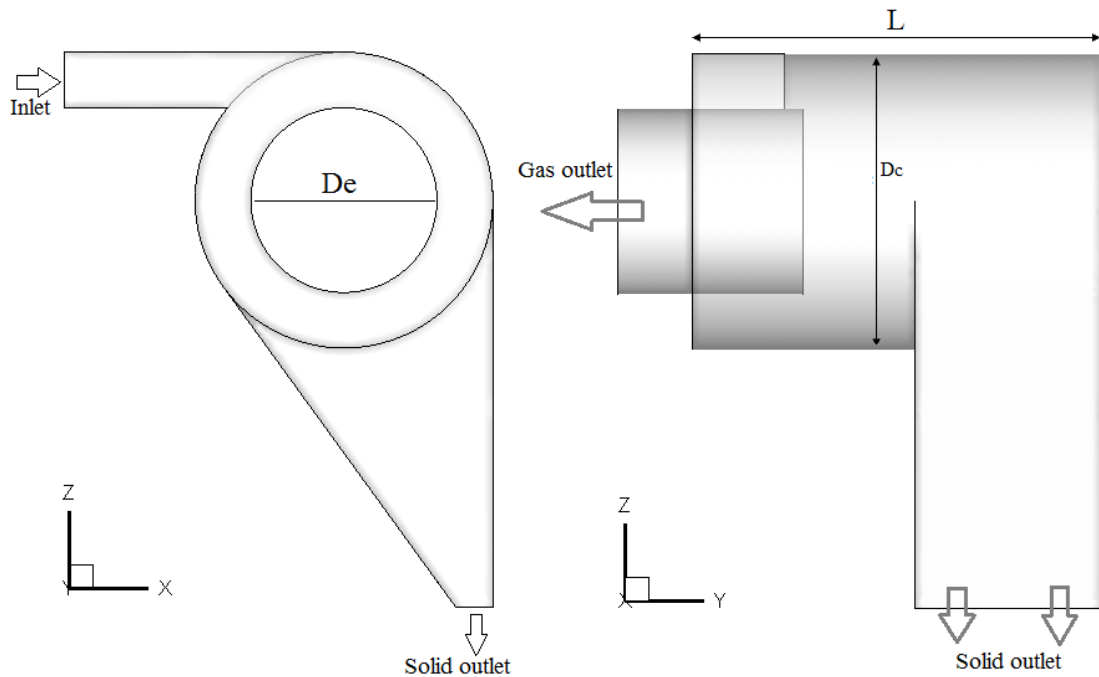


Fig. 5-1 Geometry and dimension of cyclone

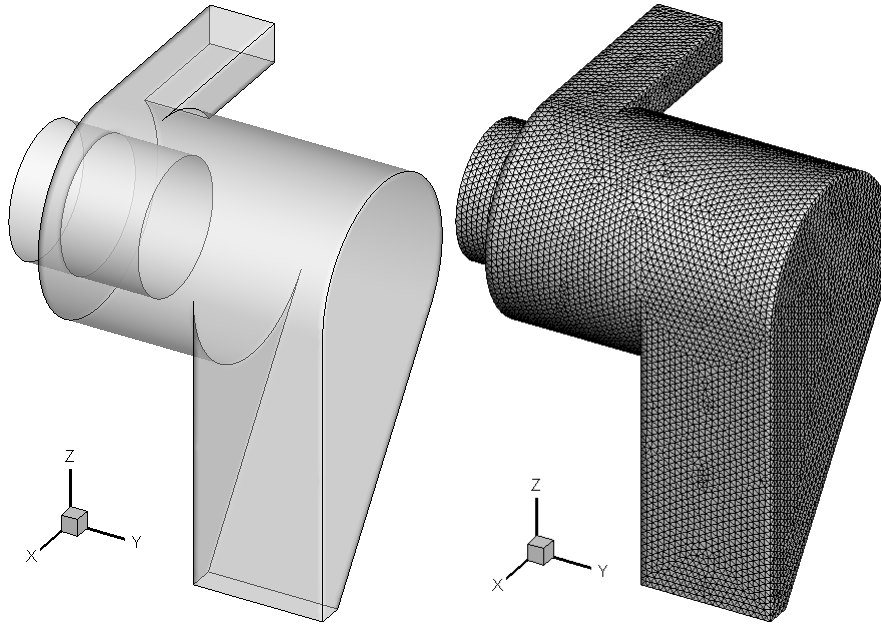


Fig. 5-2 3D geometry and generated grid used in this simulation

Table 5-1 Parameters and cyclone dimension used in these simulations

Notation	Units	Property	Value(s)
$\rho_g$	kg/m <sup>3</sup>	Gas density	1.225
$\mu_g$	kg/m-s	Gas viscosity	1.7894e-05
$V_{in}$	m/s	Flow inlet velocity	15, 20, 25, 30
$d_s$	μm	Solid diameter	150
$\rho_s$	kg/m <sup>3</sup>	Solid density	2400
$\alpha_s$	--	Solid volume fraction	0.1, 0.05
L	m	Cylindrical body length	0.44
Dc	m	Cylindrical body diameter	0.32
a	m	Inlet length	0.16
b	m	Inlet width	0.1
De	m	Gas outlet diameter	0.2
l	m	Solid outlet length	0.2
c	m	Solid outlet width	0.04

## 5.2.4 Boundary conditions

A velocity inlet boundary condition is used at the cyclone inlet, meaning that a velocity normal to the inlet is specified. Velocity inlet, particle concentration and other parameter are show in Table 5-1. A pressure flow boundary condition is used at the outlet. Gas exhaust exit tube is open to the air, and the surrounding pressure and temperature are 1 atm and 290 K respectively. The no slip boundary condition is used at the other boundaries.

## 5.3 Results and discussion

### 5.3.1 Flow fields

Fig.5-3 present velocity streamlines with inlet velocity of 20m/s at five different cross-sectional locations: Plane 1 ( $y = 0.05\text{m}$ ), plane 2 ( $y = 0.13\text{m}$ ), plane 3 ( $y = 0.17\text{m}$ ), plane 4 ( $y = 0.29\text{m}$ ) and at plane 5 ( $y = 0.33\text{m}$ ). The velocity was performed for several different gas and solid inlet velocity. Because the results show similar profile that it's not important to reported all of them. Flow behavior in the horizontal cyclone separator can be observed for both the RNG  $k-\varepsilon$  and RSM, respectively and with inlet velocity of 20m/s.

A recirculation zone exists beneath the inlet region is seen clearly in the velocity streamline plot in Fig.5-3(a) because of the collision among flow, part of gas flows inward and exhausts out quickly from the region right beneath the inlet region, which forms a short-circuiting flow. Another recirculation zone exist has seen at plane 4 (Fig.5-3(d)) due to the enlarging dust box and the friction from particles accumulating walls.

From the streamline distribution, it was seen that the suspension flow field in the horizontal cyclone separator consisted of the strong swirling flow of high velocity at the center and weak swirling flow of low velocity near the wall, and local eddies existed at the position close to inlet section as shown in Fig. 5-3(a) for both RSM and RNG  $k-\varepsilon$  model. The central flow field can be regarded as forced vortex region, while the flow near the wall can be regarded as quasi-free vortex. Hence, the flow in the horizontal cyclone separator had the characteristics of Rankine vortex, which was very advantageous for particle separation. The strong swirling flow in the center gave rise to centrifugal force and threw the particles to

the outer quasi-free vortex region, where particles were likely to be collected due to the weak swirling intensity.

Additionally, Fig.5-3 shows the evolution of the vortex core in a cross-sectional plane of the horizontal cyclone. It describes a nearly circular path around the geometrical center, rotating in the same direction as the flow.

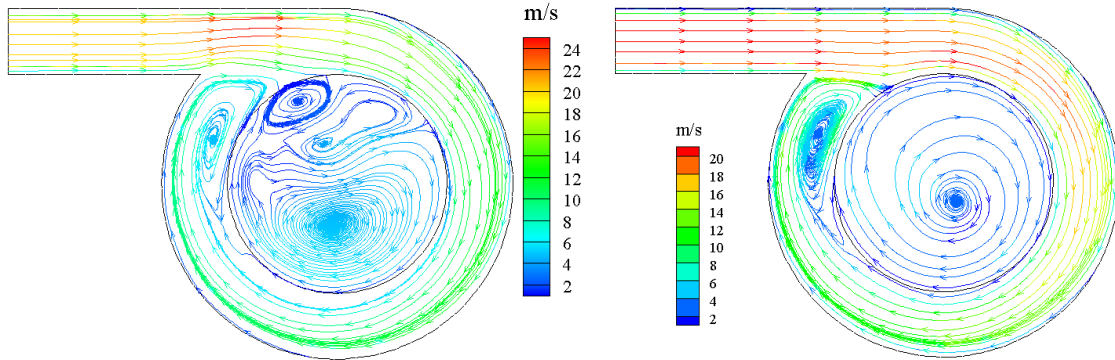


Fig. 5-3(a) Velocity streamline of RNG k-ε model (left) and RSM model (right) at plane 1

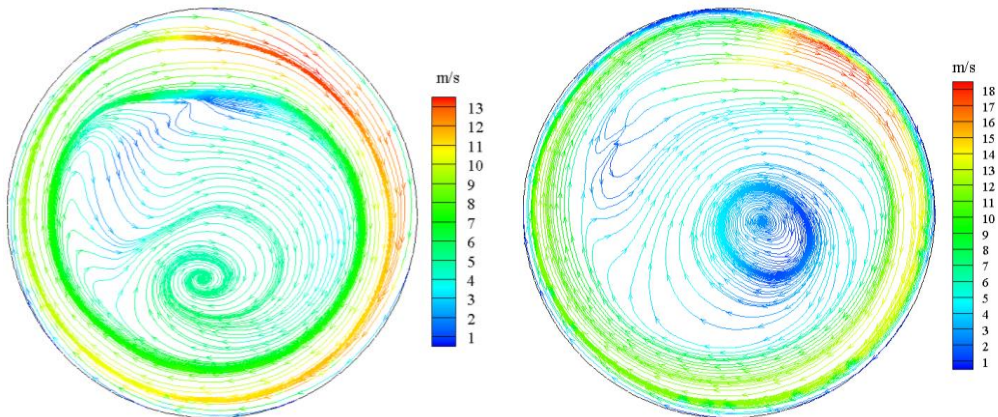


Fig. 5-3(b) Velocity streamline of RNG k-ε model (left) and RSM model (right) at plane 2

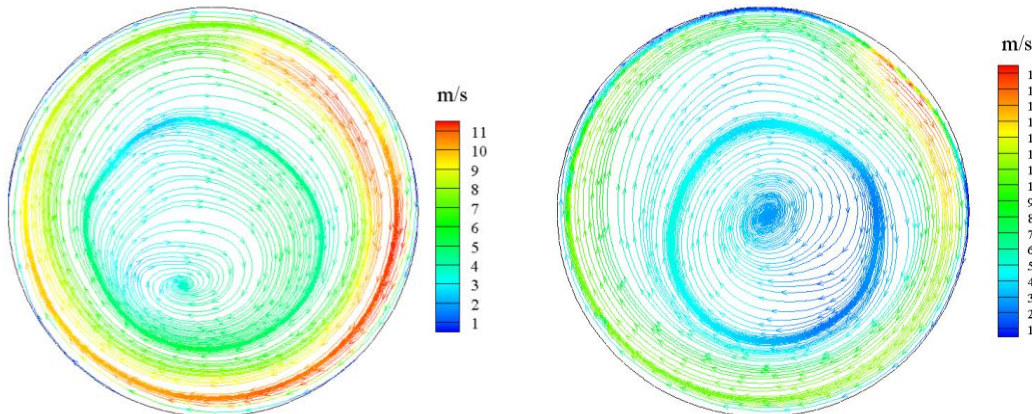


Fig. 5-3(c) Velocity streamline of RNG k-ε model (left) and RSM model (right) at plane 3

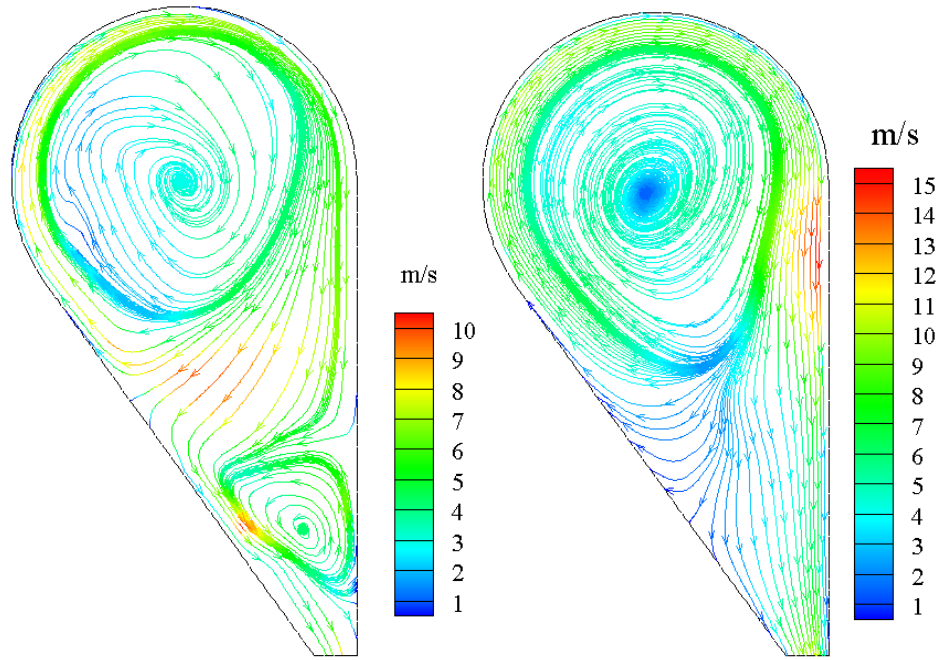


Fig. 5-3(d) Velocity streamline of RNG k- $\epsilon$  model (left) and RSM model (right) at plane 4

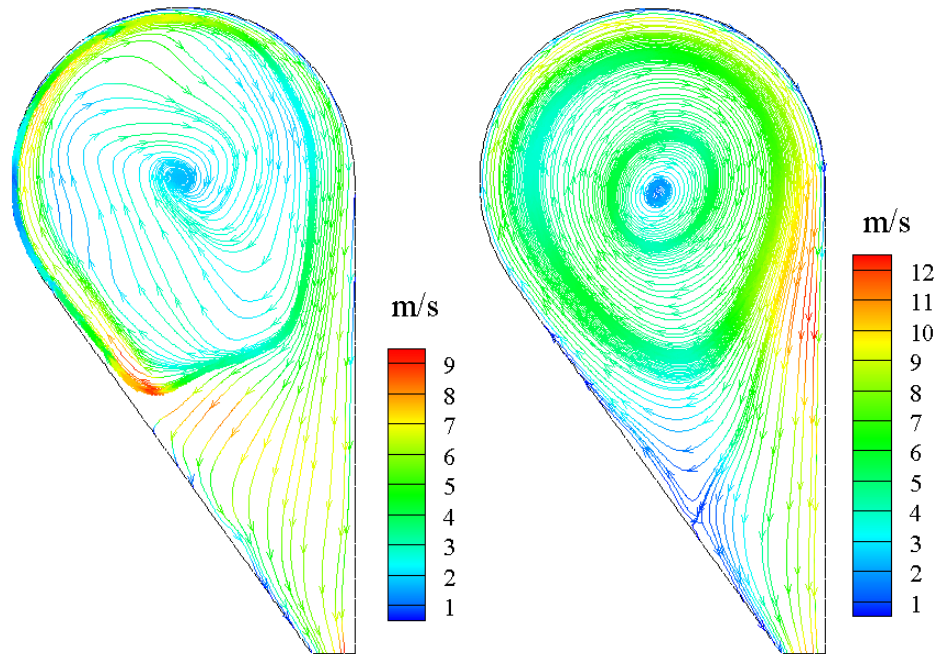


Fig.5-3(e) Velocity streamline of RNG k- $\epsilon$  model (left) and RSM model(right) at plane 5

### 5.3.2 Tangential velocity

Fig.5-4 shows the gas tangential velocity profile at different locations along axial direction of horizontal cyclone and for different gas-solid inlet velocities. Note that the tangential velocity profile is shown across the diameter and is nearly



symmetrical about the center of the cyclone separator. For different position ( $y=0.05$ ,  $y=0.17$  and  $y=0.34$  m), the tangential velocity has a positive sign and on the other side (180 degrees in the circumferential direction) has a negative sign.

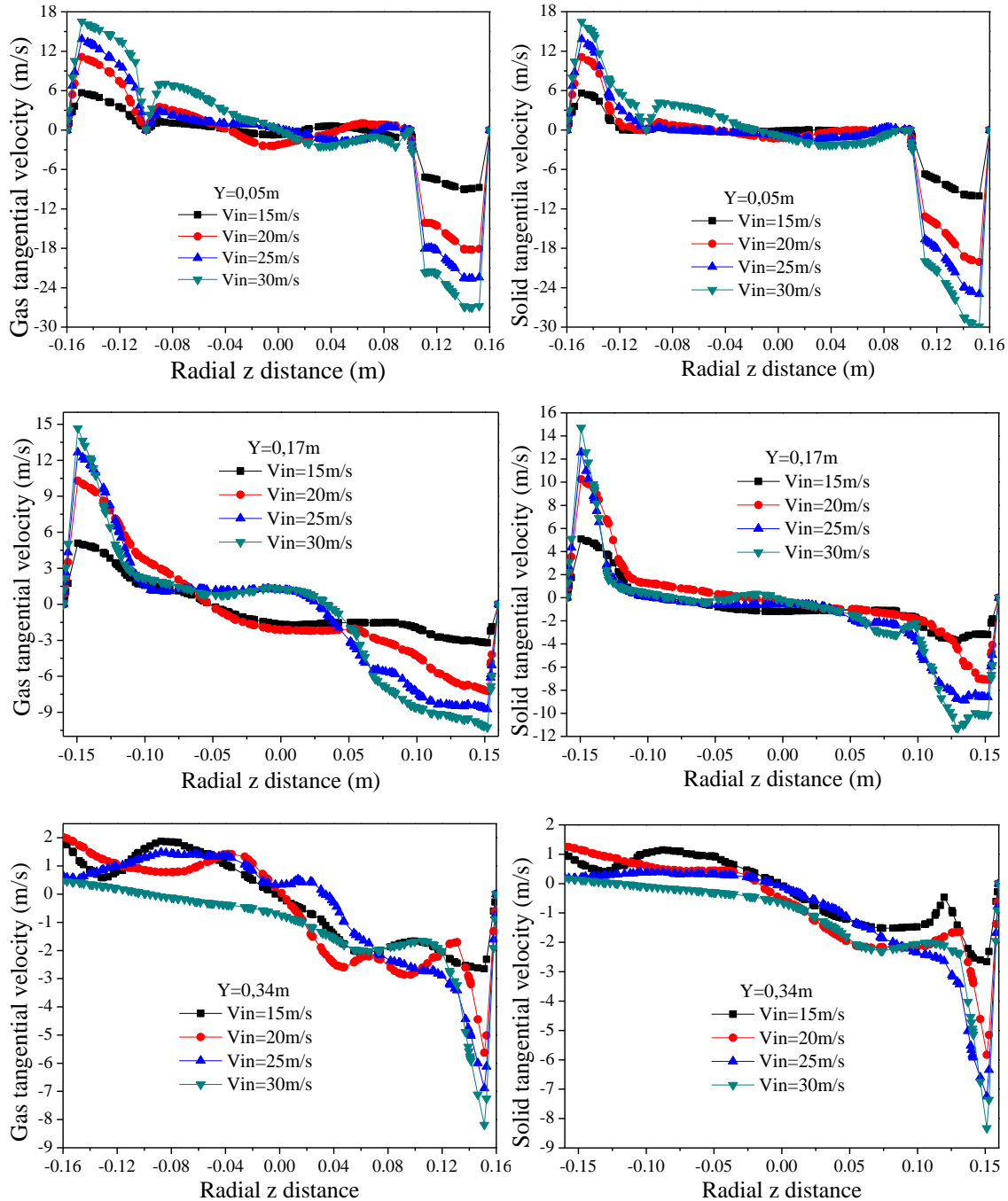


Fig.5-4 Profile of gas and tangential velocity at different  $y$  distance along axial distance of cyclone with different inlet velocity

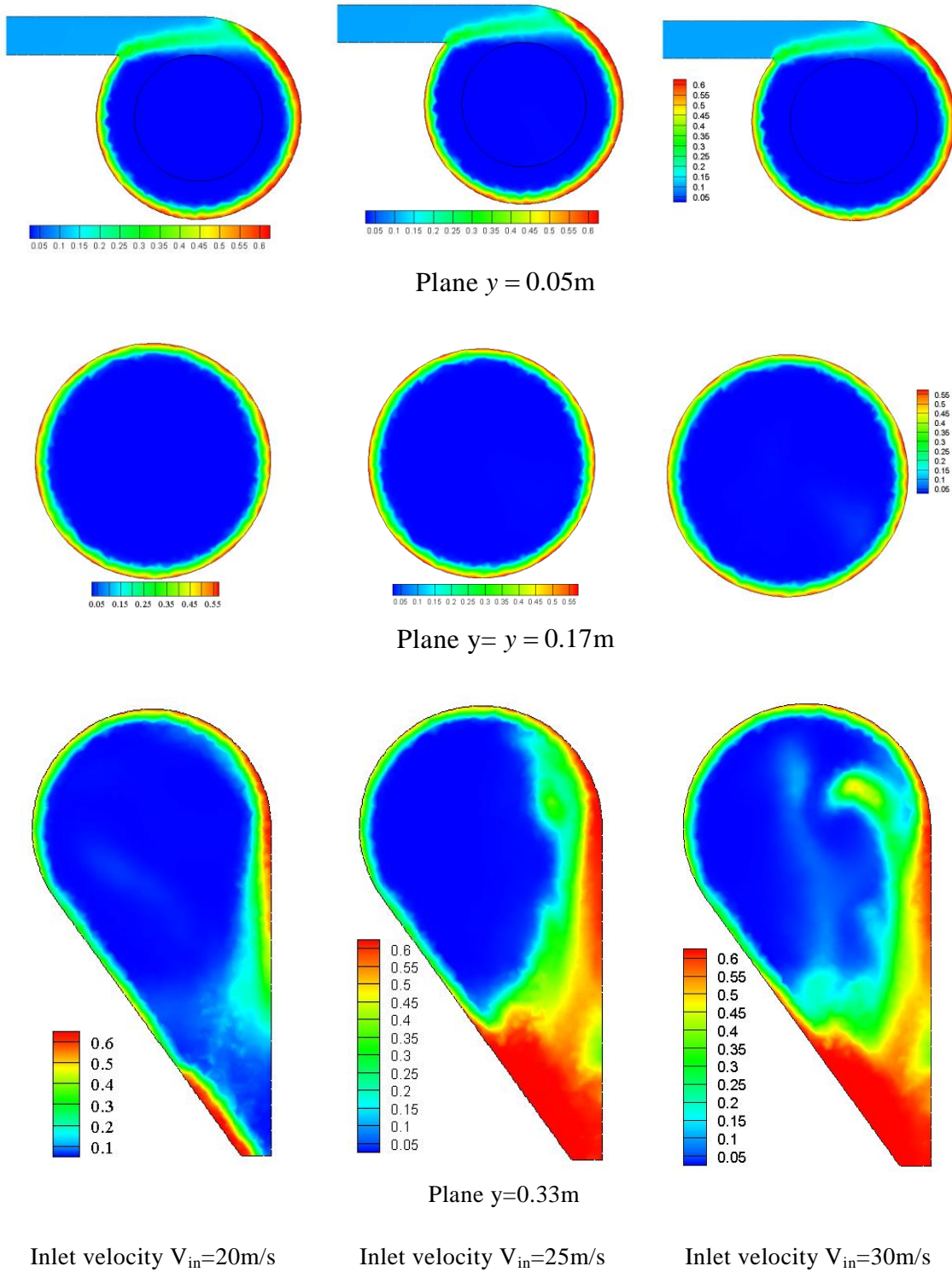


Fig.5-5 Contours plot of solid volume fraction for RNG k- $\epsilon$  model

As shown in Fig.5-4, high tangential velocity occurs in the near-wall region. This high velocity in the near-wall region decays rapidly toward the center. Notice also that the magnitude of the peak in the tangential velocity has decreased considerably from  $y=0.17\text{m}$  to  $y=0.34\text{m}$  along axial direction of cyclone. This indicates a high decay of the tangential velocity in the axial direction as well as in the circumferential direction, especially near the inlet, as shown in Fig.5-4

### 5.3.3 Volume fraction

Fig.5-5 shows the contour plot of volume fraction for RNG k- $\epsilon$  of horizontal cyclone at different cyclone location for different inlet velocity. Gil and Cortes found that in dense flow, the particles ejected radially towards the outer wall causing the increase of the effect of wall friction. This normally increases the pressure drop, but the weakness of the rotational movement in the same effect of friction, reduced. The distribution of solid volume fractions near the walls of the cyclone and in a plane at three different planes ( $y = 0.05\text{m}$ ,  $y = 0.17\text{m}$  and  $y = 0.33\text{m}$ ) is illustrated in Fig.5-5. It may be noted that high concentrations are close to the walls corresponding to separate particles and especially in the zones where velocities are reduced. For high inlet volume fraction the concentration near the walls is almost 60%. It is also observed at higher concentration of solid in plan  $y = 0.33\text{m}$  for different inlet velocity corresponding to the outlet solid part and the solid concentration have different distributions according to inlet velocity

### 5.3.4 Pressure drop

Note that the pressure drop over a cyclone is the difference of static pressure between the inlet and outlet, which can be written as in Equation (1-2). Fig.5-6 and 5-7 show the profile of pressure drop for two turbulence model and with different inlet solid volume fraction respectively.

As shown in Fig.5-6, the pressure drops in horizontal cyclone show an approximately linear increase with increasing inlet velocity. The predictions approached by RNG k- $\epsilon$  and RSM model are different, RNG k- $\epsilon$  predict a higher pressure drop compare to RSM model. However both of turbulent model a same tendency that is the pressure drop of the horizontal cyclone separator increases with increase of the inlet velocity.

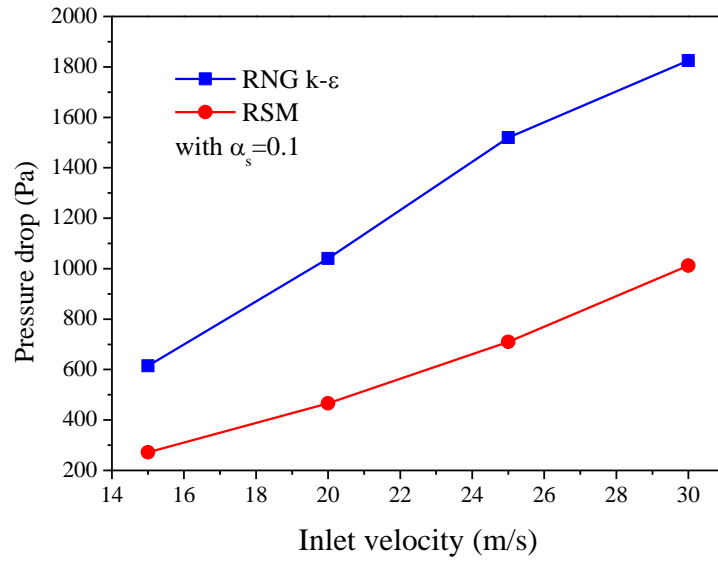
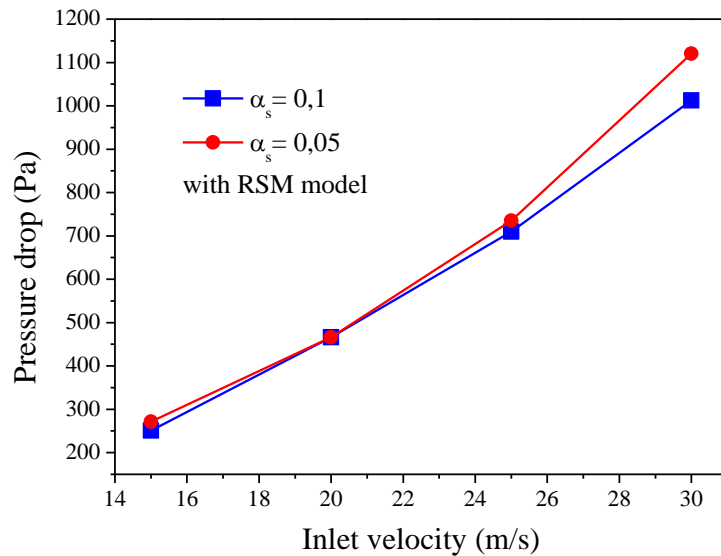
Fig. 5-6 Pressure drop as function of inlet velocity RNG k- $\epsilon$  and RSM

Fig. 5-7 Pressure drop as function of inlet velocity with different solid volume fractions

Note that the CFD has a great potential to predict the flow field characteristics and particle trajectories as well as the pressure drop inside the cyclone. The CFD code FLUENT with the RSM turbulence model predict very well the pressure drop in conventional cyclone and may be useful for cyclone design. However behind the accuracy of the complicated RSM model it does require much expensive computational effort compared to the RNG k- $\epsilon$  model. In horizontal cyclone present

there, the CFD with RNG k- $\epsilon$  turbulence model also yield a reasonably good prediction on cyclone pressure drop. The RSM turbulence model also predicts the cyclone collection efficiency better than RNG k- $\epsilon$  model, respectively for the cyclone of a different geometry.

Generally the cyclone pressure drop decreases with increased wall friction coefficient, concentration of solids or length of the apparatus. Fig.5-7 shows the pressure drop of cyclone with two different inlet solid volume fraction for RSM model, as shown in figure the pressure drop increase with increasing of inlet velocity, high solid volume fraction predict higher pressure drop compare to low inlet volume fraction.

### 5.3.5 Collection efficiency

The collection efficiencies as function of inlet gas velocities are shown in Fig. 5-8 for different turbulence model with solid volume fraction of 0.1. As can be seen from Fig.5-8, the influence of inlet velocity on collection efficiency for RNG k- $\epsilon$  and RSM turbulence model, and particle concentration is obvious. Because the tangential velocity inside the cyclone separator increases with the increasing inlet gas velocity, which leads to the increase of centrifugal forces, therefore, the collection efficiency increases accordingly.

As shown in Fig.5-8, the results show that the efficiency the horizontal cyclone increases with increasing inlet velocity. With the increase of the inlet velocity, the performance of the separation will be enhanced and the efficiency will be improved. The predictions which are achieved by RNG k- $\epsilon$  model and RSM model are not all the same. The efficiency predicted by RNG k- $\epsilon$  model is lower. However, both the two model shows that, with the increase of the inlet velocity, the efficiency improved, which is the tendency of the separation efficiency is the same.

The collection efficiencies for two different inlet solid volume fractions are shown in Fig.5-9, the simulation were performed using RSM turbulence model. As seen in Fig.5-9 the collection efficiency increase with increasing inlet velocity and decrease with increasing of solid volume fraction. Generally, the published literatures dealing with the influences of particle concentration on gas flow and particle separation showed the following results[65]: the gas flow inside the cyclone separator was primarily changed by the separated particles sliding down the wall in stream as a result of the angular momentum exchange among gas, particles and

wall.

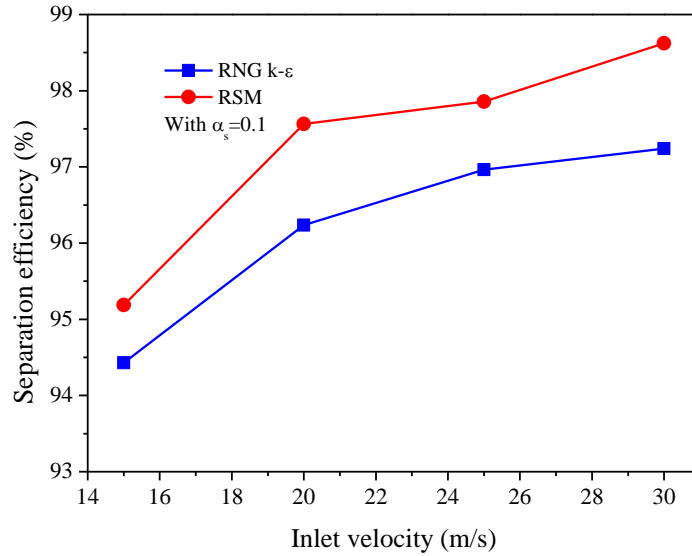


Fig.5-8. Separation efficiency of the horizontal cyclone for RNG k-ε and RSM model as function of inlet velocity

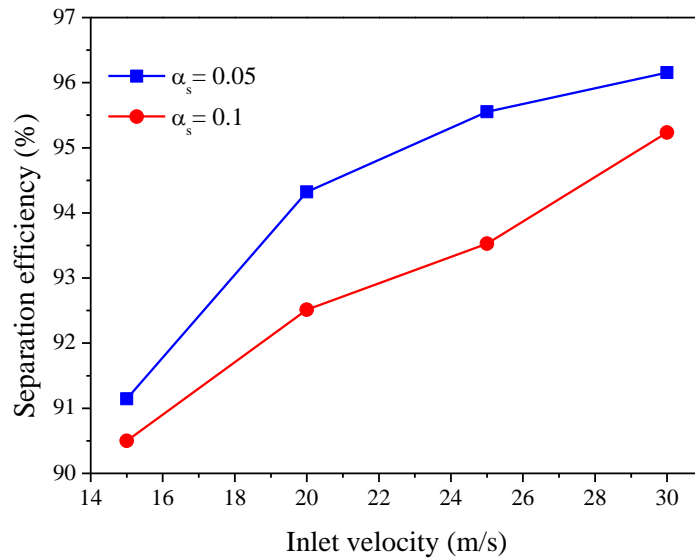


Fig.5-9 Separation efficiency of the horizontal cyclone with two different solid volume fractions.

Especially the tangential velocity of the gas inside the cyclone separator decreased distinctly with the increasing particle concentration as shown by velocity measurements using a Laser Doppler Velocimetry (LDA)[138] and by flow field simulation[139]. Thus, it might assume that the collection efficiency of cyclone

separators diminishes with the increasing particle concentration due to the smaller centrifugal forces in the cyclone separator. However, measurement results show that the collection efficiency improves steadily with the increasing particle concentrations although the centrifugal force decreases due to the smaller tangential gas velocities at high particle concentrations. Muschelknautz[39] tried to take this phenomenon into account by his mechanistic treatment on limited particle transport at high concentrations. Any material in excess of this concentration was ‘dumped’ to the cyclone separator wall, essentially without being classified, the remainder continued to the separation space proper, where it was separated roughly as if the cyclone separator was operating at low concentration. However, the collection efficiency measurements indicated that the improvement of separation performance at higher concentrations was due to particle agglomeration[66]. Derksen et al.[138] thought that the presence of solid particles in gas caused cyclone separator to lose some swirl intensity. The turbulence of the gas flow got strongly damped. Swirl intensity and turbulence had significant influence for the way the different size particles get dispersed in the gas flow, and the collection efficiency got affected in an opposite sense: negatively by the loss-of-swirl, positively by the reduced turbulence.

#### **5.4. Brief summary**

The flow behavior of gas and particles has been simulated based in Eulerian–Eulerian two-fluid modeling approach with kinetic theory of granular flow for horizontal cyclones separators. The effect of two turbulence model and solid inlet volume fraction base on the distributions of the flows fields, and cyclone performance was studied and the result illustrated that the pressure drop in horizontal cyclone increase with increasing of solid volume fraction but the collection efficiency decrease with increasing of solid volume fraction. And the same result was observe for two turbulence model which RNG k- $\epsilon$  show better separation efficiency than RSM model opposite to the pressure drop.

## Summary and Conclusion

Gas-solid separation has received considerable attention in recent years in the removal of dust from the environment. Dust abatement covers a wide range of equipment designs. A simple design of a cyclone separator is usually an initial separation step followed by more efficient means to remove air borne particles. Cyclone separators are widely used in industrial applications. The separation efficiency and pressure drop are the most important parameters to evaluate the performance of processing system. In the simulations presented in this thesis, the dense gas-solid flows separation within a different type of cyclone separator is simulated by means of computational fluid dynamics. The Reynolds stress model and RNG k-epsilon two turbulence models and Eulerian approach were combined to study and describe the dense gas-solid flows and the performance of cyclone. The flow behavior is examined in the term of tangential velocity components, static pressure and pressure drop contour plots for flow field and solid volume fraction. The effects of the turbulence model, cyclone geometry and solid volume fraction on the cyclone were discussed. And the conclusions derived from this research are presented below for different cases studied.

1. The first type of cyclone separators used in this study is the conventional cyclone separators with a various type of inlet angle. Based on the presented results, the following conclusions may be drawn. Results show that for different inlet gas-solid velocities, an axial symmetry was observed for RSM around the cylindrical section of cyclone for both tangential and axial velocities. However, the RNG k- $\epsilon$  model displays no axial symmetry. Additionally high pressure near the wall of the cyclone due to centrifugal force creates a depression on the axis of the cyclone.

The results indicate that the pressure drop increases with increasing inlet velocities for both the RSM and RNG k- $\epsilon$  models, moreover the RSM gives a higher pressure drop compared to the RNG k- $\epsilon$  model. Additionally, the RSM model provides well for the simulations of both the forced and free vortex.

The axial velocity profiles for the four inlet configurations are very similar except at the central region which the magnitude peak increases with increase inlet



configuration angle. Additionally the magnitude peak of tangential velocity in cyclone and pressure drop increase with increasing the cyclone inlet configuration angle.

2. Flow gas and solid separation in square cyclone separators with a downward gas-exit within different types of square cyclone were simulated with the condition similar to those in first section. The effect of turbulence model, inlet configuration and solid concentration based on velocity component, pressure and volume fraction were investigated in this part.

Firstly, for both turbulence models use the results indicated that the pressure drop and separation efficiency increase with increasing inlet velocities, and are higher for RSM compare to RNG k- $\epsilon$  model. Also the RSM provides well for the forced vortex and free vortex, Moreover the lower pressure in center of square cyclone is seen to be similar to that of a conventional cyclone. Additionally comparison of the pressure drop for three different solid volume fractions in a square cyclone show that the pressure increases considerably by increasing the solid volume fraction.

Secondly the flow in a square cyclone separator is numerically simulated for four types of inlet geometries. The results showed that square cyclone with different inlet geometries would increase the pressure drop and decrease the separation efficiency as function of inlet angle  $\alpha$ . Note that the effects of the cyclone inlet configuration angle  $\alpha$  on pressure drop and collection efficiency are opposite. Increasing the inlet width will save more driving power but leads to reduced collection efficiency.

3. Separation and pressure drop in horizontal cyclone separator was investigated in last part of this research. The effect of two turbulence models and solid inlet volume fraction on the horizontal cyclone were investigate based in flow vector axial velocity and performance characteristics of cyclone. The result illustrated that the pressure drop in horizontal cyclone increase with increasing of solid volume fraction but the collection efficiency decrease with increasing of solid volume fraction. And the same result was observe for two turbulence model which RNG k- $\epsilon$  shows better separation efficiency than RSM model opposite to the pressure drop.

### **Main innovative findings from the present research**

In this thesis, the dense gas-solid flow separation of cyclone was simulated within different geometries by means of CFD. The RNG k- $\epsilon$  and RSM two turbulence models and Eulerian–Eulerian approach with kinetic theory for granular flow will be combined to study and describe the dense gas-solid flow. The effect of cyclone geometry, solid volume fraction and turbulence model on collection efficiency and pressure drop were studied. The main innovative findings in this research can be summarized as follows:

- CFD has a great potential to predict the flow field characteristics as well as the pressure drop inside the cyclone. The simulation results of cylindrical cyclone, square cyclone and horizontal cyclone found that the CFD code FLUENT with the RSM turbulence model can be more reasonable to predict the separation efficiency and pressure drop in cyclones of a different geometry and may be useful for cyclone design. However behind the accuracy of the complicated RSM model it does require much expensive computational effort compared to the RNG k- $\epsilon$  model. CFD with RNG k- $\epsilon$  turbulence model also yield a reasonably good prediction on cyclone pressure drop.

- Dense gas-solid flow separation within different type of geometries was studied, and the effects of geometry on cyclone collection efficiency and pressure drop were tested and compared. Results indicate that the inlet configuration plays an important role in the cyclone collection efficiency and cyclone pressure drop. Moreover the corner is one of the major regions to cause pressure drop and was found to be beneficial to particle separation. This presents the possibility of obtaining a better performance cyclone by means of improving its geometry design.

## Reference

- [1] Jiang Y., Qiu G.Z., Wang H.G. Modelling and experimental investigation of the full-loop gas–solid flow in a circulating fluidized bed with six cyclone separators[J]. Chemical Engineering Science. 2014, 109:85-97
- [2] Chu K.W., Wang B., Yu A.B., Vince A. Computational study of the multiphase flow in a dense medium cyclone: Effect of particle density[J]. Chemical Engineering Science. 2012, 73: 123-139
- [3] Masnadi M.S., Grace J.R., Elyasi S., Bi X. Distribution of multi-phase gas–solid flow across identical parallel cyclones: Modeling and experimental study[J]. Separation and Purification Technology. 2010, 72(1): 48-55
- [4] Kuang S.B., Qi Z., Yu A.B., Vince A., Barnett B.D., Barnett P.J. CFD modeling and analysis of the multiphase flow and performance of dense medium cyclones [J]. Minerals Engineering, 2013,<http://dx.doi.org/10.1016/j.mineng.2013.10.012>
- [5] Shaaban S., Numerical optimization and experimental investigation of the aerodynamic performance of a three-stage gas–solid separator[J]. Chemical Engineering Research and Design. 2011, 89(1): 29-38
- [6] Elsayed K., Lacor C. The effect of cyclone vortex finder dimensions on the flow pattern and performance using LES[J]. Computers & Fluids. 2013, 71:224-239.
- [7] Hreiz R., Gentric C., Midoux N. Numerical investigation of swirling flow in cylindrical cyclones[J]. Chemical Engineering Research and Design. 2011, 89(12): 2521-2539
- [8] Chu K.W., Wang B., Yu A.B., Vince A. Particle scale modelling of the multiphase flow in a dense medium cyclone: Effect of vortex finder outlet pressure[J]. Minerals Engineering. 2012, 31: 46-58.
- [9] K.W. Chu, Kuang S.B., Yu A.B., Vince A., Barnett G.D., Barnett P.J. Prediction of wear and its effect on the multiphase flow and separation performance of dense medium cyclone[J]. Minerals Engineering. 2014, 56: 91-101
- [10] Wang B., Xu D.L., Chu K.W., Yu A.B. Numerical study of gas-solid flow in a cyclone separator[J]. Applied Mathematical Modeling. 2006, 30(11):

1326-1342.

- [11] Song J.F., Sun G.G., Chao Z.X., Wei Y.D, Shi M.X. Gas flow behavior and residence time distribution in a FCC disengager vessel with different coupling configurations between two-stage separators[J]. Powder Technology. 2010, 201(3) 258-265.
- [12] Safikhani H, Akhavan-Behabadi M.A., Nariman-Zadeh N, Mahmood Abadi M.J. Modeling and multi-objective optimization of square cyclones using CFD and neural networks[J]. Chemical Engineering Research and Design. 2011, 89(3):301-309.
- [13] Pirker S., Goniva C., Kloss C., Putteringer S., Houben J., Schneiderbauer S. Application of a hybrid Lattice Boltzmann–Finite Volume turbulence model to cyclone short-cut flow[J]. Powder Technology. 2013, 235: 572-580.
- [14] Kępa A. Division of outlet flow in a cyclone vortex finder-The CFD calculations[J]. Separation and Purification Technology. 2010, 75(2):127-131.
- [15] Wang Q.G., Lu J.F., Yin W.D, Yang H.R., Wei L.B. Numerical study of gas–solid flow in a coal beneficiation fluidized bed using kinetic theory of granular flow[J]. Fuel Processing Technology. 2013, 111: 29-41.
- [16] Hosseini S.H, Ahmadi G., Olazar M. CFD simulation of cylindrical spouted beds by the kinetic theory of granular flow[J]. Powder Technology. 2013, 246:303-316
- [17] Armstrong L.M., Gu S., Luo K.H. Study of wall-to-bed heat transfer in a bubbling fluidized bed using the kinetic theory of granular flow[J]. International Journal of Heat and Mass Transfer. 2010, 53(21): 4949-4959
- [18] Sambasivam D., Bhattacharya A.K, Synthesis of CFD and Monte-Carlo simulations for improved design and operation of Dense Medium Cyclones[J]. Computers & Fluids. 2014, 96: 47-62
- [19] Safikani, H. Hajiloo A, Ranjba M.A. Modeling and multi-objective optimization of cyclone separators using CFD and genetic algorithms[J]. Computers and Chemical Engineering. 2010, 35(6): 1064-1071
- [20] Sommerfeld M., Ho C.H. Numerical calculation of particle transport in turbulent wall bounded flows[J]. Powder Technology. 2003, 131(1): 1-6
- [21] Lim K., Kwon S.B., Lee K.W. Characteristics of the collection efficiency for a double inlet cyclone with clean air[J]. Journal of Aerosol Science. 2003, 34(6):1085-1095
- [22] Lee J.W., Yang H.J., Lee D.Y. Effect of the cylinder shape of a long-coned

- cyclone on the stable flow-field establishment[J]. Powder Technology. 2006, 165(1) 30-38
- [23] Darling S.L. Pyroflow compact: The next generation CFB boiler[C]. In Proceedings of the 1995 International Joint Power Generation Conference. 1995, 1: 403-412
- [24] Lu J.F., Zhang J.S., Zhang H., Liu Q., Yue G.X. Performance evaluation of a 220t/h CFB boiler with water-cooled square cyclones[J]. Fuel Processing Technology. 2007, 88(2): 129-135
- [25] Su Y.X., Mao Y.R. Experimental study on the gas-solid suspension flow in a square cyclone separator[J]. Chemical Engineering Journal, 2006 121(1): 51-58
- [26] Zhao B.T., Shen H.G., Kang Y.M. Development of a symmetrical spiral inlet to improve cyclone separator performance[J]. Powder Technology. 2004, 145(1):47-50
- [27] Makkonen P., Foster Wheeler Energia Oy, Karhula R&D Center. Foster Wheeler CFB with the new INTREXTM Superheated[M]. VGB Powertech-english Edition-. 2000, 80:30-34
- [28] Griffiths W.D., Boysan F, Computational fluid dynamics (CFD) and empirical modeling of the performance of a number of cyclone samplers[J]. Journal of Aerosol Science. 1996, 27(2): 281-304
- [29] Raoufi A., Shams M., Farzaneh M., Ebrahimi R. Numerical simulation and optimization of fluid flow in cyclone vortex finder[J]. Chemical Engineering and Processing. 2008, 47(1): 128-137
- [30] Lee J.W, Yang H.J., Lee D.Y. Effect of the cylinder shape of a long-coned cyclone on the stable flow-field establishment[J]. Powder Technology. 2006, 165(1): 30-38
- [31] Bernado S., Mori M, A. Peres A.P., Dionosio R.P. 3-D computational fluid dynamics for gas and particle flows in a cyclone with different inlet section angles[J]. Powder Technology. 2006,162(3): 190-200
- [32] Hsiao T.C., Chen D., Greenberg P.S., Street K.W. Effect of geometric configuration on the collection efficiency of axial flow cyclones[J]. Journal of Aerosol Science. 2011, 42(2): 78-86
- [33] Hoekstra A.J. Gas flow field and Collection Efficiency of cyclone separators[D]. Delft, Technical University Delft, 2000
- [34] Kaya F., Karagoz I., Performance analysis of numerical schemes in highly

- swirling turbulent flows in cyclones[J]. *Current Science*. 2008, 94(10): 1273-1278
- [35] Pant K., Crowe C.T., Irving P. On the design of miniature cyclones for the collection of bioaerosols[J]. *Powder Technology*. 2002, 125(2): 260-265
- [36] Velilla J. Study of flow at a PFBC cyclone dipleg[D]. PhD thesis, University of Zaragoza. 2005
- [37] Gil A. Experimental cold flow model of PFBC primary cyclone[D]. Zaragoza, University of Zaragoza, 2000
- [38] Muschelknautz E. Die Berechnung von Zyklonabscheidern für Gas. *Chemie-Ingenieur Technik* (in german). 1972, 44(1-2): 63-71
- [39] Trefz M., Muschelknautz E. Extended cyclone theory for gas flows with high solids concentrations[J]. *Chemical Engineering Technology*. 1993, 16(3): 153-160
- [40] Dirgo L., Leith D. Design of cyclone separators[M]. *Encyclopedia of fluid mechanics*. 1986, 4
- [41] Reznik V.A., Matsnev V.V. Comparing the characteristics of the elements in batteries of cyclones[J]. *Thermal Engineering*. 1971; 18(12): 34-39
- [42] Hoffmann A.C., Stein L.E. Gas cyclones and swirl tubes. Principles, design and operation[M]. Berlin: Springer, 2002.
- [43] Shepherd C.B., Lapple C.E. Flow pattern and pressure drop in cyclone dust collectors[J]. *Industrial & Engineering Chemistry*. 1939, 31(8): 972-984.
- [44] First M.W. Fundamental factors in the design of cyclone dust collectors[D]. Cambridge,, Harvard University. 1950
- [45] Alexander R.M. Fundamentals of cyclone design and operation, Proceedings of the Australian Institute of Mining Metals. 1953, 152-153: 203-228
- [46] Staimand C. J. Pressure drops in cyclone separators[J]. *Engineering*. 1946, 168: 409-412
- [47] W. Barth, L. Leineweber, Beurteilung und Auslegung von Zyklonabscheidern[J]. *Staub*. 1964, 24(2): 41-55.
- [48] Muschelknautz E. Auslegung von Zyklonabscheidern in der technischen Praxis[J]. *Staub Reinhaltung der Luft*. 1970, 30(5): 187-195
- [49] Casal J., Martinez-Benet J.M. A better way to calculate cyclone pressure drop [J]. *Chemical Engineering*. 1983, 90(2): 99-100
- [50] Briggs L.W., Effect of dust concentration on cyclone performance[C]. *Transaction in American Institute of Chemical Engineers*. 1946, 42(30):

511-526

- [51] Yuu S., Jotaki T., Tomita Y., Yoshida K. The reduction of pressure drop due to dust loading in a conventional cyclone[J]. Chemical Engineering Science. 1978, 33(1): 1573-1580
- [52] Hoffmann A.C., Van Santen A., Allen R.W.K., Clift R. Effects of geometry and solid loading on the performance of gas cyclones[J]. Powder Technology. 1992, 70: 83-91
- [53] Luo X.L. J.Y. Chen, M.X. Shi, Research on the effect of the particle concentration in gas upon the performance of cyclone separators[J]. Journal of Engineering Thermophysics. 1992, 13(3): 282-284(in Chinese).
- [54] Bohnet M., Lorenz T., Separation efficiency and pressure drop of cyclone at high temperatures. In: Gas Cleaning at High Temperatures[M], R. Clift, J.P.K. Seville, (Eds.), Blackie Academic and Professional, Chapman and Hall, Glasgow, UK. 1993, 17-31
- [55] Xu S.S., Xu J.Y., Xu C.K., Study of the influence of temperature and pressure on high temperature dust separation properties of cyclones separators[J]. Power Engineering. 1997, 17(2): 52-58(Chinese language)
- [56] Chen J.Y. Shi M.X. Experimental research on cyclone performance at high temperatures.[C] Proc. 9th World Filtration Congress (CD), New Orleans, U.S.A., Apr. 2004
- [57] Meißner P., Löffler F. Zur Berechnung des Strömungsfeldes im Zyklonabscheider[J]. Chemie Ingenieur Technik 1978, 50(6): 471-471
- [58] Zhao B., Su Y., Zhang J., Simulation of gas flow pattern and separation efficiency in cyclone with conventional single and spiral double inlet configuration[J]. Chemical Engineering Research and Design. 2006, 84(12): 1158-1165
- [59] Avci A., Karagoz I. Theoretical investigation of pressure losses in cyclone separators[C]. International Communications in Heat and Mass Transfer. 2001, 28(1): 107-177
- [60] Qian F., Zhang M. Effects of the inlet section angle on the flow field of a cyclone[J]. Chemical Engineering & Technology. 2007, 30(11): 1521-1525
- [61] Qian F., Wu Y. Effects of the inlet section angle on the separation performance of a cyclone[J]. Chemical Engineering Research and Design. 2009, 87(12): 1567-1572.
- [62] Schnell K.B., Brown C.A. Air Pollution Control Technology Handbook[M]

Edited by K. Frank, CRC Press LLC, Florida, 2002, Chapter 21

- [63] Gong G.C., Yang Z.Z, Zhu S.L. Numerical investigation of the effect of helix angle and leaf margin on the flow pattern and the performance of the axial flow cyclone separator[J]. Applied Mathematical Modelling, 2012, 8(36): 3916-3930
- [64] Shukla S.K., Shukla P., Ghosh P. The effect of modeling of velocity fluctuations on prediction of collection efficiency of cyclone separators[J]. Applied Mathematical Modelling. 2013, 8(37): 5774-5789
- [65] Moses H., Löffler F. Prediction of particle removal in cyclone separators[J]. International Chemical Engineering. 1988, 28(2): 251-240
- [66] Cloete S., Johansen S.T., Amini S. Performance evaluation of a complete Lagrangian KTGF approach for dilute granular flow modelling[J]. Powder Technology. 2012, 226: 43-52
- [67] El-Batsh H.M. Improving cyclone performance by proper selection of the exit pipe. Applied Mathematical Modelling, 2013, 37(7): 5286–5303
- [68] Avci A., Karagoz I, Surmen A. Development of a new method for evaluating vortex length in reversed flow cyclone separators[J]. Powder Technology 2013, 235: 460–466
- [69] Elsayed K., Lacor C. CFD modeling and multi-objective optimization of cyclone geometry using desirability function, artificial neural networks and genetic algorithms[J]. Applied Mathematical Modelling. 2013, 37 (8): 5680–5704
- [70] Funk P.A., Holt G.A., Whitelock D.P. Novel cyclone empirical pressure drop and emissions with heterogeneous particulate[J]. Journal of Aerosol Science. <http://dx.doi.org/10.1016/j.jaerosci.2014.04.001>
- [71] Chuah T.G., Gimbun J., Choong T.S. A CFD study of the effect of cone dimensions on sampling aerocyclones performance and hydrodynamics[J]. Powder Technology. 2006, 162(2): 126-132
- [72] Wan G., Sun G., Xue X., Shi M. Solids concentration simulation of different size particles in cyclones separator. Powder Technology. 2008, 183(1): 94-104
- [73] Gimbun J., Chuah T.G, Choong T.S. Fakhru'l-Razi A. A CFD study on the prediction of cyclone collection efficiency[J]. International Journal for Computational Methods in Engineering Science and Mechanics. 2005, 6(3): 161-168
- [74] Gimbun J., Chuah T.G., Fakhru'l-Razi A., Choong T.S. The influence of



- temperature and inlet velocity on cyclone pressure drop: a CFD study[J]. Chemical Engineering & Processing. 2005, 44(1): 7-12.
- [75] Gimbun J., Chuah T.G, Choong T.S., Fakhru'l-Razi A. Prediction of the effects of cone tip diameter on the cyclone performance[J]. Aerosol Science and Technology. 2005, 36(8): 1056-1065
- [76] M.D. Slack, R.O. Prasad, A. Bakker, F. Boysan, Advances in cyclone modeling using unstructured grids[J]. Chemical Engineering Research and Design. 2000, 78(8): 1098-1104
- [77] Elsayed K., Lacor C., Optimization of the cyclone separator geometry for minimum, pressure drop using mathematical models CFD simulations[J]. Chemical Engineering Science. 2010, 65(22): 6048-6058.
- [78] Elghobashi S. On predicting particle-laden turbulent flows[J]. Applied Scientific Research. 1994, 52(4): 309-29
- [79] Sommerfeld M. Theoretical and experimental modeling of particulate flows. Lecture series 2000-2006, von Karman Institute for Fluid Dynamics, 2000.
- [80] Chiesa M., Mathisen V., Melheim J.A., Halvorsen B.M. Numerical simulation of particulate flow by the Eulerian-Lagrangian and the Eulerian-Eulerian with application to fluidized bed[J]. Computer & Chemical Engineering. 2005, 29(2): 291-304
- [81] Loth E. Numerical approaches for motion of dispersed particles, droplets and bubbles[J]. Progress in Energy Combustion Science. 2000. 26(3): 161-223
- [82] Anh Ho C., Sommerfeld M. Modeling of micro-particle agglomeration in turbulent flow[J]. Chemical Engineering Science. 2002, 57(15): 3073-3084
- [83] Brilliantov N.V. and Poschel T. Kinetic theory of granular gases[M]. Oxford: Oxford University Press, 2004
- [84] Dong L.P., Fan M.Q., Yang H.L. Separation performance of a cyclone column separator with complicated positive and negative cones[J]. International Journal of Mineral Processing. 2013, 122: 43-46
- [85] Lun, C.K.K Savage, S.B. Jeffrey, D.J. Chepurnity, N. 1984. Kinetic Theory for granular flow: inelastic particles in Couette flow and slightly inelastic particles in general flow field[J]. Journal of Fluid Mechanics. 1984, 140 (223-222): 256
- [86] Safikhani H., Akhavan-Behabadi M.A., Shams M., Rahimyan M.H. Numerical simulation of flow field in three types of standard cyclone separators[J] Advanced Powder Technology. 2010, 21(4): 435-442
- [87] Liu H.F., Xu J.Y., Ying-xiang Wu Y.X., Zheng Z.C. Numerical study on oil and

- water two-phase flow in a cylindrical cyclone[J]. *Journal of Hydrodynamics*. 2010, 22(5): 832-837
- [88] Chen J.H, Liu X. Simulation of a modified cyclone separator with a novel exhausts[J]. *Separation and Purification Technology*. 2010, 73 (2): 100–105
- [89] Fukui K., Yoshida H., Jikihara L., Yamamoto T. Effects of clean-air injection on particle-separation performance of novel cyclone with sintered metal cone[J]. *Separation and Purification Technology*. 2011, 80(2): 356-363
- [90] Chu K.W., Wanga B., Yu A.B., Vince A. Computational study of the multiphase flow in a dense medium cyclone: Effect of particle density[J]. *Chemical Engineering Science*. 2012, 73: 123–139
- [91] Cloete S., Johansen S.T, Amini S. Performance evaluation of a complete Lagrangian KTGF approach for dilute granular flow modelling[J]. *Powder Technology*. 2012, 226: 43-52
- [92] Karagoz I., Avci A., Surmen A., Sendogan O. Design and performance evaluation of a new cyclone separator[J]. *Journal of Aerosol Science*. 2013 (59): 57–64
- [93] Arastoopour H. Numerical Simulation and Experimental Analysis of Gas/Solid Flow Systems: 1999 Fluor-Daniel Plenary Lecture. *Powder Technology*. 2001, 119(2): 59-67.
- [94] Benyahia S., Arastoopour H., Knowlton T.M., Massah H. Simulation of particles and gas flow behavior in the riser section of a circulating fluidized bed using the Kinetic Theory approach for the particle phase[J]. *Powder Technology*. 2000, 112(1): 24-33
- [95] Sun B., Gidaspow D. Computation of Circulating Fluidized Bed Riser Flow for the Fluidization VIII Benchmark Test[J]. *Industrial Engineering Chemistry Research*. 1999, 38(3): 787-792.
- [96] Elsayed K., Lacor C. Numerical modeling of the flow field and performance in cyclones of different cone-tip diameters[J]. *Computers & Fluids*. 2011, 51(1):48-59
- [97] Gidaspow D. Multiphase flow and fluidization: Continuum and kinetic theory description[M]. Academic Press, 1994.
- [98] Chu K.W., Kuang S.B., Yu A.B., Vince A., Particle scale modelling of the multiphase flow in a dense medium cyclone: Effect of fluctuation of solids flow rate[J]. *Minerals Engineering*. 2012, 33:34-45
- [99] Doheim M.A., Abdel Gawad A.F., Mahran G.M.A., Abu-Ali M.H., Rizk A.M.

- Numerical simulation of particulate-flow in spiral separators: Part I. Low solids concentration (0.3% & 3% solids)[J]. *Applied Mathematical Modelling*. 2013 37(1): 198-215
- [100] Karagoz I., Avci A., Surmen A., Sendogan O. Design and performance evaluation of a new cyclone separator[J]. *Journal of Aerosol Science*. 2013, 59:57-64
- [101] Gao X., Chen J., Feng J., Peng X. Numerical and experimental investigations of the effects of the breakup of oil droplets on the performance of oil-gas cyclone separators in oil-injected compressor systems[J]. *International Journal of Refrigeration*. 2013, 36(7): 1894-1904
- [102] Oh J., Choi S., Kim J., Lee S., Jin G. Particle separation with the concept of uniflow cyclone[J]. *Powder Technology* 2014, 254: 500-507
- [103] Shukla S.K., Shukla P., Ghosh P. The effect of modeling of velocity fluctuations on prediction of collection efficiency of cyclone separators[J]. *Applied Mathematical Modelling*. 2013, 37(8): 5774–5789
- [104] Hsiao T.C., Chen D., Greenberg P.S., Street K.W. Effect of geometric configuration on the collection efficiency of axial flow cyclones[J]. *Journal of Aerosol Science*. 2011, 42(2): 78-86
- [105] Gronald G., Derksen J.J. Simulating turbulent swirling flow in a gas cyclone: A comparison of various modeling approaches[J]. *Powder Technology*. 2011, 205(1): 160–171
- [106] Masnadi M.S., Grace J.R., Elyasi S., Bi X. Distribution of multi-phase gas–solid flow across identical parallel cyclones: Modeling and experimental study[J]. *Separation and Purification Technology*. 2010, 72(1): 48-55
- [107] Zhou X, Cheng L., Wang Q.H, Luo Z.Y., Cen K.F. Non-uniform distribution of gas-solid flow through six parallel cyclones in a CFB system: An experimental study[J]. *Particuology*. 2012, 10(2): 170-175
- [108] Paiva J., Salcedo R., Araujo P. Impact of particle agglomeration in cyclones[J]. *Chemical Engineering Journal*. 2010, 162(3): 861-876
- [109] Azadi M, Azadi M. An analytical study of the effect of inlet velocity on the cyclone performance using mathematical models[J]. *Powder Technology*. 2012, 217: 121-127
- [110] Choudhury, D. Introduction to the renormalization group method and turbulence modeling[M]. *Fluent Inc. Technical Memorandum TM-107*, 1993
- [111] Daly, B.J., F.H. Transport equation in turbulence[J]. *Physics of Fluids*. 1970,

13:2634-2649

- [112]Lien F.S. Leschzine M.A. Assessment of the Turbulence-transport models including non-linear RNG eddy-viscosity Formulation and Second-moment Closure[J]. Computer and Fluids. 1994, 23(8): 983-1004
- [113]Gibson M.M. Launder B.E. Ground effects on pressure fluctuations in the atmospheric boundary layer[J]. Journal of Fluid Mechanics. 1978, 86(3):491-511
- [114]Fu S., Launder B.E., Leschziner M.A. Modeling strongly swirling recirculating jet flow with Reynolds-Stress transport closures[C]. In 6th Symposium on Turbulent Shear Flows. Toulouse, France, 1987, 1: 179
- [115]Launder B.E. Second-moment closure and its use in modeling turbulent industrial flows[J]. International Journal for Numerical Methods in Fluids. 1989, 9(8): 963-985
- [116]Chapman, S., & Cowling, T. G. The Mathematical theory of non-uniform gases[M]. Cambridge: Cambridge University Press, 1970.
- [117]Schaeffer G. Instability in the evolution equations describing incompressible granular flow[J]. Journal of Differential Equations. 1987, 6(1), 19-50.
- [118]Kumar C.R., Mohanan S., Tripathy S.T., Ramamurthy Y., Venugopalan T., Suresh N. Prediction of process input interactions of floatex density separator performance for separating medium density particles[J]. International Journal of Mineral Processing. 2011, 100(3): 136-141.
- [119]Elsayed K., Lacor C., Modeling, Analysis and optimization of aircyclones using artificial neural network, response surface methodology and CFD simulation approaches[J]. Powder Technology. 2011, 212(1): 115-133
- [120]Hwang Y., Kim B.G, Bae K.H., Kim H.S. Mechanism and performance of a dry particle separator using an elastic drum[J]. International Journal of Mineral Processing. 2013, 125: 34-38
- [121]Yamamoto T., Shinya T., Fukui K., Yoshida H. Classification of particles by centrifugal separator and analysis of the fluid behavior[J]. Advanced Powder Technology. 2011, 22(2): 294-299
- [122]Wang B., Chu K.W., Yu A.B., Vince A., Barnett G.D., Barnett P.J. Computational study of the multiphase flow and performance of dense medium cyclones: Effect of body Dimensions[J]. Minerals Engineering. 2011, 24(1): 19-34
- [123]Cullivan J.C. Dyakowski, T. William, R.A. New understanding of

- hydrocyclone flow field and separation mechanism from CFD[J]. Minerals Engineering. 2004,17(5): 651-660
- [124]Raoufi A., Shams M., Farzaneh M., Ebrahimi R. Numerical simulation and optimization of fluid flow in cyclone vortex finder[J]. Chemical Engineering and Processing. 2008, 47(1): 128-137
- [125]Raoufi A., Shams M., Kanani H. CFD analysis of flow field in square cyclones[J]. Powder Technology. 2009, 191(3): 349-35
- [126]Hu L.Y. Zhou L.X., Zhang J., Shi M.X. Studies on strongly swirling flows in a full space of a volute cyclone separator[J]. AIChE Journal. 2005, 51(3):740-749
- [127]Qiu Y.F., Deng B.Q., Kim C.N. Numerical study of the flow field and separation efficiency of a divergent cyclone[J]. Powder Technology. 2012. 217:231-237
- [128]Azadi M., Azadi M., Mohebbi A. A CFD study of the effect of cyclone size on its performance parameters[J]. Journal of Hazardous Materials. 2010, 182(1):835-841
- [129]Feulvarch E., Bergheau J.M. An implicit fixed-grid method for the finite-element analysis of heat transfer involving phase changes[J]. Numerical Heat Transfer, Part B, Fundamentals. 2007, 51(6): 585–610.
- [130]Pisarev G.I., Hoffmann A.C. Effect of the ‘end of the vortex’ phenomenon on the particle motion and separation in a swirl tube separator[J]. Powder Technology. 2012, 222: 101-107
- [131]Park W.G., Park M.S., Jung Y.R, Jang K.L. Numerical study of defrosting phenomena of automotive windshield glass[J]. Numerical Heat Transfer, Part A: Applications. 2005, 47(7): 725-739
- [132]Kang K.G., Ryou H.S. Computation of Solidification and melting using the PISO Algorithm[J]. Numerical Heat Transfer, Part B: Fundamentals. 2004, 46(2):179-194
- [133]Winfield D., Cross M., Croft N., Paddison D., Craig I. Performance comparison of a single and triple tangential inlet gas separation cyclone: A CFD study[J]. Powder Technology. 2013, 235: 520-531
- [134]Haig C.W., Hursthouse A., McIlwaina S., Sykes D., The effect of particle agglomeration and attrition on the separation efficiency of a Stairmand cyclone[J]. Powder Technology. 2014, 258: 110-124
- [135]Elsayed K., Lacor C. Numerical modeling of the flow field and performance in

- cyclones of different cone-tip diameters[J]. Computers & Fluids. 2011, 51(1):48-59
- [136]Qian F., Huang Z., Chen G., Zhang M. Numerical Study of the Separation Characteristics in a Cyclone of Different Inlet Particle Concentrations[J]. Computers and Chemical Engineering. 2007, 31(9): 1111-1122
- [137]Muschelknautz E., Theorie der Fliehkraftabscheider mit besondere berucksichtigung hoher temperaturen und drucke (in German)[J]. VDI-Berichte 1980, (363): 49-60
- [138]Derksen J.J., Sundaresan S., Van Den Akker H.E.A. Simulation of mass-loading effects in gas-solid cyclone separators[J]. Powder Technology. 2006, 163(1): 59-68

## Papers published in the period of Ph.D education

- [1] **M'BOUANA No éLandry-Privace**, Zhao Feixiang, Zhang Qinghong, Lu Huilin. Numerical simulation of Gas-solid flow in Square Cyclone Separators with downward exit [J]. Journal of Harbin Institute of Technology (New Series), 2014, 21(2): 83-90 (EI 收录: 20142417813322)
- [2] **M'BOUANA No éLandry-P**, WANG Shuai, SUN Li-Yan, DU Xiaoli, LU Huilin, Numerical Simulation of Flow Behavior of Gas and Particles in Riser with Large Eddy Simulation Approach, [J] Journal of Engineering Thermophysics, 2011, 32(8): 1327-1330 (EI 收录号 20113714322575)
- [3] **M'BOUANA No é Landry P.**; LI, Dan; TANG, Yangjia; LU, Huilin. Numerical simulation of gas and particle flows in cyclone separators[C]. In: 7th International Symposium on Multiphase Flow, Heat Mass Transfer and Energy conversion. AIP Conference Proceedings, 2013, 1547, 545-554 (ISTP 收录号 WOS: 000331233800063)
- [4] **M'BOUANA No éLandry-Privace**, WANG Shuai, YANG Yun-Chao, Namory Camara, LU Hui-Lin, Modeling of Chemical Looping Combustion Process in the Coupled Reactor, Journal of Engineering Thermophysics [J] (Accepted), 2014, 35(7) (EI)
- [5] **No éLandry-Privace M'BOUANA**, Ahmed Bougamra, Zhao Feixiang, Lu Huilin. Numerical study of dense gas-solid flow in square cyclone separator [J]. Advances in Chemical Engineering and Science (Accepted), 2014

# 哈尔滨工业大学学位论文原创性声明和使用权限

## 学位论文原创性声明

本人郑重声明：此处所提交的学位论文《高浓度旋风分离器气固流动与分离特性的数值模拟》，是本人在导师指导下，在哈尔滨工业大学攻读学位期间独立进行研究工作所取得的成果，且学位论文中除已标注引用文献的部分外不包含他人完成或已发表的研究成果。对本学位论文的研究工作做出重要贡献的个人和集体，均已在文中以明确方式注明。

作者签名：



日期：2014 年 06 月 18 日

## 学位论文使用权限

学位论文是研究生在哈尔滨工业大学攻读学位期间完成的成果，知识产权归属哈尔滨工业大学。学位论文的使用权限如下：

(1) 学校可以采用影印、缩印或其他复制手段保存研究生上交的学位论文，并向国家图书馆报送学位论文；(2) 学校可以将学位论文部分或全部内容编入有关数据库进行检索和提供相应阅览服务；(3) 研究生毕业后发表与此学位论文研究成果相关的学术论文和其他成果时，应征得导师同意，且第一署名单位为哈尔滨工业大学。

保密论文在保密期内遵守有关保密规定，解密后适用于此使用权限规定。


本人知悉学位论文的使用权限，并将遵守有关规定。

作者签名：



日期：2014 年 06 月 18 日

导师签名：




日期：2014 年 06 月 18 日



## Statement of copyright and Letter or authorization

### Declarations

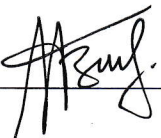
I, the undersigned, declare this work has not previously been submitted in candidature for any degree. The dissertation «Numerical Simulation of Dense Gas-Solid Separation in Cyclone Separators» is the result of my own work and investigations, except where otherwise stated. Other sources are acknowledged by giving explicit references. A complete list of references is appended.

Signed  (candidate) Date 2014.06.18

### Copyright

Powers of discretion are granted to the University Library to allow the dissertation to be copied in part without further reference to the author. This permission covers only single copies made for study purposes, subject to normal conditions of acknowledgement.

Library, Harbin Institute of Technology, No.92 West Dazhi Street, Nanggang District, Harbin 150001, P.R, China

Signed  (candidate) Date 2014.06.18

Signed  (supervisor) Date June 18, 2014

## Acknowledgements

This dissertation and study would be incomplete and impossible without people who supported me and believe in me. This dissertation is a result of four year of graduate work during which I have been accompanied and supported by many people. My deepest gratitude and heartfelt thanks are due to each and every one of them.

Most of all I would like to thank my supervisor, Prof. Lu Huilin for his support, encouragement and his supervision during this study. He is not only a god researcher with great vision but also a very kind and understanding person. His trust and faith in me encouraged me a great amount during my entire stay at Harbin Institute of Technology.

My thanks are extended to my all lab members and colleagues at the School of Energy Science and Engineering for their assistance and guidance in getting my graduate.

I am also deeply indebted to the Government of China (China Scholarship Council), and the Government of Central African Republic for providing the opportunity and financial support to take on this study.

I want to thank my family in Central African Republic; especially my father Jean and mother Catherine, Uncle Jean-Pierre and Aunt Julienne. I always had you in my mind. Thank you for your immeasurable love and support. You gave me the strength and love I needed to complete this work.

Oh, and thank you God, for not forgetting me even when I seem to forget you way too often. You never fail me.

## Resume

M'BOUANA Noé-Landry-Privace is a native of Bangui, Central African Republic (CAR). He received his Bachelor of Science major in Sciences Physics in 2005 from the Faculty of Sciences, University of Bangui (Central African Republic). He was awarded a Chinese Government Scholarship in 2007 and joined the School of Energy Science and Engineering at the Harbin Institute of Technology in September 2008 where he obtained his Master Degree of Engineering in Thermal Power Energy Engineering in July 2010. He awarded the Chinese Government Distinguished International Students Scholarship in the year of 2010 and he started his Ph.D. Degree in Thermal Power Energy Engineering in September 2010 at Harbin Institute of Technology, Harbin P.R China. After spending four years working on his research, his dissertation finally came of a close, and he is looking forward to starting his professional career.

Contact: [mbouana@hit.edu.cn](mailto:mbouana@hit.edu.cn)  
[mbouana@hotmail.fr](mailto:mbouana@hotmail.fr)